Iowa State University
Digital Repository

Retrospective Theses and Dissertations

Iowa State University Capstones, Theses and Dissertations

2002

Modeling of chemical mechanical polishing at multiple scales

Guanghui Fu
Iowa State University

Follow this and additional works at: https://lib.dr.iastate.edu/rtd

Part of the Electrical and Electronics Commons, and the Mechanical Engineering Commons

Recommended Citation
Fu, Guanghui, "Modeling of chemical mechanical polishing at multiple scales " (2002). *Retrospective Theses and Dissertations*. 995.
https://lib.dr.iastate.edu/rtd/995

This Dissertation is brought to you for free and open access by the Iowa State University Capstones, Theses and Dissertations at Iowa State University Digital Repository. It has been accepted for inclusion in Retrospective Theses and Dissertations by an authorized administrator of Iowa State University Digital Repository. For more information, please contact digirep@iastate.edu.

المنارة للاستشارات

www.manaraa.com

INFORMATION TO USERS

This manuscript has been reproduced from the microfilm master. UMI films the text directly from the original or copy submitted. Thus, some thesis and dissertation copies are in typewriter face, while others may be from any type of computer printer.

The quality of this reproduction is dependent upon the quality of the copy submitted. Broken or indistinct print, colored or poor quality illustrations and photographs, print bleedthrough, substandard margins, and improper alignment can adversely affect reproduction.

In the unlikely event that the author did not send UMI a complete manuscript and there are missing pages, these will be noted. Also, if unauthorized copyright material had to be removed, a note will indicate the deletion.

Oversize materials (e.g., maps, drawings, charts) are reproduced by sectioning the original, beginning at the upper left-hand corner and continuing from left to right in equal sections with small overlaps.

ProQuest Information and Learning
300 North Zeeb Road, Ann Arbor, MI 48106-1346 USA
800-521-0600

UMI®

Modeling of chemical mechanical polishing at multiple scales

by

Guanghui Fu

A dissertation submitted to the graduate faculty

in partial fulfillment of the requirements of the degree of

DOCTOR OF PHILOSOPHY

Major: Mechanical Engineering

Program of Study Committee:
Abhijit Chandra (Major Professor)
Shyam Bahadur
Palaniappa A. Molian
Ambar K. Mitra
Ashraf F. Bastawros

Iowa State University

Ames, Iowa

2002

UMI Number: 3061830

UMI®

UMI Microform 3061830

Copyright 2002 by ProQuest Information and Learning Company.
All rights reserved. This microform edition is protected against
unauthorized copying under Title 17, United States Code.

ProQuest Information and Learning Company
300 North Zeeb Road
P.O. Box 1346
Ann Arbor, MI 48106-1346

Graduate College
Iowa State University

This is to certify that the doctoral dissertation of

Guanghui Fu

has met the dissertation requirements of Iowa State University

Signature was redacted for privacy.

Major Professor

Signature was redacted for privacy.

For the Major Program

TABLE OF CONTENTS

ABSTRACT v

CHAPTER 1. INTRODUCTION 1
1.1 Polisher 3
1.2 Components and Their Functions 5
1.3 Thesis Outline 14

CHAPTER 2. MATERIAL REMOVAL MODEL 16
2.1 Literature Review 16
2.2 Model Development 19
2.2.1 Spherical particles 20
2.2.2 Sharp particles 24
2.3 Comparison with Experimental Data 25
2.4 Summary 33

CHAPTER 3. BOUSSINESQ'S PROBLEM 37
3.1 Literature Review 37
3.2 Theoretical Derivation 40
3.2.1 Elastic half space 40
3.2.2 Viscoelastic half space 46
3.3 Special Cases 48
3.3.1 Elastic half space 48
3.3.2 Viscoelastic half space 56
3.4 Summary 58

CHAPTER 4. WITHIN WAFER NONUNIFORMITY 60
4.1 Literature Review 61
4.2 Rigid Wafer - Elastic Pad 63
4.3 Rigid Wafer - Viscoelastic Pad 73
4.4 Deformable Wafer - Elastic Pad 85
4.5 Summary 94

CHAPTER 5. DISHING, EROSION AND STEP HEIGHT REDUCTION 96
5.1 Literature Review 96
5.2 Theoretical Derivation 98
5.3 Special Cases 103
5.4 Comparison with Experimental Data 112
5.5 Summary 115

CHAPTER 6. CONCLUSIONS AND FUTURE WORK 116
6.1 Conclusions 116
6.1.1 Material removal mechanism 118

6.1.2 Within wafer nonuniformity 118
6.1.3 Dishing, erosion and step height reduction 119
6.2 Future Work 120
6.2.1 Particle scale model 120
6.2.2 Wafer scale model 121
6.2.3 Die scale model 122
6.2.4 Feature scale model 123

REFERENCES 124

ABSTRACT

Chemical Mechanical Polishing (CMP) has grown rapidly during the past decade as part of mainstream processing method in submicron integrated circuit manufacturing because of its global or near-global planarization ability. However, CMP process is influenced by many factors and is poorly understood. It makes process control and optimization very difficult. This study focuses on the modeling and simulation to facilitate better understanding and better control of the CMP process. The thesis outlines the modeling of CMP process in three scales: particle scale for material removal mechanism, wafer scale for within wafer nonuniformity issues and feature scale for dishing and erosion in metal CMP.

At the particle scale, material removal mechanism is assumed to be due to local plastic deformation of wafer surface at the abrasive - wafer interface. Pad is assumed to deform like a beam to obtain an approximate force partition between abrasives and direct wafer-pad contact. A mechanistic material removal model is derived that delineates the influence of abrasive (shape, size and concentration), pad (rigidity) and process parameters (pressure and relative velocity) on the material removal rate (MRR).

Wafer scale model is based on the solution of indentation of elastic half space by a rigid frictionless polynomial punch. The elastic solution is derived through potential theory and complex analysis method. It is valid for any polynomial punch with integer power or non-integer power. The load-displacement relationship is also derived and the conditions for unbonded or bonded contact are obtained from the boundary condition at punch edge. The corresponding viscoelastic solution is obtained through Laplace transform and elastic-viscoelastic analogy. The elastic solution is used to explain the edge effect. The elastic analytical

solution is first verified against numerical results from Finite Element Method (FEM) simulation. It shows wafer curvature, indentation depth and load will influence the interface pressure distribution throughout the wafer surface and it introduces parameters control as a potential avenue for completely eliminating the within wafer nonumiformity. Viscoelastic solution is used to explain within wafer nonuniformity, i.e., edge effect and wafer to wafer nonuniformity, i.e., removal rate decay for unconditioned pad. The relationships among wafer-pad interface pressure, wafer shape and wafer loading condition are also investigated.

Feature scale model for dishing and erosion is based on Preston's relationship for material removal and constant downforce. It shows dishing will reach a limit and is governed by polishing conditions (overpolishing, pressure, velocity), slurry (selectivity), pad characteristics (pad stiffness and bending ability), as well as wafer surface feature topography (pattern density, linewidth and pitch). This model is also valid for step height reduction when the same surface material is polished.

Due to process complexity and coupling of various parameters, more fundamental research needs to be carried out and carefully designed experiments need to be done to verify the models. Recommendations for future research work is presented at the end.

CHAPTER 1. INTRODUCTION

Chemical Mechanical Polishing, or CMP, has become part of mainstream processing method in IC manufacturing. With this technique, global or near-global planarization can be achieved because the CMP process removes elevated features without much removal of lower areas, thus planarizing the topography (Plummer et al 2000). While standard plasma etchback processes achieve local planarization, global planarization is obtained through CMP. CMP is a room-temperature process and fits the process design trend of using lower process temperature, which will lead to less diffusion of dopants in Si substrate. It is also compatible to the thermal stability requirement of some of the low-K dielectric materials.

CMP is used in submicron IC manufacturing because of the following (Ouma 1998):

- Without CMP, higher levels of metallization will be difficult to carry out. Uneven surface after the deposition processes has to be made flat so a reliable and compact higher level metal interconnect structure can be made.
- To satisfy the lithography depth of focus requirement. With further shinkage of feature size, higher system resolution and smaller depth of focus is required. All of those demand a very flat wafer surface to guarantee the image from mask to be accurately transferred to wafer surface.
- To make the increment of device density possible, e.g., through the application of Shallow Trench Isolation (STI).

As its name implies, CMP is a combination of chemical and mechanical polishing. Wafers are held face down against a spinning polishing pad made of a roughened polyurethane plate. A slurry with certain chemical solution and abrasives is introduced between the

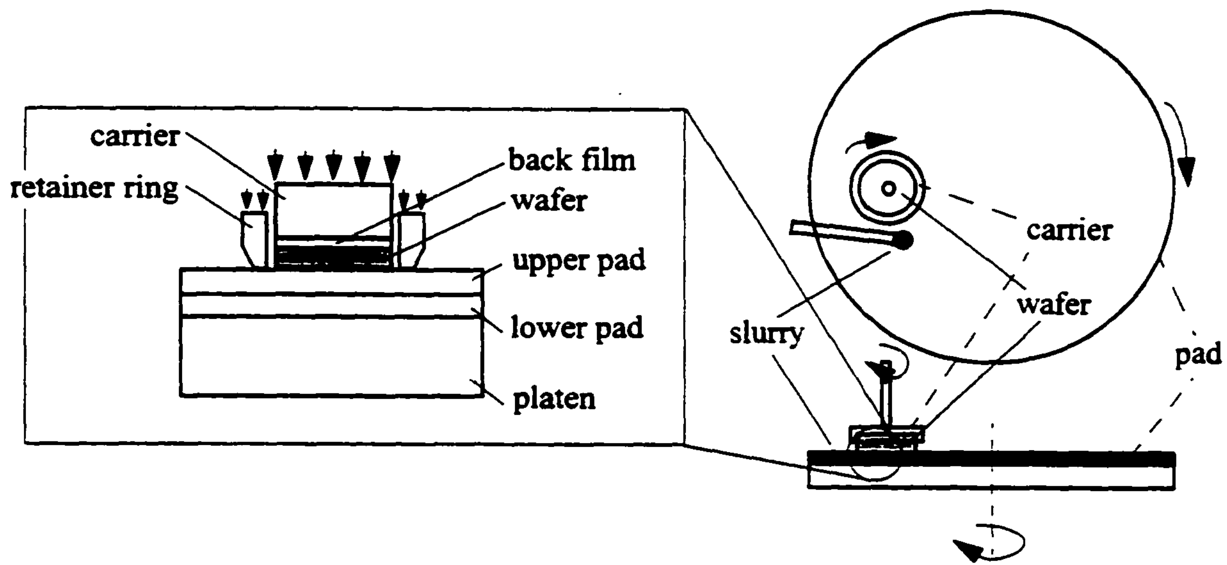

Fig. 1.1 Schematic picture of CMP setup

pad and the wafer, as shown in Fig. 1.1. The chemical composition and pH of the slurry are important and depend on the material being polished. For planarizing an oxide layer, a high pH alkali-based solution is often used, while a low pH, oxidizer-based solution is commonly used for metals. In general the chemical reaction at the wafer surface makes the surface material susceptible to mechanical abrasion by the abrasive in the slurry. For silicon dioxide removal, it is believed that the hydroxide in the slurry reacts with oxide to form a hydrated silicate layer, which is then removed mechanically by abrasion (Brown 1987). For metal removal, the solution oxidizes the surface and the product reacts with the acid to form salt which is then polished in a similar fashion to the oxide removal (Nguyen et al 2000). Removal rate stability (wafer to wafer variation), nonuniformity (both wafer-scale and die-scale) control and cost of ownership are some of the important issues in CMP application in IC manufacturing.

1.1 Polisher

CMP equipment has its root in glass polishing. To make it suitable for IC manufacturing, many research and development efforts have been made. The improvement is driven by the need for higher throughput and lower cost of ownership. The throughput can be increased either by increasing the material removal rate through increased pressure and velocity or by polishing more wafers at a given time. There are now three generations of CMP tools (Bibby and Holland 2000):

a. 1st Generation Polishers

They are based on rotating platen and rotating wafer design. The rotating axes of platen and wafer are parallel but have certain amount of offset. Larger the offset, higher the relative velocity between wafer and pad. If wafer and platen rotate with the same direction and the same speed, the relative velocity between wafer and pad is the same throughout the wafer surface. Slurry is deposited near the center of pad and centrifugal force causes it to move radially outward. Slurry built-up happens at the carrier edge while most falls off the pad and is discharged from the system, which leads to low slurry usage efficiency. The throughput is low and is in the order of 10-18 wafer/hour.

b. 2nd Generation Polishers

2nd generation polishers increase throughput to the range of 30-60 wafer/hour and increase footprint utilization from 0.5 to >1 wafer/hour per square foot of floor space. They are still based on rotating platen and rotating wafer design but include many "evolutionary" changes. Mutliwafer per platen and single wafer per platen multiplaten are the two general types of polisher design.

The major concerns in multiwafer per platen system are: (a) the breakage of one wafer will cause scratching and gouging of other wafers; (b) the variation of polishing results when wafer is loaded unevenly. The major concerns in single wafer per platen multiplaten system are: (a) the throughput limitation by the slowest polish step; (b) difficulty to decide which pad is the cause of wafer defects.

c. 3rd Generation Polishers

They are based on "revolutionary" approaches to improve CMP process through: (a) high relative velocity; (b) generalized pad and wafer motion; (c) unique methods of slurry delivery. Its main characteristics are high speed, low down force and single polyurethane pad. There are three types:

(a) Linear polishers

The rotating wafer is pressed against a rapidly moving pad which is a continuous belt kept in tension by rollers, as shown in Fig. 1.2. The slow carrier rotation will lead to almost uniform relative velocity throughout the wafer surface.

(b) Orbital polishers

Its major advantage is high relative speed with small tool footprint. Several tool con-

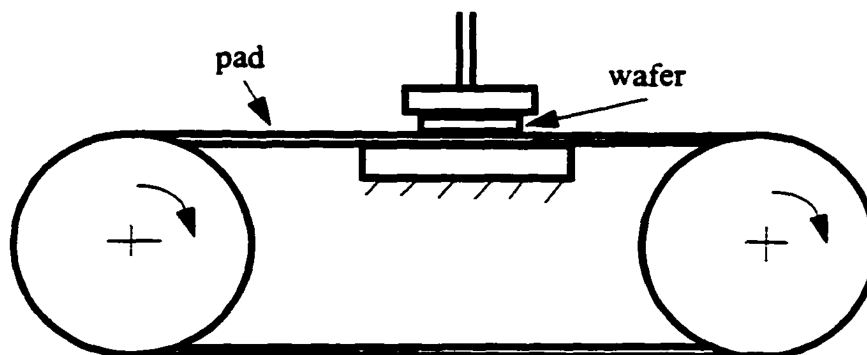

Fig. 1.2 Linear polisher

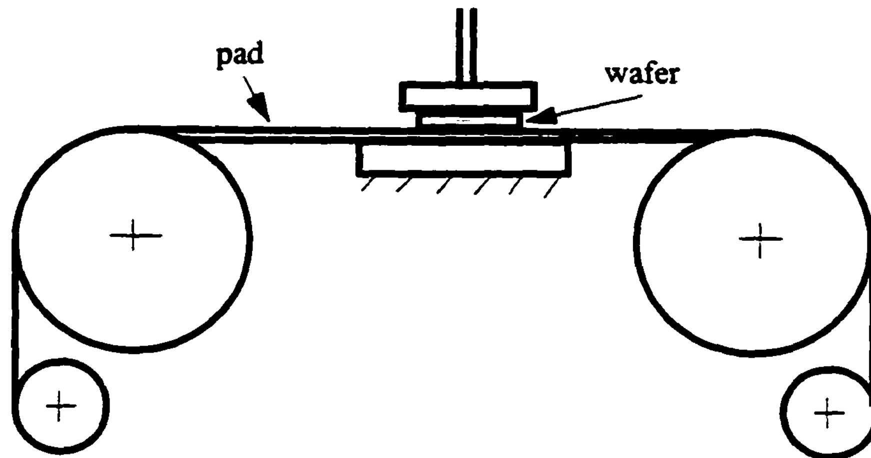

Fig. 1.3 Pad feed polisher

cepts based on orbital motion exists: some orbit the carrier while rotating the platen; some orbit the polish pad while rotating the carrier; some use orbital motion of carrier on a fixed pad.

(c) Pad feed polishers

Polish pads are in a roll like camera film as shown in Fig. 1.3. First, pad is fed out to the polish table and a wafer is polished. Then, the pad is conditioned and incrementated forward for the next wafer polish. Its major advantage is tool utilization. Fab can process wafers without changing the pad for up to a week.

1.2 Components and Their Functions

Slurry, pad and carrier are the three major components with different functions in a CMP system setup. Understanding their functions is the first step in the modeling and simulation of CMP processes.

a. Slurry

Slurry, a kind of liquid sandpaper, is made of abrasives and solution. The function of abrasives is mainly mechanical. The abrasives act as cutting tools and take part in the repeated plowing action leading to material removal. The main function of solution is chemical. It reacts with the wafer surface material to produce a softer surface layer which is easier to be removed by the abrasives.

(a) Abrasives

Abrasives are generally inorganic oxides. Silica - SiO_2, alumina -Al_2O_3 and Ceria - CeO_2 are the most commonly used. In general, they must be ultrapure and have almost uniform size and shape so that consistent polishing result can be achieved.

Abrasive size is in the order of 50-200 nm and its distribution is tightly controlled. However, due to various reasons (e.g., particle agglomeration), large particle will be present which may cause CMP scratches. To decrease unwanted large particles, milling during the slurry manufacture or filtration during the slurry distribution in CMP is commonly used (Li et al 2000).

Silica is often used in oxide CMP and there are two kinds of it due to different manufacturing methods: one is fumed silica whose shape is irregular, the other is colloidal silica whose shape is spherical (Li et al 2000). There are also two kinds of alumina: γ phase and α phase, and α phase is harder than γ phase.

How abrasives cause material removal in polishing is a research topic for a long time (Izumitani 1979). Some speculate that molecular order of surface material is removed by the abrasives through mechanical wear. The local heat generation and friction by the high contact pressure between abrasive and surface will cause plastic flow. In chemical mechanism for Si

polishing, a silica gel layer in silicon surface is believed to be formed through the chemical reaction with water and this layer is removed by the abrasives.

The particle parameters that are generally believed to influence material removal are:

- particle shape
- particle size and its distribution
- concentration
- polishing environment (wet polishing vs. oil/dry polishing)
- abrasive hardness

In the early days of CMP research, some people believed that there exists an uninterrupted fluid layer between wafer and pad while others believed that material removal is by abrasion through direct solid-solid contact (Steigerwald et al 1996). In fluid-based model, abrasive particles impact the wafer surface with certain velocity and impact angle. The energy of the impact weakens the bonds and leads to material removal (Cook 1990). In abrasion model, the particles are held by the pad and act as cutting tools, similar to material removal mechanism of sand paper. Now many believe the asperities of pad surface will be in direct contact with wafer surface and abrasion happens in those regions. There is also an interrupted fluid layer which aids slurry distribution and transport the abraded material out of the system.

As pad is not continuously in contact with every point of wafer surface due to its asperities, the material removal by the abrasives is not continuous. In the region where pad is not in direct contact with wafer, wafer surface is exposed to the slurry and reacts quickly to form a soft surface layer which is then removed through abrasion by the abrasives when pad and wafer is in direct contact.

In the common polishing practice, abrasives are between wafer-pad interface and is

free to move. There are some researchers working on fixed abrasive (FA) or bonded abrasive technology in which abrasives are built into the pad surface. On the pad surface, there are micro-replicated post structures which contain sub-micron particles evenly dispersed and captured within a toughened composite binder.

(b) Solution

Water in the solution acts as coolant on the surfaces of abrasives, wafer and pad, removes the abraded material out of the polishing system, aids the distribution of chemicals and at the same time may cause certain chemical reactions on the wafer and pad surfaces.

In oxide CMP, slurry solution acts as a hydrolizer and the following chemical reaction happens: $SiO_2+2H_2O \leftrightarrow Si(OH)_4$. The original Si-O bond is very strong; however, Si-OH is weak and much easier to be removed. In oxide CMP, common solution are KOH-based (most popular) or NH_4OH-based with high pH values. In this environment, SiO_2 is partially dissolved so that the chemical reaction (hydration) is further accelerated; on the other hand, higher pH value solutions lead to better suspended slurry which can decrease particle agglomeration and reduce CMP scratches (Li et al 2000).

In metal CMP, the solution acts as an oxidizer and selectivity is a major issue because the same slurry is used for metal interconnect, barrier layer and dielectric material. The oxidizer converts metal into metal oxide and it reacts with the acid to form salt, which is removed by the abrasives. The selectivity between different materials should be controlled so that dishing in metal region and erosion in dielectric region can be minimized.

Metal CMP has evolved from Al and W CMP to Cu CMP. In Cu CMP, oxidizer (e.g., H_2O_2) reacts with Cu in an acidic slurry and Cu^{2+} ion is formed (according to Pourbaix diagram (Pourbaix 1996) in Fig. 1.4, only Cu^{2+} or Cu are possible in acidic solutions with pH

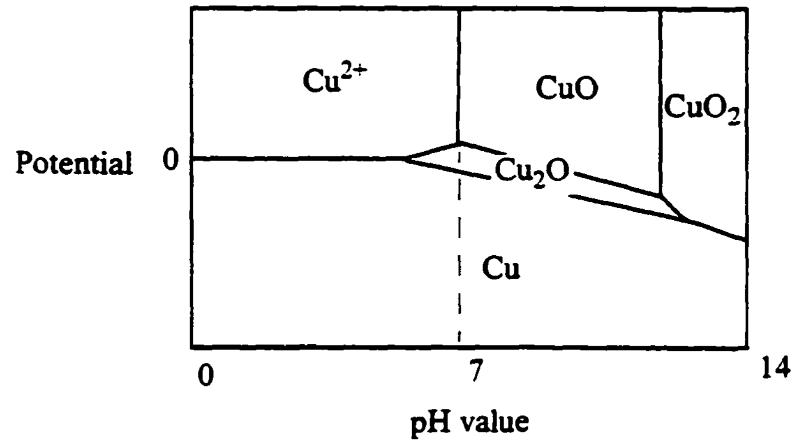

Fig. 1.4 Pourbaix diagram of the copper - H_2O system

4~5). The anions of the acid react with Cu^{2+} ions to from an insoluble salt which passivates the surface and prevents further chemical reactions below this layer. The passivative layer is then removed by abrasion in CMP (Nguyen et al 2000).

b. Pad

The mechanical properties of pad are affected by a large number of process and structural variables. For example, water soaking will decrease pad's Young's modulus because water breaks hydrogen bonds which crosslink the urethane structure (Steigerwald et al 1996). This implies that dry pad properties are not applicable to wet pad in CMP.

The mechanical properties which are generally believed to influence pad performance are:

- Young's modulus
- poisson ratio
- hardness and compressibility
- viscoelastic properties
- surface roughness and texture

- liquid permeability

Pad needs to have the ability to bring slurry on to the wafer surface, gives enough time to let the chemical reaction happen for softer surface layer formation; and, to aid the abrasive plowing action and remove the abraded material out of the system. To aid slurry transport, pad is either perforated (e.g., IC 1000 pad) or grooved (e.g., IC 1400). Newly-developed pads have trench grids for the same purposes.

In the material removal process, pad must hold abrasives and transfer the load to the abrasives. Izumitani (1979) found that to satisfy these requirements, pad has to be viscoelastic so that the polishing grain can be embedded and at the same time, it has to be rigid enough to transmit the load. In other words, pad should have viscoelastic characteristics and is generally made of polyermic materials such as polyurethane for CMP pads.

The viscoelastic deformation of pad also plays an important role in the planarization process. As the wafer transverses the pad surface according to its kinematic design, high areas and low areas of wafer surface may contact with pad. As the pad passes from a high area to a low area, it cannot deform immediately due to viscosity so that less pressure is on the low area. On the other hand, as the pad passes from a low area to a high area, it cannot conform immediately to the high area so that a higher pressure is on the high area. From this prospective, viscosity of pad improves the planarization efficiency.

The applied pressure by pad on the wafer surface depends on the topography of the wafer surface. Since pads are not perfectly rigid, they conform to the surface to a limited degree, but not exactly. As a result the pressure at each point varies, with protruding points receiving high pressure, and sunken or shadowed points receiving little or no pressure (Warnock 1991). Because of the flexibility of the pads, the resulting profiles depend on both the

stiffness of the pad as well as the density and spacing of elevated features on the wafer surface.

When the polishing rate is different for different materials and the pad is not perfectly rigid, dishing will happen, e.g., when CMP is done on metal for via formation on an oxide dielectric layer. Overpolish is required to remove all metallic residue on dielectric surface to ensure electrical isolation between adjacent circuits (Pan et al 1999). But metals generally polish faster than oxide in the metal polishing slurry. Due to the flexibility of the pad and the difference in polishing rates, this causes the metal in some places to removed below the top of the oxide layer. The shape of the resulting metal surface is curved and is called dishing. During dishing, the oxide layer is also slightly polished, especially at the edges, it is called erosion. Dishing and erosion are one of the major defects in metal CMP because the polished surface is actually not planarized and adds to the difficulties of following metallization processes.

To satisfy the different requirement for CMP, different kinds of pads have been developed. Some are for bulk polishing where removal rate is the major concern; others are for final finish where surface finish and defect reduction are major concerns. Cook (2000) classified pads into four kinds according to their structural characteristics:

- Felts and polymer impregnated felts (e.g., Suba IV)

Its structure is felted fiber with polymer binder and its micro structure is continuous channels between fibers. It is mainly used for Si stock polish and W damascene CMP.

- Microporous synthetic leathers

Its structure is high porosity film on substrate and its micro structure is complex foam with vertically oriented channels. It is mainly used for Si final polish, metal damascene CMP

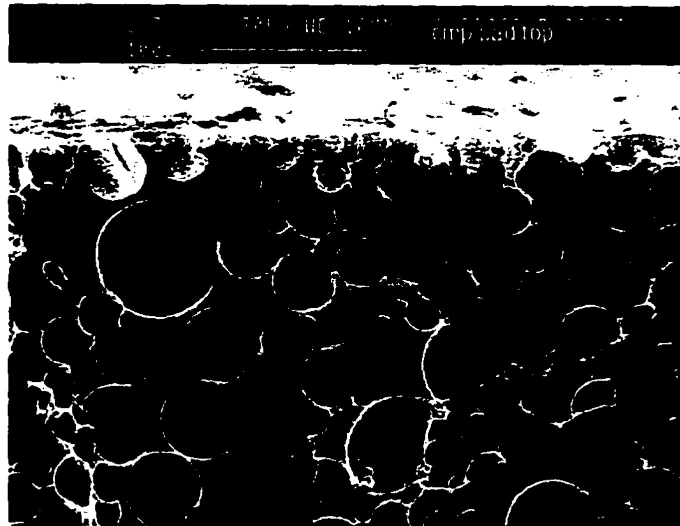

Fig. 1.5 SEM picture of IC 1000 pad (Borucki 2001)

and post-CMP buff.

- Filled polymer films (e.g., IC 1000 and IC 1400)

Its structure is solid urethane sheet with filler such as voids, SiO_2, CeO_2, etc and its micro structure is closed cell and open cell foam. It is mainly used for ILD CMP and metal damascene. Fig. 1.5 shows a SEM picture of IC 1000 pad and it is a closed cell polyurethane foam with voids that average about 30 microns in diameter (Borucki 2001).

- Unfilled textured polymer films

Its structure is solid polymer sheet with surface texture and it is mainly used for ILD CMP, Shallow Trench Isolation (STI) and metal dual damascene.

Pad manufacturing processes (e.g., felting, casting, laminating) will decide its micro-structure. The micro or macro structures of pad will influence the polishing result.

During CMP, pad surface is also planarized. Pad asperities are flattened by the abrasion of slurry particles and wafer surface. The abraded pad material, abrasive particles and redeposited wafer surface material are filling in the pad pores, causing glaze (Bajaj et al 1994,

Bibby and Holland 2000). Pad becomes smoother and less abrasive. The result is that the slurry cannot be effectively transported to the wafer surface and the removed material cannot be moved out of the system. Also, pad deformation due to its viscoelastic properties leads to bowl-shaped trench into the pad surface. It is very important to have pad treated to have reproducible and consistent polishing results.

To stabilize pad surface, pad conditioning is used to (Bibby and Holland 2000)

- bring the pad back to flat
- remove materials from the pores
- rebuild the nap

c. Carrier

Carrier is one of the most critical components in CMP tool designs and its functions are (Bibby and Holland 2000):

- to keep the wafer in certain kinematic motion while it is polished
- to provide a means (e.g., vacuum) to load and unload the wafer
- to prevent the wafer from becoming dislodged during the polishing by using a retainer ring
- to compensate for small amounts of wafer bow, tilt, or warp by using carrier film at the back of the wafer
- to load wafer in such a way that within wafer nonuniformity (WIWNU) can be minimized

There are mainly two kinds for carriers: gimbaled carrier and floating carrier (Bibby and Holland 2000).

(a) Gimbaled Carrier

It is used in the early stages of CMP tool design for its simplicity and is based on the

assumption that the applied force will be distributed uniformly across the wafer through the backing plate. However, the resulted WIWNU is not so good and the improvements are either on the redesign of back pressure or the use of curved carriers.

(b) Floating Carrier

Its goal is to apply more uniform pressure between the wafer and the pad through the use of hydraulic pressure. There are various forms of designs: one is that hydraulic pressure is applied to a flexible membrane on the wafer backing plate and the pressure applied to the retainer ring is adjusted separately from that of the carrier; another design uses concentric pistons with independent pressure control in each zone.

One of the biggest concerns in carrier head design is WIWNU. The goal is to obtain uniform pressure throughout the wafer-pad interface. The major hurdle is lack of a clear understanding of the interaction among pad, retainer ring and wafer.

1.3 Thesis Outline

The thesis is divided into six chapters. In Chapter 2, material removal mechanism is examined and material removal rate model is developed.

Chapter 3 is the basis for Chapter 4. It presents the analytical solution for Boussinesq's problem and the condition for its validity. It also gives the corresponding solution for viscoelastic half space.

Chapter 4 is about wafer scale nonuniformity issues, e.g., edge effect and polishing rate decay. Rigid wafer - elastic pad, rigid wafer - viscoelastic pad and deformable wafer - elastic pad are modeled to obtain the pressure distribution on the wafer surface. Models show

how the wafer shape, displacement and loading influence the within wafer noniformity and MRR rate decay.

Chapter 5 focused on modeling of dishing, erosion and step height reduction and shows how polishing conditions, slurry, pad and wafer surface topography influence the polishing results in the feature scale.

The conclusions as well as recommendations for future work are presented in chapter 6.

CHAPTER 2. MATERIAL REMOVAL MODEL

2.1 Literature Review

Early models of CMP has its roots in glass polishing, and material removal has been described by the Preston's equation (Preston 1927) as $dH/dt = C \cdot P \cdot V$ where, dH/dt is the average height removal per unit time, P is the pressure, V is the relative velocity between the pad and the wafer, and C is the Preston's coefficient. Preston's equation represents a phenomenological model without explanation about material removal mechanism.

Based on the understanding of CMP processes, researchers have modeled the material removal either as a hydrodynamic process or as an abrasion process. In a series of papers, Runnels (1994), Runnels and Eyman (1994) and Runnels (1996) have investigated the phenomenon of material removal based on the hydrodynamic model. They focus primarily on the effects of slurry flow and its associated fluid dynamics. Runnels and Eyman (1994) have used the steady-state incompressible Navier-Stokes equation to model the slurry flow at the wafer-pad interface. Their model is physically based, but is constructed on idealized geometry. The wafer surface is assumed to be smooth and spherical with a large radius of curvature, which imply that issues relating to the polishing mechanism is neglected. The fluid layer thickness and the angle of attack between the pad and the wafer are obtained through an iterative procedure satisfying force and momentum balance. Several researchers (e.g., Tichy et al 1999) have investigated the contact mechanics and lubrication hydrodynamics of CMP processes.

Runnels (1994) also proposes a modification to Preston's equation, where the relative velocity is replaced by the tangential stress at the wafer-pad interface. Runnels' modified

equation is expressed as $dH/dt = C' \cdot \sigma_n \cdot \sigma_t$ where, σ_n and σ_t represent local normal and the tangential stresses, respectively. The hydrodynamic model, is predicated on the existence of a continuous slurry film of around 60 μm in thickness. However, due to pad porosity and surface asperities, such a slurry film is almost certain to be interrupted by solid-solid contact (e.g., Levert et al 1998, Zhang and Busnaina 1998, Ouma 1998) because the hydrodynamic force is not likely to support the load. Based on these observations, it is speculated here that hydrodynamic lubrication is responsible for distributing the slurry, while majority of material removal occurs through abrasion by solid-solid contact.

Assuming solid-solid contact, various researchers have investigated the mechanical aspects of a free abrasive finishing process. Brown et al (1981) have developed a model based on elastic contact and they obtain a governing equation that displays the same linear dependencies of the removal rate with applied pressure and velocity, as that in the Preston's equation. They also deduce the Preston's coefficient to be $\frac{1}{2E}$, where E is the Young's modulus of the wafer surface. Cook (1990) has utilized Brown's model and investigated the chemical processes in glass polishing. Based on kinematics and elastic theory, Liu et al (1996) describe the wear mechanism of the silicon wafer surface during a CMP process. Their model can correlate the effects of mechanical properties of the slurry particles with the removal rate. This model is based on the assumption that the pressure on the abrasive particle is large enough to cause its rupture during the contact. Zhao and Shi (2000) have proposed a model of CMP based on elastic contact and soft pad response. They propose a dependence of $(\text{pressure})^{2/3}$ for the removal rate, and introduce the concept of a threshold pressure. These elastic contact models provide a valuable infrastructure, but they cannot accommodate many important effects due to slurry and pad properties.

Bulsara et al (1997) have developed a mechanistic model to determine the number and size of abrasive particles involved in material removal in a dry polishing process. They also determine the forces acting on these particles and simulate the effect of particle size on a variety of process parameters. When polishing with abrasives with a broad band of size distribution, they observe that only a very small percentage of the particles, usually larger ones, are actively involved in the polishing action. Samuels (1982) has observed that while the polishing force per particle is low and in itself insufficient to cause considerable elastic deformation, the force is transmitted to the surface through asperity contacts, and contact pressure at such region may approach the hardness of the work material, resulting in plastic deformation. Thus, it is of significant interest to deduce the magnitude and distribution of polishing forces and their dependence on various polishing parameters. Evans et al (1998) have attempted to investigate the effects of grit size and their concentration in lapping of brittle materials.

Yu et al (1993) have developed a statistical model to deal with the dependence of the removal rate on pad asperities. The contact properties: contact area, load and effective Young's modulus are assumed to follow the Hertzian distribution. Assuming spherical asperities and a normal distribution in variations in asperity height and radius, surface roughness of the polishing pad is characterized. Preston's equation is then utilized to predict polishing rates based on these asperity contacts.

Luo and Dornfeld (2001) develop a removal rate model based on plastic contact over wafer-abrasive and pad-abrasive interfaces. They consider the effects of particle size distribution and pad asperities. A wafer-abrasive-pad contact model is developed to investigate the abrasive size distribution influences on material removal rate. How the number of active abrasives and the size of them influence the material removal is also considered.

Expressing the removal rate as a linear function of both normal and shear stresses, Tseng and Wang (1997) have proposed a modification to the linear Preston's equation. Using the principles of elasticity and fluid mechanics, they have derived a model with $(\text{pressure})^{5/6}$ and $(\text{velocity})^{1/2}$ dependence on the removal rate.

2.2 Model Development

Motivated by the observations of excessive plasticity during glass polishing and the hydroxylated "mushy zone" at water-silica interfaces (Brown 1987), we assume that the leading edge of an abrasive particle in a CMP process is completely enveloped in a perfectly plastic solid of the wafer surface material. Workpiece material in the contact zone reaches its yield strength, and this stress supports the normal load and the tangential load on the abrasive particle. Because the "mushy zone" is solely observed at Si and wafer reaction region, the model is only valid for oxide CMP. Whether or not it can be used in metal CMP needs further investigation.

Following the procedure by Brown et al (1981), the total volume ΔV removed in abrasive motion Δs with cross section A_s by N particles can be expressed as,

$$\Delta V = NA_s\Delta s \tag{2.1}$$

The overall height reduction rate over an area A is,

$$\frac{\Delta V}{A\Delta t} = \frac{N}{A}A_s\frac{\Delta s}{\Delta t} \text{ or } \frac{dH}{dt} = \frac{N}{A}A_s\frac{ds}{dt} \tag{2.2}$$

In the model, the particles are assumed to be rigid (Tomozawa 1997), and two cases involving spherical particles and sharp particles are considered.

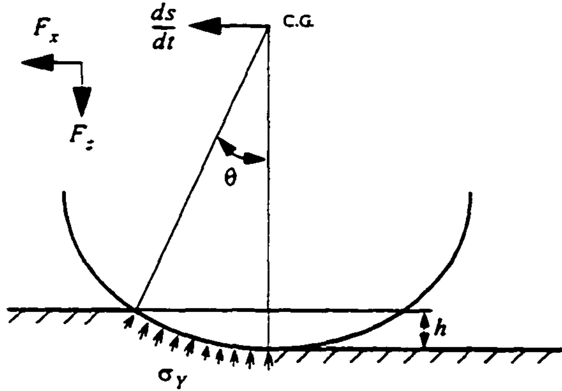

Fig. 1(a)

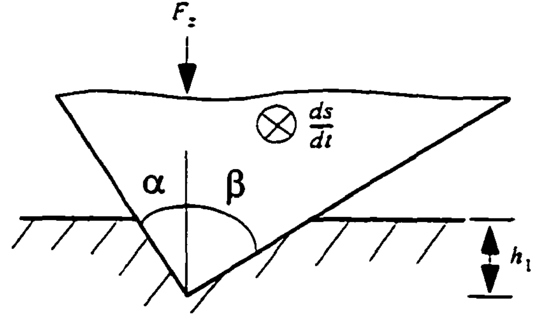

Fig. 1(b)

Fig 2.1 Schematic of particle contact (a) Spherical Particle, (b) Sharp Particle

2.2.1 Spherical Particles

Neglecting the pile-up before the abrasive particle during the plowing action, and assuming a spherical particle-workpiece interface, forces in the vertical direction on an individual abrasive particle (with radius R) can be expressed (referring to Fig. 2.1(a)) as,

$$F_z \sim \int_0^{\pi}\int_0^{\theta}\sigma_Y R^2 \sin\theta\cos\theta d\theta d\varphi \tag{2.3}$$

$$F_x \sim \int_0^{\pi}\int_0^{\theta}\sigma_Y R^2 \sin^2\theta\sin\varphi d\theta d\varphi \tag{2.4}$$

where θ is the angle of contact and σ_Y is the yield stress of the hydrolized wafer surface layer.

Assuming the angle of contact between the workpiece and the abrasive particle to be small, we have

$$F_z \sim \sigma_Y R h \tag{2.5}$$

$$F_x \sim \sigma_Y R^{\frac{1}{2}} h^{\frac{3}{2}} \tag{2.6}$$

For small particle indentation depth h, the radius of the contact impression a is,

$$a = \sqrt{R^2-(R-h)^2} = \sqrt{2Rh-h^2} \cong \sqrt{2Rh} \tag{2.7}$$

and the cross sectional area of contact A_s is,

$$A_s \cong \frac{2}{3}\cdot 2a\cdot h = \frac{4}{3}\sqrt{2}R^{\frac{1}{2}}h^{\frac{3}{2}} \tag{2.8}$$

Using the expression for force in the vertical direction (2.3), we have,

$$h \sim \frac{F_z}{\sigma_Y R} \tag{2.9}$$

and,

$$A_s \sim R^{\frac{1}{2}}\left(\frac{F_z}{\sigma_Y R}\right)^{\frac{3}{2}} \tag{2.10}$$

In the following model development, two regions of wafer-pad contact are considered: one is that wafer and pad do not touch each other; the other is that wafer and pad touch each other.

a. wafer and pad do not touch each other

The total area A is converted to a square of sides $\sqrt{A}$. As shown in Fig. 2.2, the abrasive particles are assumed to be distributed uniformly in a square grid on the wafer surface. The distance between the neighboring particles can written as, $l = \frac{\sqrt{A}}{\sqrt{N}-1}$. Noting $\sqrt{N} \gg 1$, we have

$$l = \sqrt{\frac{A}{N}} \tag{2.11}$$

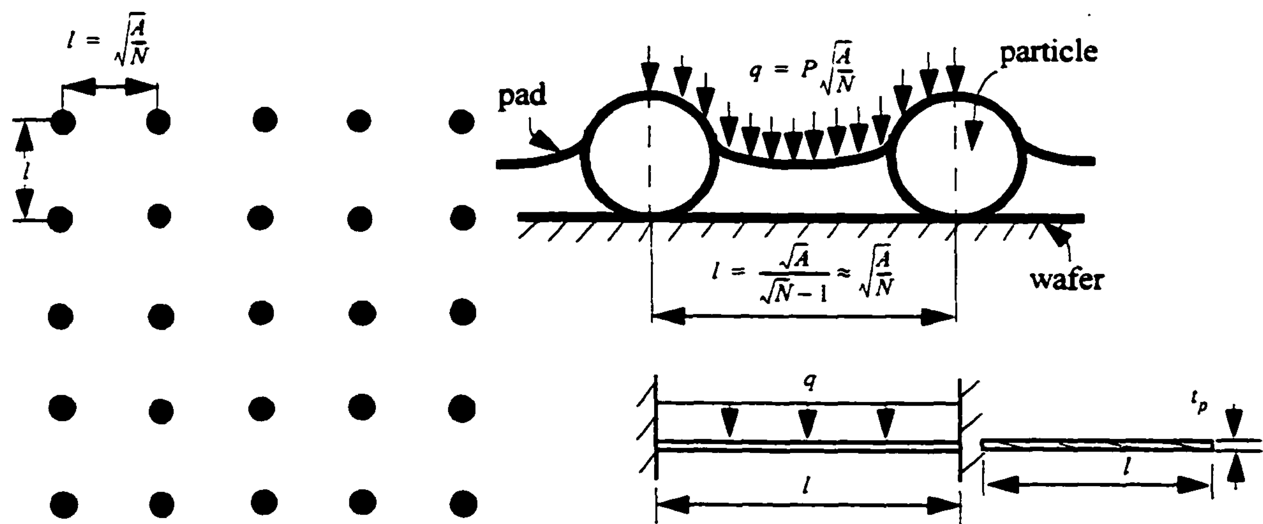

Fig. 2.2 Beam model for a span of the pad suspended between two abrasive particles

Pad is assumed to deform like a beam. The span of the pad between two abrasive particles l, is under uniform distributed load $q = P\sqrt{\frac{A}{N}}$. E_p and t_p represent, respectively, the Young's modulus and the thickness of the beam. For such a beam (w, w', w'' being the deflection, slope and curvature of the beam, respectively), the maximum deflection will occur at the mid-span,

$$w_{max} = w\left(\frac{l}{2}\right) = \frac{ql^4}{384E_pI} \tag{2.12}$$

Under the condition that pad and wafer don't touch each other, we have

$$w_{max} < 2R \tag{2.13}$$

Putting eqn. (2.9) and eqn. (2.10) into eqn. (2.11), we have,

$$\frac{P}{64E_pt_p^3} < \left(\frac{N}{A}\right)^2 R \tag{2.14}$$

as the necessary condition for the requirement that the pad and the wafer do not touch each other.

As shown in Fig. 2.2, for a relatively stiff pad and high abrasive concentration in the slurry, we assume that the pad and the wafer surface do not touch and the inequality in (2.14) is satisfied. In that case, the average pressure on the pad surface is $P = \frac{NF_z}{A}$, and we write,

$$A_s \sim R^{\frac{1}{2}}\left\{P \cdot \frac{A}{N} \cdot \frac{1}{\sigma_Y R}\right\}^{\frac{3}{2}} \tag{2.15}$$

Substituting eqn.(2.15) into eqn.(2.2), the average height reduction rate is,

$$\frac{dH}{dt} \sim \left(\frac{P}{\sigma_Y}\right)^{\frac{3}{2}} \cdot \left(\frac{A}{N}\right)^{\frac{1}{2}} \cdot \frac{1}{R} \cdot \frac{ds}{dt} \tag{2.16}$$

If both the pad and the wafer are rigid, for the same concentration of abrasive particles (in a monolayer) in the slurry, we have,

$$wt\% = \frac{\rho_{particle}V_{particle}}{\rho_{fluid}V_{fluid} + \rho_{particle}V_{particle}} = 1/\left[\frac{3}{2\pi} \cdot \left(\frac{\rho_{fluid}}{\rho_{particle}}\right) \cdot \frac{1}{R^2} \cdot \left(\frac{A}{N}\right) + \left(1 - \frac{\rho_{fluid}}{\rho_{particle}}\right)\right] = constant \tag{2.17}$$

Thus, for the extreme case involving rigid pad and wafer, and for same weight concentration of abrasive particles in the slurry, we get,

$$\frac{1}{R^2} \cdot \left(\frac{A}{N}\right) = const \tag{2.18}$$

Hence,

$$\frac{dH}{dt} \sim \frac{1}{(\sigma_Y)^{\frac{3}{2}}} \cdot P^{\frac{3}{2}} \cdot \frac{ds}{dt} \tag{2.19}$$

b. extended contact between the pad and the safer

From Fig. 2.3, pad and wafer will touch each other when the pad is soft enough, or when the abrasive concentration is low enough. For the same pad stiffness and abrasive concentration, reducing the abrasive size will also make the pad and the wafer touch each other. For such situations, the wafer and the pad surfaces will touch each other, and only a fraction of the total force is carried by the abrasives.

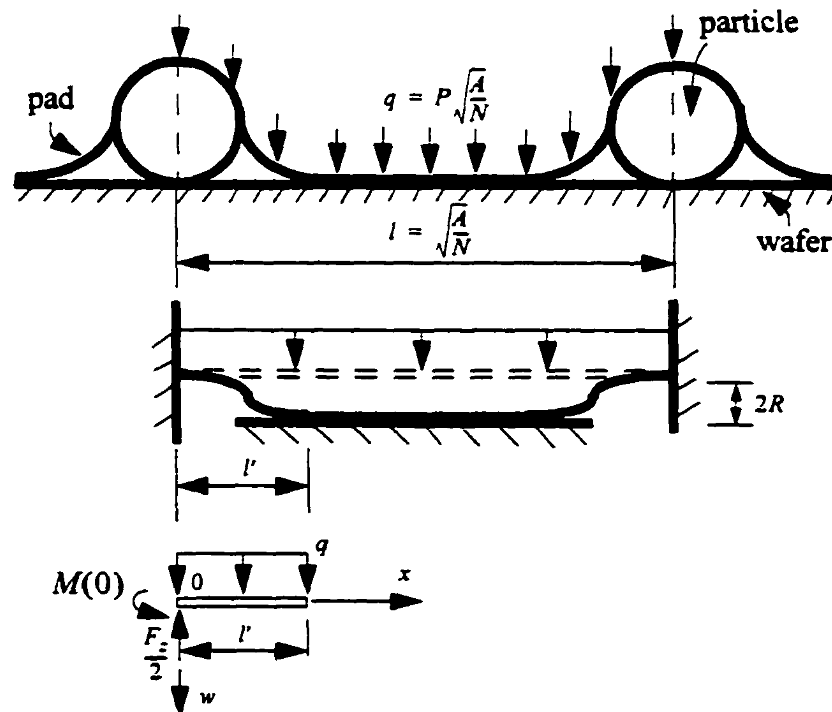

Fig. 2.3 Beam model for soft pad and low abrasive concentration

In this case, boundary conditions for the beam are:

$$w(0) = 0,\ w'(0) = 0,\ w(l') = 2R,\ w'(l') = 0 \text{ and } w''(l') = 0 \tag{2.20}$$

with the free span l' yet to be determined.

This yields

$$l' = \left(\frac{144RE_pI}{q}\right)^{\frac{1}{4}} \tag{2.21}$$

Force per particle is,

$$F_z = \frac{4}{3}q(l') = (4^5/3^3)^{1/4}\left[E_p t_p^3 R\left(\frac{A}{N}\right)^2 P^3\right]^{1/4} \tag{2.22}$$

The cross sectional area of contact A_s can be expressed as,

$$A_s \sim t_p^{9/8} \cdot \frac{1}{R^{5/8}} \cdot \left(\frac{A}{N}\right)^{3/4} \cdot \left(\frac{E_p P^3}{\sigma_Y^4}\right)^{3/8} \tag{2.23}$$

and utilizing equation (2.2), the removal rate is,

$$\frac{dH}{dt} = \frac{N}{A}A_s\frac{ds}{dt} \sim t_p^{\frac{9}{8}} \cdot \frac{1}{R^{\frac{5}{8}}} \cdot \left(\frac{N}{A}\right)^{\frac{1}{4}} \cdot \left(\frac{E_p P^3}{\sigma_Y^4}\right)^{\frac{3}{8}} \cdot \frac{ds}{dt} \tag{2.24}$$

2.2.2 Sharp particles

As shown in Fig. 2.1(b), the cross-sectional area of the trace due to the sharp particle plowing the wafer surface can be expressed as,

$$A_s = \frac{1}{2} \cdot h_1 \cdot (h_1 \cdot \tan\alpha + h_1 \cdot \tan\beta) = \frac{(\tan\alpha + \tan\beta)}{2} \cdot h_1^2 \sim h_1^2 \tag{2.25}$$

Using equ (2.2), we then have,

$$\frac{dH}{dt} = \frac{N}{A} \cdot A_s \cdot \frac{ds}{dt} \sim \frac{N}{A} \cdot h_1^2 \cdot \frac{ds}{dt} \tag{2.26}$$

Noting that for sharp particles $F_z \sim \sigma_Y \cdot h_1^2$, we have,

$$\frac{dH}{dt} \sim \frac{N}{A} \cdot h_1^2 \cdot \frac{ds}{dt} \sim \frac{N}{A} \cdot \frac{F_z}{\sigma_Y} \cdot \frac{ds}{dt} \tag{2.27}$$

Following the same procedure as for spherical particles, we consider two regions of wafer-pad contact:

a. wafer and pad do not touch each other

For situations involving a relatively stiff pad, and high abrasive concentration, the pad section suspended between abrasive particles cannot deform enough to make contact with the wafer surface. In such cases,

$$\frac{dH}{dt} \sim \frac{N}{A} \cdot \frac{F_z}{\sigma_Y} \cdot \frac{ds}{dt} = \frac{1}{\sigma_Y} \cdot \frac{NF_z}{A} \cdot \frac{ds}{dt} = \frac{1}{\sigma_Y} \cdot P \cdot \frac{ds}{dt} \tag{2.28}$$

The load is transferred from the pad to the wafer surface only by the abrasives and only limited deformation of the pad is permitted.

b. extended contact between the pad and the wafer

Assuming R' to be the equivalent size of the sharp particles, the height reduction rate in this regime can be written as,

$$\frac{dH}{dt} \sim \frac{N}{A} \cdot \frac{F_z}{\sigma_Y} \cdot \frac{ds}{dt} \sim \frac{1}{\sigma_Y} \cdot \frac{N}{A} \cdot \left[(E_{pad} t_{pad}^3) \cdot R' \cdot \left(\frac{A}{N}\right)^2 \cdot P^3 \right]^{\frac{1}{4}} \cdot \frac{ds}{dt} \sim \frac{1}{\sigma_Y} \cdot (E_{pad} t_{pad}^3)^{\frac{1}{4}} \cdot \left(\frac{N}{A}\right)^{\frac{1}{2}} \cdot R'^{\frac{1}{4}} \cdot P^{\frac{3}{4}} \cdot \frac{ds}{dt} \tag{2.29}$$

2.3 Comparison with Experimental Data

In this section, model predictions are compared against existing experimental observations in two phases. To verify the assumption of plastic flow at the particle - wafer contact region, model predictions are first compared with existing experimental observations from nano-indentation tests. Model predictions are also compared to experimental observations in CMP by fitting a single data point for each experimental observation.

a. Comparisons to Nano-indentation Tests

The experimental data for TiN film on High Speed Steel (Lichinchi et al 1998) and

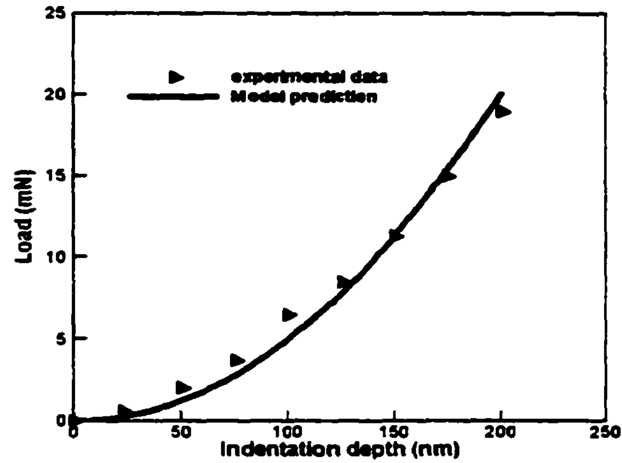

Fig 2.4 Comparison of model predictions with experimental data (Lichinchi et al 1998) for TiN film on HSS

diamond-like carbon (DLC) film over Silicon (Knapp et al 1998) are considered here. Fig. 2.4 shows the comparison of model predictions with the experimental data of Lichinchi et al (1998), and Fig. 2.5 shows the comparisons against the experimental data of Knapp et al (1998). The comparisons involve a fitting parameter obtained by fitting the model prediction ($F_z = 24.56\sigma_Y h^2$) to a single data point. This is equivalent to choosing the yield stress to be 20.4 GPa for the TiN film, and 36.2 GPa for the DLC film. It may be observed that in both

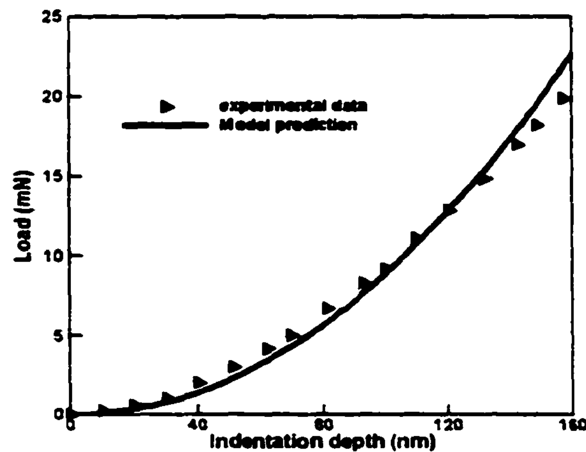

Fig 2.5 Comparison of model predictions with experimental data (Knapp et al 1998) for DLC film on Si

instances the model reliably depicts the trend in the experimental observations. This lends credibility to the assumption that there exists plastic deformation during nano-indentation of TiN and DLC films.

b. Comparisons Against CMP Experimental Data

The first set of experimental CMP data is taken from Ouma (1998). These tests were

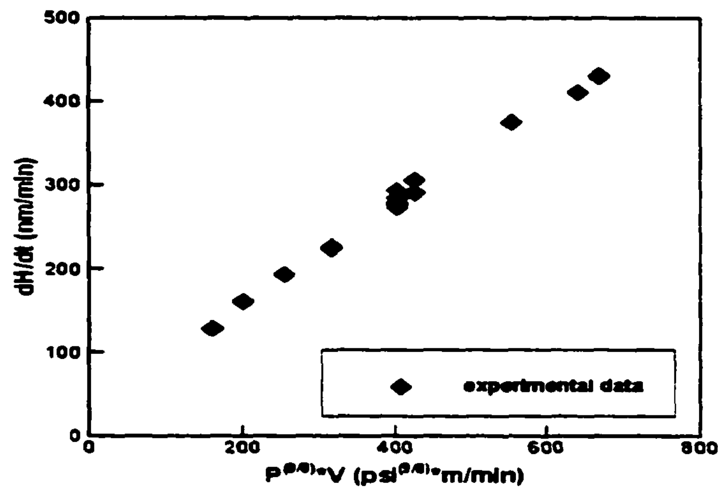

(a) Spherical abrasive particles

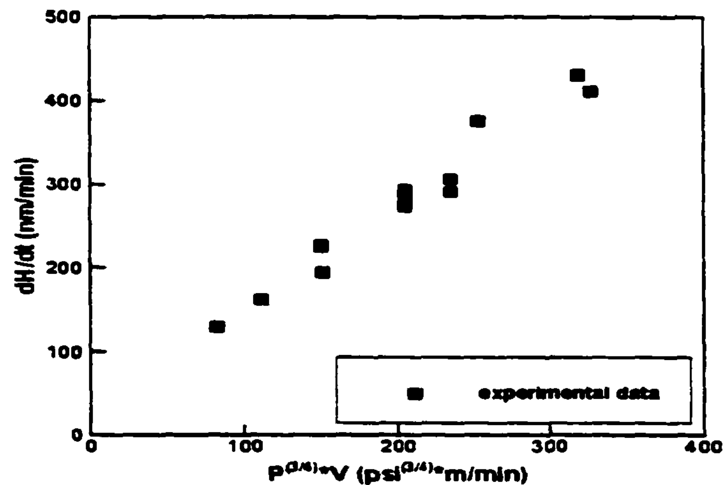

(b) Sharp abrasive particles

Fig 2.6 Comparison of model predictions to experimental observation for IC 1000 pad (Ouma 1998)

carried out on Avante^{TM} 472 polisher (IPEC Planar/Westech) at pressures of 4.8 - 7.2 psi (33.1 - 49.6 Pa), and table speeds of 20 - 80 rpm with an offset of 170 mm. Two different pad set-ups, one using an IC 1400 pad (K-grooved), and the other one using an IC 1000 (K-

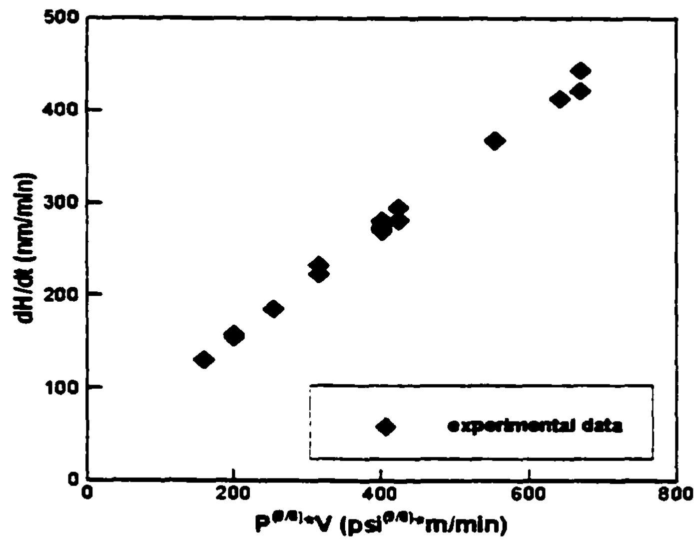

(a) Spherical abrasive particles

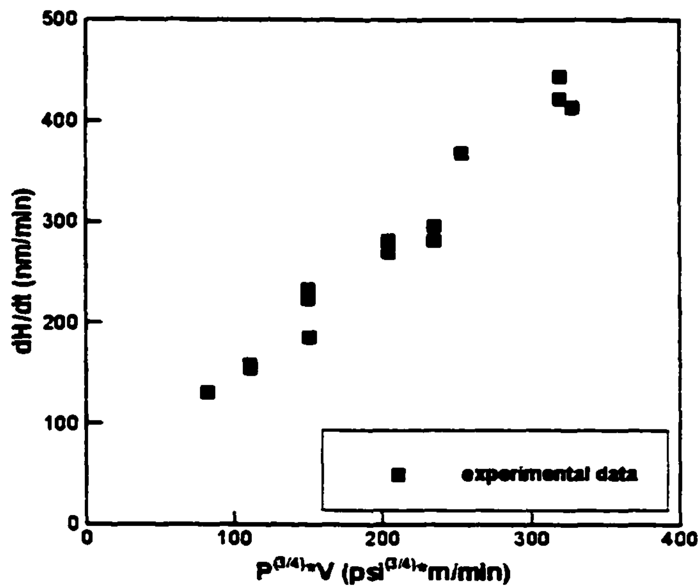

(b) Sharp abrasive particles

Fig 2.7 Comparison of model predictions to experimental observation for IC 1400 pad (Ouma 1998)

grooved) upper pad stacked on Suba IV lower pad, were used. A commercial slurry SS25 from Cabot Corp. was used at a flow rate of 900 ml/min. The polished material was LPCVD-TEOS (tetraethyl orthosilicate) on 200 mm wafer. Figs 2.6(a) and 2.7(a) show the correlations between model predictions (soft pad - low abrasive concentration regime) of MRR (material removal rate) for spherical particles, while the comparisons for sharp particles are shown in Figs 2.6(b) and 2.7(b). First, we assume that all abrasive particles are blunt (or spherical). It is observed that the experimental data fits the $P^{9/8}V$ dependence for spherical particles in the soft pad - low abrasive concentration regime very well. Next, all abrasive particles are assumed to be sharp. The experimental data also fits the $P^{3/4}V$ dependence for sharp particles reasonably well. More scatter is observed in this case. However, in both instances, the intercept on the ordinate, at zero pressure and velocity, is positive and very small. It should also be noted that in real life CMP, some of the abrasive particles may be sharp, while others may be spherical. Thus, the best fit to the experimental data may be a trend that is intermediate between $P^{9/8}V$ and $P^{3/4}V$.

The second set of experimental data is obtained from glass polishing experiments of

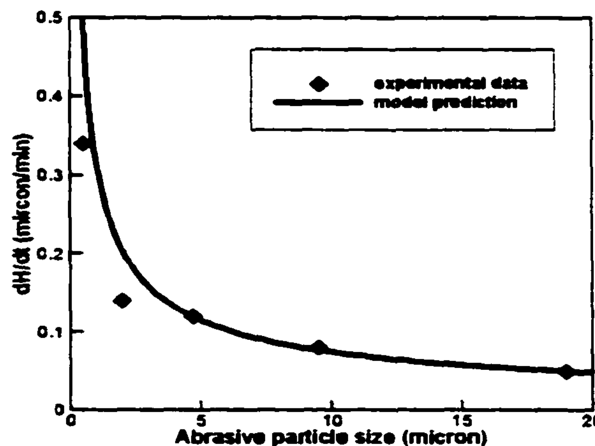

Fig. 2.8 Comparison of model prediction for spherical particles with experimental data (Izumitani 1979)

Izumitani (1979). Izumitani reports variations of MRR with abrasive particle size and concentration. Fig. 2.8 shows the correlation between model prediction (for spherical particles) and the experimental observations of Izumitani (1979) when abrasive particle (α-alumina) size is varied from 0.5 μm to 19 μm. Izumitani observed the MRR to increase considerably as the particle size is reduced, which is consistent with our model predictions for spherical particles. Fig. 2.9 shows the comparison of model predictions with the experimental data of Bielman et al (1999) on tungsten CMP. It is observed from the micrographs by Bielman et al (1999), that the abrasive particles are spherical in this case. Accordingly, as expected, MRR decreases with increasing particle size. This trend compares very well to our model predictions when wafer-pad contacts are included. This may be due to the fact that a soft pad, and relatively low abrasive concentration have been used in the experiments, resulting in direct wafer-pad contacts. From experimental data, Bielman et al (1999) estimate a slope between -0.52 and -0.76 for the log(MRR) vs. log(particle size) plot. Our model predicts a slope of -0.625 for the same plot.

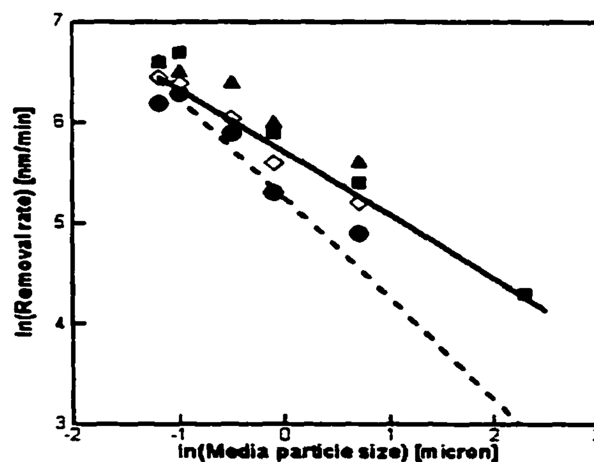

Fig. 2.9 Comparison of model prediction for spherical particles with experimental data (Bielman et al 1999): solid line is model prediction for wafer-pad contact; dashed line is model prediction for no wafer-pad contact.

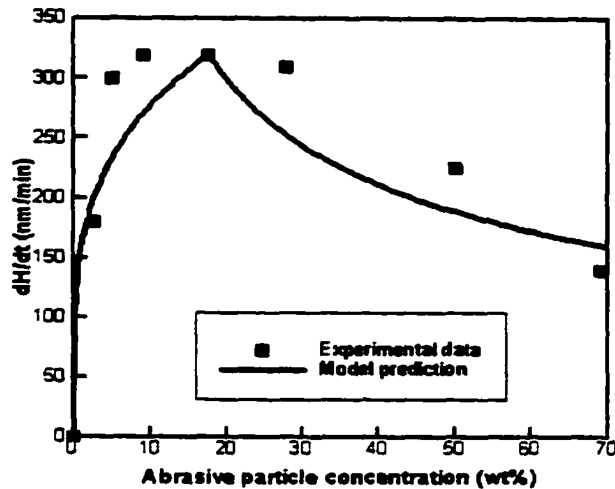

Fig. 2.10 Comparison of model prediction for spherical particles with experimental data (Izumitani 1979)

Fig. 2.10 shows the variation in MRR with abrasive concentration while polishing BK7 glass with cerium oxide. Izumitani has observed that the MRR initially increases as cerium oxide concentration (wt%) is increased from zero to 30%, and steadily decreases to about one-third of the maximum polishing rate as the cerium oxide concentration is increased from 30 to 70%. A similar trend is also observed from model predictions for spherical particles. At the low abrasive concentration regime, MRR increases with abrasive concentration, while at the high abrasive concentration regime, MRR decreases with increasing abrasive concentration.

The next set of experimental data is obtained from CMP tests of Luo et al (1998). While doing CMP on copper with 300 nm α-alumina abrasives in 0.005 M BTA, 0.1 M $Fe(NO_3)_3$ slurry, they have observed a monotonous increase in MRR as abrasive concentration is increased from 1%-8% by weight. Fig. 2.11 shows the correlation between model predictions for sharp particles, and the experimental observations. It may be observed that the proposed plasticity based model reliably depict the experimental trend.

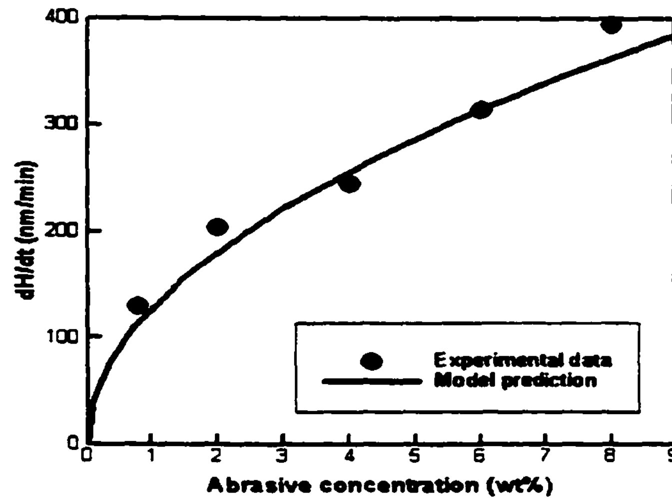

Fig. 2.11 Comparison of model prediction for sharp particles with experimental data (Luo et al 1998)

The last set of experimental data is obtained by Evans et al (1998) using rapidly renewable lapping of nickel-phosphorus with an overarm polisher (10 pores/cm SiC Rapidly Renewable Lap, Mylar film, water-based slurries, 0.9 g/mm2 pressure, 35 rpm spindle speed, 10 strokes/min arm speed). As abrasive size is increased from 3 μm to 25 μm, the MRR was observed to rapidly increase at the beginning as abrasive size was increased to 6 micron. With

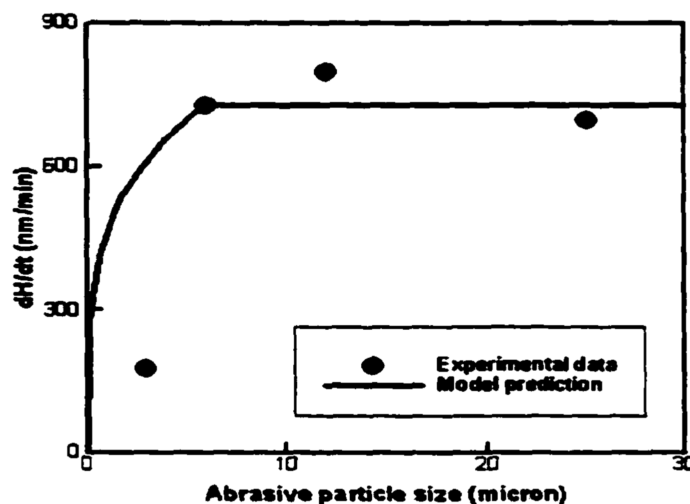

Fig. 2.12 Comparison of model prediction for sharp particles with experimental data (Evans et al 1998)

further increase in abrasive size, the MRR was observed to hold constant. Assuming that the transition from extended contact between pad and wafer, to no contact between pad and wafer occurs at around 6 micron abrasive size, the model predictions for sharp particles also correlate well to these experimental observations as shown in Fig. 2.12.

2.4 Summary

The presented model assumes onset of plastic deformation as the hydroxilated softer layer at the wafer surface is abraded by the abrasive particle. Based on the assumption of perfectly plastic contact between abrasive particles and the wafer surface layer, a mechanistic description of material removal is developed. Thus, the present model is applicable to oxide CMP. Nano-indentation tests on metals (e.g., copper and aluminum) show significant plastic deformation at the indenter - workpiece interface. Hence, the present assumption of plastic contact is also reasonable for metal CMP.

Depending on processing conditions and the Consumables used, two distinct regimes of material removal rate (MRR) during a CMP process are identified. The first regime is valid for relatively stiff pad and high abrasive concentration, when the pad and the wafer will not touch each other and all of the load is transferred through the abrasive. The second regime depicts relatively soft pad and low abrasive concentration, when extended contact between pad and wafer is possible, and part of the load is carried through wafer-pad contact. The present work identifies these two distinct regimes, and appropriate MRR models are developed in each of these regimes. A condition for transition from one regime to the other is also derived.

The proposed model facilitates understanding of the MRR variations with respect to slurry and pad properties. It is observed from the investigations, that various parameters, e.g., pressure, relative velocity, slurry properties (abrasive shape, size and concentration), as well as pad stiffness influence the MRR very differently in these two distinct regimes. The shape of the abrasive, whether sharp or spherical (blunt), distinctly influences the MRR, and alters the nature of variations in MRR with respect to various design parameters. As expected, the yield strength of the hydroxylated interface layer also influences the MRR, and the nature of dependence on yield strength (or wet nano-hardness) also changes with particle shape and the operative regime (depending on whether pad and wafer touch each other) of CMP operations.

It is observed, that in the soft pad - low abrasive concentration regime (which is typical in CMP) MRR varies as $P^{9/8}V$ for spherical particles, but as $P^{3/4}V$ for sharp particles. These do not represent significant departure from the Preston model and the traditional PV representation of MRR. In reality, a slurry may consist of a mixture of sharp and blunt particles. Thus, the Preston model may also hold true for a particular proportion of sharp and blunt particles. When the pad and the wafer do not touch each other, which is the case not only for stiff pads and high abrasive concentrations, but also for soft pads under very low pressures, the plasticity based model for sharp particles yields the same PV relationship for the MRR. Thus, Preston's phenomenological description may also be operative for sharp particles under very low pressures.

The proposed model also allows investigation of MRR variations with respect to pad (stiffness) and slurry properties (abrasive shape, size and concentration). Thus, it can facilitate exploration of an expanded design space for CMP processes. For spherical particles, the

model prediction of decreasing MRR with increasing particle size matches well with experimental observations of Izumitani (1979) on glass polishing. It is also consistent with the observations of Bielman et al (1999) on CMP of tungsten with alumina abrasives. As abrasive concentration is increased, the MRR first increases, reaches saturation, and then decreases, which are similar trends to those observed experimentally by Izumitani (1979). For sharp particles, the MRR is found to be independent of particle size and concentration in the stiff pad and high abrasive concentration regime, while the MRR increases with both particle size and concentration in the soft pad and low abrasive concentration regime. These are consistent with experimental observations of Luo et al (1998) and Evans et al (1998). For both sharp and spherical particles, the MRR is found to be independent of pad properties if the pad and the wafer do not touch. When the pad and wafer touch each other (soft pad - low abrasive concentration regime), higher pad stiffness leads to higher MRR.

CMP typically uses soft pads, and it is generally believed that there is extended pad-wafer contact in a CMP process. Thus, in addition to abrasive-wafer contact, part of the load is transferred through pad-wafer contact. It has been observed in the present work, that model predictions fit the experimental data well when extended pad-wafer contact is assumed. Model also provides a condition for transition from no pad-wafer contact to extended pad-wafer contact. It may be observed that (for a given CMP process) at pressures below a critical threshold, there will be no pad-wafer contact. This may explain the apparent nonlinearity that is observed in a CMP process at very low pressures.

Like many of its predecessors, the present model also assumes that the complete volume of material in the track of an abrasive particle is removed in a single pass. In nano-plowing tests, pile-up of workpiece material is observed, and it may be inferred that the material is

separated (or removed) from the workpiece surface only after a number of such passes (similar to fatigue wear).

CHAPTER 3. BOUSSINESQ'S PROBLEM

To construct a mechanistic model of the contact between a wafer and a soft pad, the contact of a simply-connected axisymmetric punch with an elastic half space is examined. The problem is mathematically formulated by using potential theory and complex variable analysis. The final solution of these equations is obtained by assuming a polynomial punch profile. The conditions for complete contact and incomplete contact are also derived. The solutions give the pressure profile at the punch - elastic half space interface for any polynomial punch profile, even for non-integer power polynomials, as long as the contact region is simply-connected. The results show that some classic solutions in linear elasticity are special cases of the derived solution and determine the range of validity for those solutions. The corresponding solution for the indentation of a visoelastic half space is also derived through Laplace transform and elastic-visoelastic analogy. These solutions will be used extensively in Chapter 4 for wafer scale nonuniformity model.

3.1 Literature Review

Contact pressure distribution between two surfaces has always been of great interest to engineers. Perhaps the most widely used equation for bearing application is Hertz's solution. Boussinesq solution for flat-ended punch finds its application in the safety evaluation of foundations in civil engineering (Sneddon 1946). Researchers used Love and Sneddon solution for conical punch to explain nanoindentation experimental data (e.g., Hay et al 1999). In Elastic Emission Machining (EEM), the material is removed through the atomic scale elastic fracture without plastic deformation (Komanduri 1997). Indentation model for different particle shape

is needed to investigate this process. Shield and Bogy (1989) investigated the indentation of a flat-ended punch into layered elastic half space. The solution may be used in the evaluation of protective coating to prevent the substrate from wear under sliding contact.

When a rigid axisymmetric punch indents normally into an elastic half space, there are two possibilities: one is that the whole punch surface contacts with the half space; the other is that only part of the punch contacts with the half space. Following the terminology by Gladwell (1980), the first contact is called complete or bonded, and the second one is termed incomplete or unbonded. In the second case, the contact pressure will drop to zero at the boundary of the contact region. Complete contact can be classified further into critical complete contact and general complete contact. In general complete contact, pressure at the punch edge goes to infinity; in critical complete contact, pressure drops to zero at the punch edge and the pressure profile is similar to that of incomplete contact.

The axisymmetric solutions for a punch whose shape is flat-ended, conical or parabolic have been known for years. Hertz found the solution for the parabolic punch in 1882 when he investigated the pattern of interference fringes between glass lenses (e.g., Johnson 1985). His solution is only valid when the contact is incomplete. Bousinessq obtained the pressure distribution for a flat-ended punch in 1885 and found the square root singularity at the punch edge (e.g., Johnson 1985). To solve conical punch problem, Love (1939) used potential theory and Sneddon (1948) used integral transform method to get the same result. They found that there exists a logarithmetic singularity at the conical tip, and their solutions are also for incomplete contact. For circular annular punch problem, Collins (1963) used potential theory and superposition method to obtain the solution.

Popov (1962) shows: If a normal pressure distribution on the plane $z = 0$ over a circular area with radius a has a square-root singularity at the edge and is in the form $P_{2n}[(1-r^2/a^2)^{1/2}]/(1-r^2/a^2)^{1/2}$ ($P_n(x)$ is Legendre polynomial), then the vertical displacement on the plane $z = 0$ over the circular area will be proportional to $P_{2n}[(1-r^2/a^2)^{1/2}]$, which is an even polynomial.

In this chapter, we consider a rigid frictionless axisymmetric punch with a polynomial profile and axis of revolution as z-axis, indenting normally into the plane $z = 0$ of a half space $z \geq 0$. The problem is considered in linear theory of elasticity and the half space is assumed to be isotropic and homogeneous. The punch is assumed to be rigid with sharp corners, which may lead to singularities in the contact pressure at those corners. The problem is solved by using potential theory and complex variable analysis. Green's solution (1954) is utilized and with the aid of mathematical software MATHEMATICA (Wolfram 1991), the final solution is obtained. Also, the conditions for the complete and incomplete contacts are derived. The solutions give the pressure profile at the punch - elastic half space interface for any polynomial punch profile, even for non-integer power polynomials so long as the contact region remains simply-connected. As special cases of the obtained solution, we show the results for five kinds of punches: flat-ended punch, square-root punch, conical punch, three-half power punch and parabolic punch. The force-displacement curves are also shown for these five punches.

The corresponding viscoelastic solution is quite straightforward if the contact area is fixed. Generally, after Laplace transform, elastic-viscoelastic analogy is applied and through inverse Laplace transform, the final viscoelastic solution is obtained (Christensen 1982). As special cases of the solution, we show the results for constant load and constant displacement

for a flat-ended punch and a parabolic punch.

3.2 Theoretical Derivation

3.2.1 Elastic half space

The following equations give the relevant displacement and stresses in terms of an unknown harmonic potential function $\phi(r, z)$. The vertical component of the displacement is denoted by u_z, and the stress components have two subscripts corresponding to the appropriate coordinates. E and ν are Young's Modulus and Poisson's ratio for the elastic half space.

$$\frac{E}{1+\nu}u_z = z\frac{\partial^2\phi}{\partial z^2} - 2(1-\nu)\frac{\partial\phi}{\partial z} \tag{3.1}$$

$$\tau_{zx} = z\frac{\partial^3\phi}{\partial x\partial z^2} \tag{3.2}$$

$$\tau_{zy} = z\frac{\partial^3\phi}{\partial y\partial z^2} \tag{3.3}$$

$$\sigma_{zz} = z\frac{\partial^3\phi}{\partial z^3} - \frac{\partial^2\phi}{\partial z^2} \tag{3.4}$$

Assuming that various limits exist as $z \to 0$, on the plane $z = 0$, we have,

$$\frac{E}{1+\nu}u_z = -2(1-\nu)\frac{\partial\phi}{\partial z} \tag{3.5}$$

$$\tau_{zx} = \tau_{zy} = 0 \tag{3.6}$$

$$\sigma_{zz} = -\frac{\partial^2\phi}{\partial z^2} \tag{3.7}$$

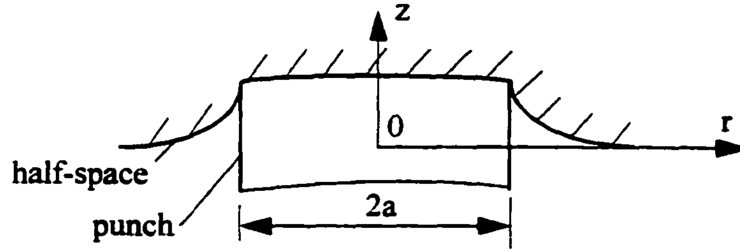

Fig. 3.1 Normal indentation of an elastic half space

As Fig. 3.1 shows, the boundary conditions for the indentation problem are:

$$\tau_{zr} = \tau_{z\theta} = 0, (0 \le r < \infty) \tag{3.8}$$

$$\sigma_{zz} = 0, (r > a) \tag{3.9}$$

and, $u_z = f(r), (0 \le r \le a)$ (3.10)

where $f(r)$ is the final position of the punch.

This boundary value problem can be changed into the following equivalent potential theory problem (Green and Zerna 1954):

$$\frac{\partial\omega}{\partial z} = 0, (r > a) \tag{3.11}$$

$$\omega = f(r), (0 \le r \le a) \tag{3.12}$$

where $\omega(r,z) = \frac{2(1-v^2)}{E}\frac{\partial\phi}{\partial z}$, $\nabla^2\omega = 0$ (3.13)

The normal stress under the punch is $\sigma_{zz}|_{z=0} = \frac{1}{2}\cdot\frac{E}{1-v^2}\cdot\frac{\partial\omega}{\partial z}\Big|_{z=0}$ (3.14)

Green (1954) considers the following potential function for ω, which can be obtained through Fourier cosine transform (Gladwell 1980):

$$\omega(r,z) = \frac{1}{2}\int_0^a \frac{g(t)dt}{\sqrt{r^2+(z+it)^2}} + \frac{1}{2}\int_0^a \frac{g(t)dt}{\sqrt{r^2+(z-it)^2}} \tag{3.15}$$

Green (1954) found that if $f(r)$ is continuously differentiable in $0 \le r \le a$, then

$$g(t) = \frac{2}{\pi}\frac{d}{dt}\int_0^t \frac{rf(r)}{\sqrt{t^2-r^2}}dr \tag{3.16}$$

His further derivation leads to

$$\sigma_{zz}\big|_{z=0} = \frac{1}{2}\cdot\frac{E}{1-\nu^2}\cdot\frac{1}{r}\cdot\frac{\partial}{\partial r}\int_r^a \frac{tg(t)}{\sqrt{t^2-r^2}}tdt,\ (0 \le r \le a) \tag{3.17}$$

Until now, the above equation has only been utilized to solve the pressure distribution for a flat-ended punch. The present work will derive the solution for punches with general polynomial profiles.

We express the displacement field under the punch as a polynomial:

$$f(r) = \sum_{\alpha=0}^{\alpha_n} a_\alpha r^\alpha,\ (\alpha = 0, \alpha_1, \alpha_2, \ldots, \alpha_n \text{ and } \alpha \ge 0) \tag{3.18}$$

where the function $\sum_{\alpha=\alpha_1}^{\alpha_n} a_\alpha r^\alpha$ describes the shape of the punch, a_0 describes the depth of indentation and is non-negative, and α is not necessarily an integer.

a. The Solution When α is not an Integer but is a Positive Real Number

In this case, the symbolic manipulation program MATHEMATICA (Wolfram 1991) is utilized and the identities used in the derivation are:

$$\int_0^t \frac{r^{1+k}}{\sqrt{t^2-r^2}}dr = \frac{\sqrt{\pi}}{2}\cdot\frac{\Gamma\left(\frac{2+k}{2}\right)}{\Gamma\left(\frac{3+k}{2}\right)}t^{1+k} \tag{3.19}$$

$$\int_r^a \frac{t^{1-k}}{\sqrt{t^2-r^2}}dt = \frac{\sqrt{\pi}}{2}\cdot\frac{\Gamma\left(-\frac{1+k}{2}\right)}{\Gamma\left(-\frac{k}{2}\right)}r^{1-k} + \frac{a^{1+k}}{1+k}\cdot {}_2F_1\left(\frac{1}{2}, \frac{1+k}{2}; \frac{1-k}{2}; \frac{r^2}{a^2}\right) \tag{3.20}$$

$$\frac{\partial}{\partial r}\left[{}_2F_1\left(\frac{1}{2},-\frac{1+k}{2};\frac{1-k}{2};\frac{r^2}{a^2}\right)\right] = -\frac{1+k}{r}\left[\frac{1}{\sqrt{1-\frac{r^2}{a^2}}} - {}_2F_1\left(\frac{1}{2},-\frac{1+k}{2};\frac{1-k}{2};\frac{r^2}{a^2}\right)\right] \tag{3.21}$$

From those identities and eqn. (3.15) and eqn. (3.16), We have

$$\sigma_{zz}\big|_{z=0} = \frac{1}{2\sqrt{\pi}}\cdot\frac{E}{1-\nu^2}\sum_{\alpha=0}^{\alpha_n} a_\alpha(1+\alpha)\cdot\frac{\Gamma\left(\frac{2+\alpha}{2}\right)}{\Gamma\left(\frac{3+\alpha}{2}\right)}\Phi(r,\alpha) \tag{3.22}$$

where $\Phi(r,\alpha) = \frac{\sqrt{\pi}}{2}\cdot(1+\alpha)\cdot\frac{\Gamma\left(-\frac{1+\alpha}{2}\right)}{\Gamma\left(-\frac{\alpha}{2}\right)}r^{-1+\alpha} - \frac{a^{1+\alpha}}{r^2}\left[\frac{1}{\sqrt{1-\frac{r^2}{a^2}}} - {}_2F_1\left(\frac{1}{2},-\frac{1+\alpha}{2};\frac{1-\alpha}{2};\frac{r^2}{a^2}\right)\right]$ (3.23)

and ${}_2F_1(a,b;c;z) = \sum_{n=0}^{\infty}\frac{(a)_n(b)_n}{(c)_n}\cdot\frac{z^n}{n!}$.

b. The Solution When α is Zero or a Positive Even Integer

Noting $\Gamma(-\alpha/2) = \infty$ and from eqn. (3.22), we have

$$\sigma_{zz}\big|_{z=0} = \frac{1}{2\sqrt{\pi}}\cdot\frac{E}{1-\nu^2}\sum_{\alpha=0}^{\alpha_n} a_\alpha(1+\alpha)\cdot\frac{\Gamma\left(\frac{2+\alpha}{2}\right)}{\Gamma\left(\frac{3+\alpha}{2}\right)}\Phi(r,\alpha) \tag{3.24}$$

where $\Phi(r,\alpha) = -\frac{a^{1+\alpha}}{r^2}\left[\frac{1}{\sqrt{1-\frac{r^2}{a^2}}} - {}_2F_1\left(\frac{1}{2},-\frac{1+\alpha}{2};\frac{1-\alpha}{2};\frac{r^2}{a^2}\right)\right]$ (3.25)

In this case, $\Phi(r,\alpha)$ can also be expressed by elementary functions. The original format for $\Phi(r,\alpha)$ is

$$\Phi(r,\alpha) = \frac{1+\alpha}{r^2}\int_r^a\frac{t^{1+\alpha}}{\sqrt{t^2-r^2}}dt - \frac{a^{1+\alpha}}{r^2}\frac{1}{\sqrt{1-\frac{r^2}{a^2}}} \tag{3.26}$$

Letting $\alpha = 2m$ $(m = 0, 1, 2, \ldots)$, we have $\int_r^\rho \frac{t^{1+\alpha}}{\sqrt{t^2-r^2}}dt = \int_r^\rho \frac{t^{1+2m}}{\sqrt{t^2-r^2}}dt$ (3.27)

Letting $t = r\sec\theta$, we have

$$\int_r^\rho \frac{t^{1+2m}}{\sqrt{t^2-r^2}}dt = r^{2m+1}\sum_{i=0}^{m}\frac{\Gamma(m+1)}{\Gamma(m+1-i)\Gamma(i+1)}\cdot\frac{\left(\frac{\sqrt{a^2-r^2}}{r}\right)^{2i+1}}{2i+1} \tag{3.28}$$

Thus,

$$\Phi(r,\alpha) = (1+\alpha)r^{\alpha-1}\left[\sum_{i=0}^{\frac{\alpha}{2}}\frac{\Gamma\left(\frac{\alpha}{2}+1\right)}{\Gamma\left(\frac{\alpha}{2}+1-i\right)\Gamma(i+1)}\cdot\frac{\left(\frac{\sqrt{a^2-r^2}}{r}\right)^{2i+1}}{2i+1}\right]-\frac{a^{1+\alpha}}{r^2}\frac{1}{\sqrt{1-\frac{r^2}{a^2}}} \tag{3.29}$$

c. The Solution When α is a Positive Odd Integer

Noting in this case, eqn. (3.23) becomes $\Phi(r,\alpha) = \infty - \infty$ and its limit is difficult to obtain. A new formulation has to be derived. Starting from eqn. (3.26).

Letting $\alpha = 2m+1$ $(m = 0, 1, 2, \ldots)$, we have $\int_r^\rho \frac{t^{1-\alpha}}{\sqrt{t^2-r^2}}dt = \int_r^\rho \frac{t^{2-2m}}{\sqrt{t^2-r^2}}dt$ (3.30)

Letting $t = r\sec\theta$, we have $\int_r^\rho \frac{t^{2-2m}}{\sqrt{t^2-r^2}}dt = r^{2m-2}\sum_{i=0}^{m-1}\frac{\Gamma(m+2)}{\Gamma(m+2-i)\Gamma(i+1)}I_i(r)$ (3.31)

Where $I_i(r) = \int_0^{\cos^{-1}\frac{r}{a}}\tan^{2i}\theta\sec\theta d\theta$ $(i = 0, 1, 2\ldots)$ (3.32)

There is a recurrence relationship for the function $I_i(r)$:

$$I_i = \frac{1}{2i}\cdot\frac{a}{r}\cdot\left(\frac{\sqrt{a^2-r^2}}{r}\right)^{2i-1}-\frac{2i-1}{2i}I_{i-1} \text{ with } I_0(r) = \frac{1}{2}\ln\left(\frac{a+\sqrt{a^2-r^2}}{a-\sqrt{a^2-r^2}}\right) \tag{3.33}$$

Thus, we have

$$\Phi(r,\alpha) = (1+\alpha)\cdot r^{\alpha-1}\sum_{i=0}^{\frac{\alpha+1}{2}}\frac{\Gamma\left(\frac{\alpha+3}{2}\right)}{\Gamma\left(\frac{\alpha+3}{2}-i\right)\Gamma(i+1)}I_i(r)\frac{a^{1-\alpha}}{r^2}\frac{1}{\sqrt{1-\frac{r^2}{a^2}}} \tag{3.34}$$

d. Total Load

Noting eqn. (3.22), we have the total vertical force needed to cause the displacement a_0 is

$$F_z = -\int_0^a \sigma_{zz}\big|_{z=0}\cdot 2\pi r dr = \sqrt{\pi}\frac{E}{1-\nu^2}\sum_{\alpha=0}^{\alpha_n} a_\alpha\cdot\frac{\Gamma\left(\frac{2+\alpha}{2}\right)}{\Gamma\left(\frac{3+\alpha}{2}\right)}a^{1-\alpha} \tag{3.35}$$

e. Condition for Using the Solution

If the whole punch contacts with the half space, i.e., the contact region is simply-connected, we need to have

$$\sigma_{zz}\big|_{z=0}\le 0\ \ (0\le r\le a)\ \text{or}\ \lim_{r\to a^-}\sigma_{zz}\big|_{z=0}\le 0 \tag{3.36}$$

At the punch edge we need to have $\sigma_{zz}\big|_{z=0,\,r=a}\le 0$ and

$$\text{noting}\ {}_2F_1\left(\frac{1}{2},-\frac{1-\alpha}{2};\frac{1-\alpha}{2};1\right) = -\frac{\sqrt{\pi}}{2}\cdot(1+\alpha)\cdot\frac{\Gamma\left(-\frac{1+\alpha}{2}\right)}{\Gamma\left(-\frac{\alpha}{2}\right)}, \tag{3.37}$$

we have

$$\sum_{\alpha=0}^{\alpha_n}(1+\alpha)\cdot a_\alpha\cdot\frac{\Gamma\left(\frac{2+\alpha}{2}\right)}{\Gamma\left(\frac{3+\alpha}{2}\right)}a^{\alpha}\ge 0 \tag{3.38}$$

Fig. 3.2, Fig. 3.3 and Fig. 3.4 summarize the characteristics for normal indentation problems.

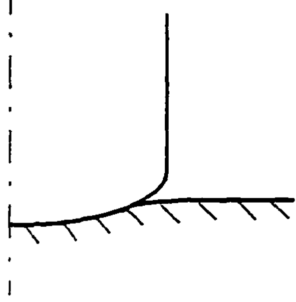

Fig. 3.2 Incomplete (unbonded) contact:
1) Pressure drops to zero at the edge;
2) The following condition is satisfied:

$$\sum_{\alpha=0}^{\alpha_n} (1+\alpha)\cdot a_\alpha \cdot \frac{\Gamma\left(\frac{2+\alpha}{2}\right)}{\Gamma\left(\frac{3+\alpha}{2}\right)} a^\alpha < 0$$

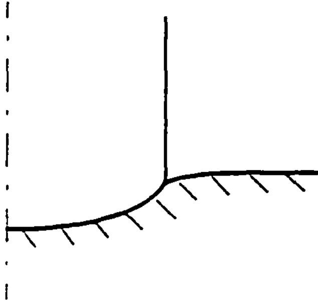

Fig. 3.3 Critical complete (bonded) contact:
1) Pressure drops to zero at the edge;
2) The following condition is satisfied:

$$\sum_{\alpha=0}^{\alpha_n} (1+\alpha)\cdot a_\alpha \cdot \frac{\Gamma\left(\frac{2+\alpha}{2}\right)}{\Gamma\left(\frac{3+\alpha}{2}\right)} a^\alpha = 0$$

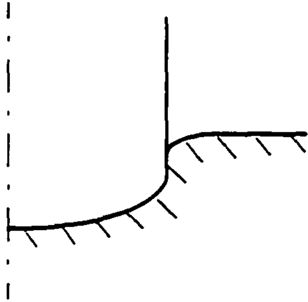

Fig. 3.4 General complete (bonded) contact:
1) Pressure has singularity at the punch edge;
2) The following condition is satisfied:

$$\sum_{\alpha=0}^{\alpha_n} (1+\alpha)\cdot a_\alpha \cdot \frac{\Gamma\left(\frac{2+\alpha}{2}\right)}{\Gamma\left(\frac{3+\alpha}{2}\right)} a^\alpha > 0$$

3.2.2 Viscoleastic half space

The governing equations for the corresponding viscoelastic half space problem are:

$$2\varepsilon_{ij}(t) = u_{i,j}(t) + u_{j,i}(t) \text{ (compatibility equation)} \tag{3.39}$$

$$\sigma_{ij}(t) = \int_{-\infty}^{t} \left[2G(t-\tau)\frac{\partial}{\partial\tau}\varepsilon_{ij}(\tau) + \delta_{ij}\lambda(t-\tau)\frac{\partial}{\partial\tau}\varepsilon_{kk}(\tau)\right]d\tau \text{ (constitutive equation)} \tag{3.40}$$

where $\lambda(t)$ and $G(t)$ are relaxation moduli.

$$\sigma_{ij,j} = 0 \text{ (force equilibrium)} \tag{3.41}$$

The boundary conditions are:

$$\sigma_{zr}(r,0,t) = \sigma_{z\theta}(r,0,t) = 0\ ,\ r \geq 0 \tag{3.42}$$

$$\sigma_{zz}(r,0,t) = 0\ ,\ r \geq a \tag{3.43}$$

$$u_z(r,0,t) = a_0(t) + \sum_{k=1}^{n} a_k(t) r^k\ ,\ 0 \leq r \leq a \tag{3.44}$$

where $a_0(t)$ is the depth of indentation and $a_k(t)$ decides the shape of the punch. If a_k $(k = 1, 2, \ldots, n)$ does not change with respect to time, punch shape is fixed; if $a_k = a_k(t)$ $(k = 1, 2, \ldots, n)$, punch shape will change with time.

Initially, no interaction happens between the punch and the half space and we have the initial conditions:

$$u_i(t) = \varepsilon_{ij}(t) = \sigma_{ij}(t) = 0\ ,\ -\infty \leq t \leq 0 \tag{3.45}$$

$$a_0(t) = 0\ ,\ -\infty \leq t \leq 0 \tag{3.46}$$

Assuming Laplace transform of all the time variables exists, we have

$$2\bar{\varepsilon}_{ij} = \bar{u}_{i,j} + \bar{u}_{j,i} \tag{3.47}$$

$$\bar{\sigma}_{ij}(t) = 2\bar{\mu}\overline{\varepsilon_{ij}'} + \delta_{ij}\bar{\lambda}\overline{\varepsilon_{kk}'}$$

$$= 2\bar{\mu}[s\overline{\varepsilon_{ij}} - \varepsilon(0)] + \delta_{ij}\bar{\lambda}[s\overline{\varepsilon_{kk}} - \varepsilon(0)]$$

$$= 2s\bar{\mu}\overline{\varepsilon_{ij}} + \delta_{ij}s\bar{\lambda}\overline{\varepsilon_{kk}} \tag{3.48}$$

$$\bar{\sigma}_{ij,j} = 0 \tag{3.49}$$

$$\overline{\sigma_{zr}}(r,0,s) = \overline{\sigma_{z\theta}}(r,0,s) = 0\ ,\ r \geq 0 \tag{3.50}$$

$$\overline{\sigma_{zz}}(r,0,s) = 0\ ,\ r \geq a \tag{3.51}$$

$$\bar{u}_z(r,0,s) = \sum_{k=0}^{n} \bar{a}_k(s) r^k, \; 0 \le r \le a \tag{3.52}$$

Using elastic-visoelastic analogy (Christensen 1982), we have interface pressure

$$\left.\overline{\sigma_{zz}}\right|_{z=0} = \frac{1}{2\sqrt{\pi}} \cdot \frac{s\bar{E}}{1-(s\bar{v})^2} \sum_{k=0}^{n} \bar{a}_k \cdot (1+k) \cdot \frac{\Gamma\left(\frac{2+k}{2}\right)}{\Gamma\left(\frac{3+k}{2}\right)} \cdot \Phi(r,k) \tag{3.53}$$

Thus,

$$\left.\sigma_{zz}\right|_{z=0} = \frac{1}{2\sqrt{\pi}} \cdot \sum_{k=0}^{n} L^{-1}\left[\frac{s\bar{E}\bar{a}_k}{1-(s\bar{v})^2}\right] \cdot (1+k) \cdot \frac{\Gamma\left(\frac{2+k}{2}\right)}{\Gamma\left(\frac{3+k}{2}\right)} \cdot \Phi(r,k) \tag{3.54}$$

Similarly, we have the total load

$$\bar{F}_z = \sqrt{\pi}\frac{s\bar{E}}{1-(s\bar{v})^2} \sum_{k=0}^{n} \bar{a}_k \cdot \frac{\Gamma\left(\frac{2+k}{2}\right)}{\Gamma\left(\frac{3+k}{2}\right)} a^{1+k} \tag{3.55}$$

Thus,

$$F_z = \sqrt{\pi} \sum_{k=0}^{n} L^{-1}\left[\frac{s\bar{E}\bar{a}_k}{1-(s\bar{v})^2}\right]\left[\frac{\Gamma\left(\frac{2+k}{2}\right)}{\Gamma\left(\frac{3+k}{2}\right)} a^{1+k}\right] \tag{3.56}$$

3.3 Special Cases

3.3.1 Elastic half space

a. Flat-ended punch

When $f(r) = a_0 \; (0 \le r \le a)$, we have

$$\left.\sigma_{zz}\right|_{z=0} = -\frac{a_0}{\pi} \cdot \frac{E}{1-v^2} \cdot \frac{1}{\sqrt{a^2-r^2}} \tag{3.57}$$

Which is the same as Boussinesq's solution and there is a square-root singularity at the punch edge.

b. One-half Power Punch

In this case, punch vertical displacement field is defined as $f(r) = a_0 + a_{\frac{1}{2}} r^{\frac{1}{2}}$ $(0 \le r \le a)$.

$$\text{When } a_0 \frac{\Gamma(1)}{\Gamma\left(\frac{3}{2}\right)} + \frac{3}{2} \cdot a_{\frac{1}{2}} \cdot \frac{\Gamma\left(\frac{5}{4}\right)}{\Gamma\left(\frac{7}{4}\right)} \cdot a^{\frac{1}{2}} \ge 0 \tag{3.58}$$

$$\sigma_{zz}\big|_{z=0} = -\frac{a_0}{\pi} \cdot \frac{E}{1-\nu^2} \cdot \frac{1}{\sqrt{a^2-r^2}} + \frac{3}{4\sqrt{\pi}} \cdot \frac{E}{1-\nu^2} \cdot a_{\frac{1}{2}} \cdot \frac{\Gamma\left(\frac{5}{4}\right)}{\Gamma\left(\frac{7}{4}\right)} \cdot \Phi\left(r, \frac{1}{2}\right) \tag{3.59}$$

$$\text{where } \Phi\left(r, \frac{1}{2}\right) = \frac{3\sqrt{\pi}}{4} \cdot \frac{\Gamma\left(-\frac{3}{4}\right)}{\Gamma\left(-\frac{1}{4}\right)} r^{-\frac{1}{2}} \frac{a^{\frac{3}{2}}}{r^2} \left[\frac{1}{\sqrt{1-\frac{r^2}{a^2}}} - {}_2F_1\left(\frac{1}{2}, -\frac{3}{4}; \frac{1}{4}; \frac{r^2}{a^2}\right) \right] \tag{3.60}$$

Fig. 3.5 shows the pressure distributions for a punch with radius 1 and profile $f(r) = a_0 - 0.001 r^{\frac{1}{2}}$ under different depth of indentation a_0. When $a_0 = 0.001311$, it is critical complete contact. There is a singularity at the tip only when the indentation depth is no more than

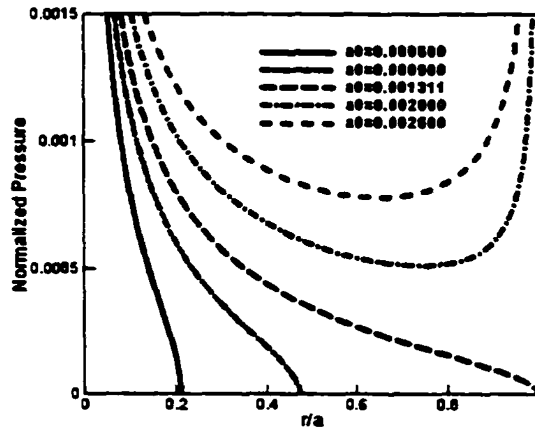

Fig. 3.5 One-half power punch. The pressure is normalized with respect to $\frac{-E}{1-\nu^2}$

the one for critical complete contact. There will be singularities at both the tip and the edge when the indentation depth is greater than the one for critical complete contact.

c. Conical Punch

In this case, punch vertical displacement field is defined as $f(r) = a_0 + a_1 r \ (0 \le r \le a)$.

When $a_0 \frac{\Gamma(1)}{\Gamma\left(\frac{3}{2}\right)} + 2a_1 \frac{\Gamma\left(\frac{3}{2}\right)}{\Gamma(2)} a > 0$, (3.61)

$$\sigma_{zz}\big|_{z=0} = \frac{1}{2\sqrt{\pi}} \cdot \frac{E}{1-\nu^2} \cdot a_1 \cdot 2 \cdot \frac{\Gamma\left(\frac{3}{2}\right)}{\Gamma(2)} \cdot \left[\frac{1}{2}\ln\left(\frac{a+\sqrt{a^2-r^2}}{a-\sqrt{a^2-r^2}}\right)\right]$$

$$+ \frac{1}{2\sqrt{\pi}} \cdot \frac{E}{1-\nu^2} \cdot \left[\frac{a_0}{a}\frac{\Gamma(1)}{\Gamma\left(\frac{3}{2}\right)} + 2a_1 \frac{\Gamma\left(\frac{3}{2}\right)}{\Gamma(2)}\right] \cdot \left[\frac{a^2}{r^2}\left(\sqrt{1-\frac{r^2}{a^2}} - \frac{1}{\sqrt{1-\frac{r^2}{a^2}}}\right)\right] \quad (3.62)$$

There is a square-root singularity at the punch edge and a logarithmic singularity at the punch tip.

When $a_0 \frac{\Gamma(1)}{\Gamma\left(\frac{3}{2}\right)} + 2a_1 \frac{\Gamma\left(\frac{3}{2}\right)}{\Gamma(2)} a = 0$, $\sigma_{zz}\big|_{z=0} = \frac{a_1}{4} \cdot \frac{E}{1-\nu^2} \cdot \ln\left(\frac{a+\sqrt{a^2-r^2}}{a-\sqrt{a^2-r^2}}\right)$. It leads to the same solutions as those of Love (1939) and Sneddon (1948). At the punch edge, pressure drops to zero and there is a logarithmetric singularity at the punch tip.

Fig. 3.6 shows the pressure distributions for a conical punch with radius 1 and profile $f(r) = a_0 - 0.001r$ under different depth of indentation a_0. When $a_0 = 0.001570$, it is critical complete contact. There is a logarithmetric singularity at the tip when the indentation depth is no more than the one for critical complete contact. There will be singularities at both the tip (log-

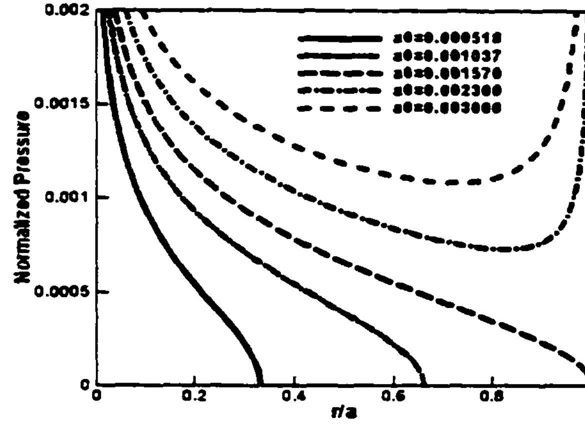

Fig. 3.6 Conical punch. The pressure is normalized with respect to $\frac{-E}{1-\nu^2}$

arithmetric singularity) and the edge (square-root singularity) when the indentation depth is greater than the one for critical complete contact.

d. Three-half Power Punch

In this case, punch vertical displacement field is defined as $f(r) = a_0 + a_{\frac{3}{2}} r^{\frac{3}{2}}$ $(0 \le r \le a)$.

When $a_0 \dfrac{\Gamma(1)}{\Gamma\left(\frac{3}{2}\right)} + \dfrac{5}{2} \cdot a_{\frac{3}{2}} \cdot \dfrac{\Gamma\left(\frac{7}{4}\right)}{\Gamma\left(\frac{9}{4}\right)} \cdot a^{\frac{3}{2}} \ge 0$, (3.63)

$$\sigma_{zz}\big|_{z=0} = -\frac{a_0}{\pi} \cdot \frac{E}{1-\nu^2} \cdot \frac{1}{\sqrt{a^2-r^2}} + \frac{5}{4\sqrt{\pi}} \cdot \frac{E}{1-\nu^2} \cdot a_{\frac{3}{2}} \cdot \frac{\Gamma\left(\frac{7}{4}\right)}{\Gamma\left(\frac{9}{4}\right)} \cdot \Phi\left(r, \frac{3}{2}\right) \tag{3.64}$$

where $\Phi\left(r, \frac{3}{2}\right) = \dfrac{5\sqrt{\pi}}{4} \cdot \dfrac{\Gamma\left(-\frac{5}{4}\right)}{\Gamma\left(-\frac{3}{4}\right)} r^{\frac{1}{2}} \dfrac{a^{\frac{5}{2}}}{r^2} \left[\dfrac{1}{\sqrt{1-\frac{r^2}{a^2}}} - {}_2F_1\left(\frac{1}{2}, -\frac{5}{4}; -\frac{1}{4}; \frac{r^2}{a^2}\right) \right]$ (3.65)

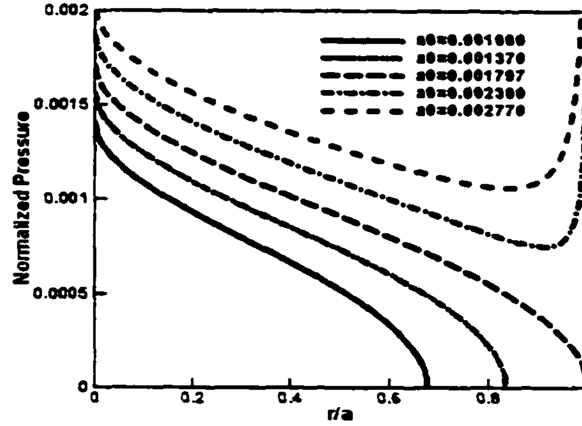

Fig. 3.7 Three-half power punch. The pressure is normalized with respect to $\frac{-E}{1-v^2}$

Fig. 3.7 shows the pressure distributions for a punch with radius 1 and profile $f(r) = a_0 - 0.001 r^{\frac{3}{2}}$ under different depth of indentation a_0. When $a_0 = 0.001797$, it is critical complete contact. There is a singularity at the tip when the indentation depth is no more than the one for critical complete contact. There will be singularities at both the tip and the edge when the indentation depth is greater than the one for critical complete contact.

e. Parabolic Punch

In this case, punch vertical displacement field is defined as $f(r) = a_0 + a_2 r^2$ $(0 \le r \le a)$.

When $a_0 \cdot \frac{\Gamma(1)}{\Gamma\left(\frac{3}{2}\right)} + 3a_2 \cdot \frac{\Gamma(2)}{\Gamma\left(\frac{5}{2}\right)} \cdot a^2 > 0$, (3.66)

$$\sigma_{zz}\big|_{z=0} = -\frac{1}{2\sqrt{\pi}} \cdot \frac{E}{1-v^2} \cdot \left[\frac{\Gamma(1)}{\Gamma\left(\frac{3}{2}\right)} a_0 \frac{1}{\sqrt{a^2-r^2}} - 3\frac{\Gamma(2)}{\Gamma\left(\frac{5}{2}\right)} a_2 \frac{2r^2-a^2}{\sqrt{a^2-r^2}}\right] \tag{3.67}$$

There is a square-root singularity at the punch edge.

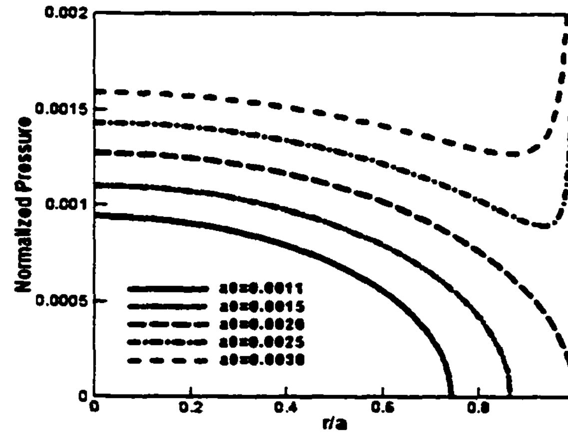

Fig. 3.8 Parabolic punch. The pressure is normalized with respect to $\frac{-E}{1-\nu^2}$

When $a_0 \cdot \frac{\Gamma(1)}{\Gamma\left(\frac{3}{2}\right)} + 3a_2 \cdot \frac{\Gamma(2)}{\Gamma\left(\frac{5}{2}\right)} \cdot a^2 = 0,$ (3.68)

we have $\sigma_{zz}\big|_{z=0} = \frac{4}{\pi} \cdot \frac{E}{1-\nu^2} \cdot a_2 \cdot \sqrt{a^2 - r^2}$ (3.69)

The pressure drops to zero at the punch edge and the solution is the same as Hertz's.

Fig. 3.8 shows the pressure distributions for a parabolic punch with radius 1 and profile $f(r) = a_0 - 0.001r^2$ under different depth of indentation a_0. When $a_0 = 0.0020$, it is critical complete contact. There is no singularity when the indentation depth is no more than the one for critical complete contact. There will be a square-root singularity at the edge when the indentation depth is greater than the one for critical complete contact.

f. Load-displacement Relationships

Here, we will show the comparison of load-displacement relationship for the five kinds of punches in 4.1-4.5. We can express those punch profiles generally by $f(r) = a_0 + a_\alpha r^\alpha$ $(0 \le r \le a)$.

(a) Critical complete contact

The indentation depth is $a_0 = -(1+\alpha)\cdot a_\alpha \cdot \frac{\Gamma\left(\frac{3}{2}\right)}{\Gamma(1)} \cdot \frac{\Gamma\left(\frac{2+\alpha}{2}\right)}{\Gamma\left(\frac{3+\alpha}{2}\right)} \cdot a^\alpha$. (3.70)

The total load is $F_z = -\sqrt{\pi} \cdot \frac{E}{1-\nu^2} \cdot \alpha \cdot a_\alpha \cdot \frac{\Gamma\left(\frac{2+\alpha}{2}\right)}{\Gamma\left(\frac{3+\alpha}{2}\right)} \cdot a^{\alpha+1}$. (3.71)

(b) Incomplete contact

The size of the contact region is $a = \left[\frac{\Gamma(1)}{\Gamma\left(\frac{3}{2}\right)} \cdot \frac{a_0}{a_\alpha} \cdot \frac{1}{1+\alpha} \cdot \frac{\Gamma\left(\frac{3+\alpha}{2}\right)}{\Gamma\left(\frac{2+\alpha}{2}\right)}\right]^{\frac{1}{\alpha}}$. (3.72)

The load-displacement relationship is

$$F_z = \frac{2E}{1-\nu^2} \cdot \left[\frac{\Gamma(1)}{\Gamma\left(\frac{3}{2}\right)}\right]^{\frac{1}{\alpha}} \cdot \frac{a_0^{\frac{1-\alpha}{\alpha}}}{(-a_\alpha)^{\frac{1}{\alpha}}} \cdot \left[\frac{\Gamma\left(\frac{3+\alpha}{2}\right)}{\Gamma\left(\frac{2+\alpha}{2}\right)}\right]^{\frac{1}{\alpha}} \cdot \frac{\alpha}{(1+\alpha)^{\frac{1-\alpha}{\alpha}}} \sim a_0^{\frac{1-\alpha}{\alpha}} \tag{3.73}$$

(c) Complete contact

The load-displacement relationship is

$$F_z = \sqrt{\pi} \cdot \frac{E}{1-\nu^2} \cdot \left[a_0 \cdot \frac{\Gamma(1)}{\Gamma\left(\frac{3}{2}\right)} \cdot a + a_\alpha \cdot \frac{\Gamma\left(\frac{2+\alpha}{2}\right)}{\Gamma\left(\frac{3+\alpha}{2}\right)} \cdot a^{1+\alpha}\right] = C_1 a_0 + C_2, \tag{3.74}$$

Where C_1, C_2 are constants and

$$C_1 = \sqrt{\pi} \cdot \frac{E}{1-\nu^2} \cdot a_0 \cdot \frac{\Gamma(1)}{\Gamma\left(\frac{3}{2}\right)} \cdot a, \; C_2 = \sqrt{\pi} \cdot \frac{E}{1-\nu^2} \cdot a_\alpha \cdot \frac{\Gamma\left(\frac{2+\alpha}{2}\right)}{\Gamma\left(\frac{3+\alpha}{2}\right)} \cdot a^{1+\alpha}. \tag{3.75}$$

If all punch radius is the same and the indentation depth is greater than the one for critical complete contact, the force vs. the displacement curve will be linear and parallel to each

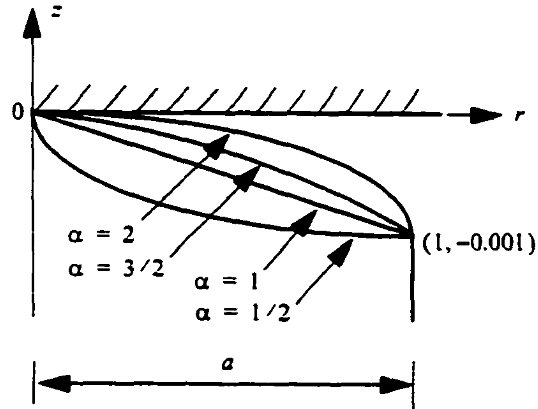

(a) Indenter shape

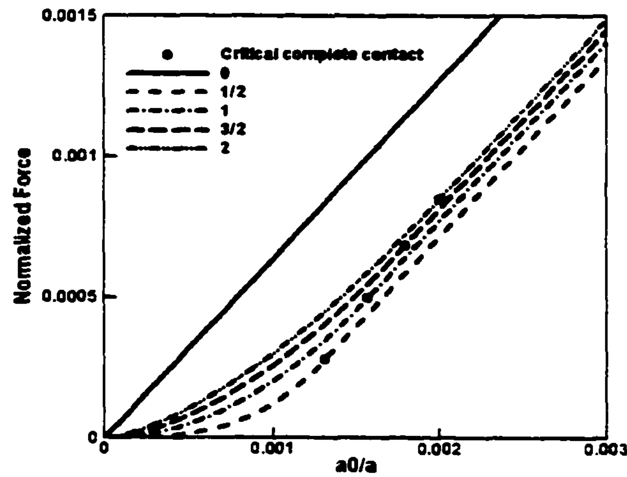

(b) load-displacement curves

Fig. 3.9 Load-displacement curve. The load is normalized with respect to $\frac{\pi a^2}{1-\nu}$

other. Fig. 3.9 shows the comparison of the five punches ($\alpha = 0, \frac{1}{2}, 1, \frac{3}{2}, 2$) for their load-displacement curves. When the depth of indentation is greater than the one for critical complete contact, they are all parallel to each other.

3.3.2 Viscoelastic half space

To make it simple, we assume Poisson's ratio to be constant.

a. Flat-ended Punch

(a) Constant displacement

In this case, the displacement is $a_0(t) = a_0 h(t)$ (3.76)

where a_0 is the amplitude and $h(t)$ is the step function.

From eqn. (3.54) we have $\sigma_{zz}\big|_{z=0} = -\frac{a_0}{\pi}\cdot\frac{1}{1-\nu^2}\cdot\frac{E(t)}{\sqrt{a^2-r^2}}$ (3.77)

It is observed from eqn. (3.71), the pressure distribution will keep the same; but its magnitude will change in the same way as the stress relaxation function.

From eqn. (3.56), we have $F_z = \frac{2a}{1-\nu^2}L^{-1}\left[s\bar{E}\frac{\bar{a}_0}{s}\right] = \frac{2aa_0}{1-\nu^2}E(t)$ (3.78)

The load will change in the same way as stress relaxation function.

(b) Constant load

The loading history is expressed as $F_z(t) = F_0 h(t)$ (3.79)

where F_0 is the amplitude and $h(t)$ is the step function.

From eqn. (3.55), we have $\bar{a}_0 = \frac{1-\nu^2}{2a}\bar{F}_z\cdot\bar{J}\cdot s = \frac{1-\nu^2}{2a}F_0\bar{J}$ (3.80)

Using Inverse Laplace Transform for eqn. (3.74) we have

$$a_0 = \frac{1-\nu^2}{2a}F_0 J(t) \quad (3.81)$$

The indentation depth of the punch will vary in the same way as creep function.

Putting eqn. (3.81) into eqn. (3.54), we have

$$\sigma_{zz}\big|_{z=0} = -\frac{1}{\pi}\cdot\frac{L^{-1}[s\bar{E}\bar{a}_0]}{1-\nu^2}\cdot\frac{1}{\sqrt{a^2-r^2}} = -\frac{F_0}{2\pi a}\frac{h(t)}{\sqrt{a^2-r^2}} \tag{3.82}$$

Pressure distribution will not change and is the same as flat-ended punch solution.

b. Parabolic Punch (Fixed Shape $a_2 = const$)

(a) Constant displacement

The displacement is $a_0(t) = a_0 h(t)$ (3.83)

where a_0 is the amplitude and $h(t)$ is the step function.

$$\sigma_{zz}\big|_{z=0} = \frac{1}{\pi}\cdot\frac{1}{1-\nu^2}\cdot\frac{1}{\sqrt{a^2-r^2}}\cdot[-a_0+(a_2a^2-2a_2r^2)]\cdot E(t) \tag{3.84}$$

$$F_z = \frac{2aa_0}{1-\nu^2}E(t)+\frac{\sqrt{\pi}}{1-\nu^2}E(t)a_2\cdot\frac{4}{3\sqrt{\pi}}\cdot a^3 = \frac{2a}{1-\nu^2}\left(a_0+\frac{2}{3}a_2a^2\right)E(t) \tag{3.85}$$

From eqn. (3.84) and eqn. (3.85), we have the similar results as those of flat-ended punch: pressure distribution will keep the same and only its magnitude will change in the same way as stress relaxation function; load also changes in the same way as stress relaxation function.

(b) Constant load

The loading history is $F_z(t) = F_0 h(t)$ (3.86)

where F_0 is the amplitude and $h(t)$ is the step function.

Noting eqn. (3.55), we have $\bar{F}_z = \frac{\sqrt{\pi}}{1-\nu^2}s\bar{E}\left(\bar{a}_0\frac{2}{\sqrt{\pi}}a+\frac{a_2}{s}\cdot\frac{4}{3\sqrt{\pi}}\cdot a^3\right)$ (3.87)

Solving for $\bar{a}_0$, $\bar{a}_0 = \frac{1-\nu^2}{2a}\cdot F_0\cdot\bar{J}-\frac{2}{3}a_2a^2\frac{1}{s}$ (3.88)

Under Inverse Laplace Transform, we have $a_0 = \frac{1-\nu^2}{2a}F_0J(t)-\frac{2}{3}a_2a^2h(t)$ (3.89)

Putting eqn. (3.89) into eqn. (3.54), we have,

$$\sigma_{zz}\big|_{z=0} = -\frac{1}{\pi}\cdot\frac{1}{1-\nu^2}L^{-1}[s\bar{E}\bar{a}_0]\frac{1}{\sqrt{a^2-r^2}}+\frac{2}{\pi}\cdot\frac{E(t)}{1-\nu^2}\cdot a_2\cdot\frac{a^2-2r^2}{\sqrt{a^2-r^2}}$$

$$= \left[-\frac{F_0h(t)}{2\pi a}+\frac{2a_2a^2}{3\pi(1-\nu^2)}E(t)\right]\frac{1}{\sqrt{a^2-r^2}}+\frac{2}{\pi}\cdot\frac{E(t)}{1-\nu^2}\cdot a_2\cdot\frac{a^2-2r^2}{\sqrt{a^2-r^2}} \tag{3.90}$$

3.4 Summary

The solutions obtained in this chapter can be the basis for finding contact pressure between two smooth surfaces with arbitrary shape profile.

For the nanoindentation using an axisymmetric indenter in an elastic media, these solutions will provide a good theoretical basis for interpreting the load-displacement curve and evaluating Young's modulus and Poisson's ratio.

For punch displacement profile in the formula of $f(r) = a_0 + a_{2m}r^{2m}$ (m is positive integer), the pressure distribution will not have singularities when the indentation depth is not more than the one for critical complete contact and will have square-root singularity at the punch edge when the indentation depth is greater than the one for critical complete contact.

For punch displacement profile in the formula of $f(r) = a_0 + a_{2m-1}r^{2m-1}$ (m is positive integer), the pressure distribution will always have a logarithmetric singularity at the punch tip and will have square-root singularity at the punch edge when the indentation depth is greater than the one for critical complete contact.

The pressure will alternate when it is the indentation of viscoelastic half space. Under constant displacement, the pressure distribution will be the same; but its magnitude will

change in the same way as stress relaxation function. Under constant load, the pressure distribution and its shape will change respect to time.

It should be emphasized that the solution is only valid when the contact region is a simply-connected domain. When a general punch profile is considered such as $f(r) = \sum_{\alpha=0}^{\alpha_n} a_\alpha r^\alpha$, one should first investigate if the contact area is simply-connected before using the present solution.

The derived solution can be the basis for further investigation of the indentation of half space when the interface friction is considered.

CHAPTER 4. WITHIN WAFER NONUNIFORMITY

It has been widely observed in CMP that the MRR, even under uniform nominal downpressure on the wafer, is not uniform across the entire wafer surface. Compared to the central region of the wafer, the MRR in a region 3-5 mm from the wafer edge has been observed to be significantly higher. This implies that for a specific polishing time, if the thickness removed in the central region is within the tolerance band, the thickness removed at the wafer edge is not. Although the wafer edge area is a narrow annular region, it contains about 20-25% of the dies for a 300 mm wafer, which represents a revenue stream of the order of $2.75 billion for a single IC fab (Witt and Cook 2000).

It is well-known that within wafer non-uniformity (WIWNU) due to the variation in material removal rate (MRR) in CMP significantly affects the yield of good dies. The process control for a batch CMP operation is further complicated by wafer to wafer non-uniformity (WTWNU) caused by MRR decay when a number of wafers are polished with the same unconditioned pad. Accordingly, the present work focuses on modeling the WIWNU and WTWNU in CMP processes. For a single wafer polish related to WIWNU, elastic pad deformation is assumed. For pad life related to WTWNU, viscoelastic pad deformation is assumed because pad is made of polymeric material and its long term mechanical properties (e.g., viscoelastic deformation) are important to understand its performance. Various material removal models suggest that the MRR is strongly influenced by the interface pressure. In the present work, an analytical expression for pressure distribution (and its associated MRR) at the wafer-pad interface for an elastic pad and a viscoelastic pad are developed.

The relationships among wafer displacement, wafer deformation and loading condi-

tion are also investigated. A good understanding of those will be helpful in carrier head design and of CMP process performance.

4.1 Literature Review

In CMP, the widely used material removal rate model is given by Preston's equation (Preston 1927): $\dot{H} = C \cdot P \cdot V$, where $\dot{H}$ is the average thickness removal rate, P is the pressure, V is the relative velocity between the pad and the wafer, and C is the Preston's coefficient. Preston's equation is based on the observation in glass polishing and is an empirical model; however, it gives a good estimation about material removal in CMP. Since the variation in relative velocity throughout the wafer is small in a typical orbital CMP process (Ouma 1998), we may assume that the WIWNU in MRR is mainly caused by the variation of the pressure distribution on the wafer surface, though other factors such as slurry distribution, may also play a role. From this, it is apparent that within wafer non-uniformity (WIWNU) may depend primarily on the pressure distribution.

Many researchers have focused on the modeling of the interface pressure distribution between the pad and the wafer (at wafer scale). Runnels and Renteln (1993) have used continuum mechanics modeling to investigate wafer edge effects and wafer curvature effects during polishing. They attribute the increase in MRR over several millimeters from the edge to the increased contact pressure. Their Finite Element Method (FEM) based elasticity solutions, however, have always shown larger pressure at wafer center, dropping to zero at the wafer edge. They hypothesized the cause to be partial contact between the pad and the wafer. Baker (1996) has developed a model for interfacial pressure based on plate theory, and has shown

that the predicted pressure variation in the edge region matches well with the non-uniform material removal. Wang et al (1997) and Srinivasa-Murthy et al (1997) have investigated the effects of various process parameters on the degree of wafer scale nonuniformity. They have observed that the von Mises stress correlates with the polishing nonuniformity, and uniformity improves with decreasing polishing pad compressibility. Sasaki et al (1998) have conducted a detailed FEM analysis of the pressure distribution under a wafer, and investigated the influences of back film, wafer chamfer and retainer ring on the pressure distribution. Byrne et al (1999) have considered the effects of pad wear. Utilizing finite element analysis, they predict that the MRR in the center region will be reduced over time due to pad wear.

For WIWNU investigation, elastic pad assumption is a good approximation because CMP in each wafer is carried out in a few minutes. However, pad is generally made of polymeric materials such as polyurethane, and its properties are time-dependent. For pad life investigation, such as WTWNU, viscoelastic pad deformation may not be neglected. Although viscoelastic properties of pads are one of the important factors for CMP performance, very few investigations have incorporated such pad characteristics. Steigerwald et al (1996) give a detailed presentation about viscoelastic properties of the pad and how it influences the planarization in the feature scale. Kim et al (2000) measure the viscoelastic parameters of several commonly used pads based on their viscoelastic material model.

Another issue is how to explain the decreasing MRR during CMP for unconditioned pad. Bajaj et al (1994) indicate it is because of the deterioration of pad surface due to cold flow caused by shear stress. These stresses lead to smoothening of pad surface and closing of the pores which result in lower mechanical abrasion at the pad surface and reduced slurry transporting. However, the experimental observations of Stein et al (1996) contradict such

inference: flat mesa-like structures formed on the pad during the first five minutes of polishing, and the pad structure was observed to remain unaltered thereafter. Some researchers (e.g., Byrne et al 1999) have also implied pad wear as one of the causes for decreasing MRR.

Little work has been done on the relationships among interface pressure, loading condition and wafer deformation though it is very important for carrier head design. In the last section, a preliminary study on this topic is presented.

4.2 Rigid Wafer - Elastic Pad

In the present work, an analytical expression for pressure distribution at the wafer and pad interface is developed. It is observed that depending on the wafer curvature and polishing conditions, the interface pressure may exhibit significant variation. The analytical model predictions are first verified against Finite Element Method (FEM) simulations. The predicted analytical pressure profiles are then utilized in Preston's equation to estimate the MRR, and these MRR predictions are also compared to experimental observations. The analytical results suggest, that for a specified wafer curvature there exists a certain polishing condition (and vice versa) that will enable holding the WIWNU within a specified tolerance band. The proposed model facilitates the design space exploration for such optimal polishing conditions.

a. Model development

Motivated by the observations that the WIWNU in MRR is primarily caused by variations in contact pressure. An analytical expression for the contact pressure distribution at the pad - wafer interface is first developed. For this purpose, the pad is assumed to deform like an elastic half-space. The wafer shape is assumed to be fixed (in comparison to the pad) and

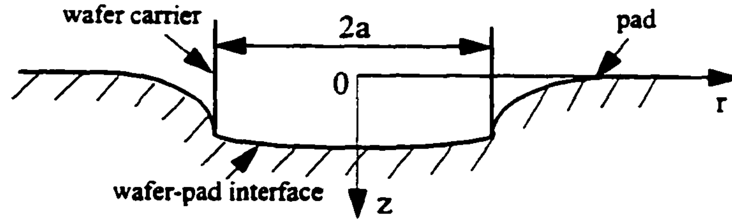

Fig. 4.1 Schematic of the contact problem between the wafer and the pad

wafer is undeformable though in reality its shape can change depending on the compressive characteristics of the deposited film, the wafer-pad interactions and the carrier head design (e.g., back film).

It is assumed that material removal occurs primarily due to solid-solid contact, while the slurry distribution is governed by the hydrodynamic effects.

Considering friction in the hoop direction only, and neglecting the friction in the radial direction, we need to solve the contact problem (Fig. 4.1) with the following boundary conditions at $z = 0$:

$$\tau_{zr} = 0, (0 \le r < \infty) \tag{4.1}$$

$$\sigma_{zz} = \tau_{z\theta} = 0, (r > a) \tag{4.2}$$

$$u_z = f(r) \text{ and } \tau_{z\theta} = \mu\sigma_{zz}, (0 \le r \le a) \tag{4.3}$$

Where $f(r)$ describes the final position of the wafer, which is assumed to be a polynomial form $f(r) = \sum_{k=0}^{n} a_k r^k$, and μ is the friction coefficient between the wafer and the pad.

This problem can be decomposed into two cases with a weak coupling between them:

Case (I): Normal indentation without friction and the Boundary conditions at $z = 0$ are:

$$\tau_{zr}^{(I)} = \tau_{z\theta}^{(I)} = 0, \; (0 \le r < \infty) \tag{4.4}$$

$$\sigma_{zz}^{(I)} = 0, \; (r > a) \tag{4.5}$$

$$u_z^{(I)} = f(r), \; (0 \le r \le a) \tag{4.6}$$

From eqn. (3.22), we have

$$\sigma_{zz}^{(I)}\Big|_{z=0} = \frac{1}{2\sqrt{\pi}} \cdot \frac{E}{1-\nu^2} \sum_{k=0}^{n} a_k (1+k) \cdot \frac{\Gamma\left(\frac{2+k}{2}\right)}{\Gamma\left(\frac{3+k}{2}\right)} \Phi(r,k) \tag{4.7}$$

Case (II): Friction in the hoop direction and the Boundary conditions at $z = 0$ are:

$$\tau_{zr}^{(II)} = \sigma_{zz}^{(II)} = 0, \; (0 \le r < \infty) \tag{4.8}$$

$$\sigma_{z\theta}^{(II)} = 0, \; (r > a) \tag{4.9}$$

$$\tau_{z\theta}^{(II)} = \mu \sigma_{zz}^{(I)}, \; (0 \le r \le a) \tag{4.10}$$

Noting eqn. (4.7), we have,

$$\tau_{z\theta}^{(II)}\Big|_{z=0} = \mu \sigma_{zz}^{(I)}\Big|_{z=0} = \frac{\mu}{2\sqrt{\pi}} \cdot \frac{E}{1-\nu^2} \sum_{k=0}^{n} a_k (1+k) \cdot \frac{\Gamma\left(\frac{2+k}{2}\right)}{\Gamma\left(\frac{3+k}{2}\right)} \Phi(r,k) \tag{4.11}$$

The total moment needed to overcome the friction under the wafer can be expressed as,

$$M_z^{(II)} = \int_0^a \tau_{z\theta}^{(II)}\Big|_{z=0} \cdot 2\pi r^2 dr = \frac{\pi^{\frac{3}{2}}}{2} \mu \cdot \frac{E}{1-\nu^2} \cdot \sum_{k=0}^{n} a_k \cdot \frac{1+k}{2+k} \cdot \frac{\Gamma\left(\frac{2+k}{2}\right)}{\Gamma\left(\frac{3+k}{2}\right)} a^{2+k} \tag{4.12}$$

Using superposition of case I and case II to obtain the final solution for the original problem:

$$\sigma_{zz}\big|_{z=0} = \sigma_{zz}^{(I)}\big|_{z=0} = \frac{1}{2\sqrt{\pi}} \cdot \frac{E}{1-\nu^2}\sum_{k=0}^{n} a_k(1+k) \cdot \frac{\Gamma\left(\frac{2+k}{2}\right)}{\Gamma\left(\frac{3+k}{2}\right)}\Phi(r,k) \tag{4.13}$$

$$\tau_{z\theta}\big|_{z=0} = \tau_{z\theta}^{(II)}\big|_{z=0} = \frac{\mu}{2\sqrt{\pi}} \cdot \frac{E}{1-\nu^2}\sum_{k=0}^{n} a_k(1+k) \cdot \frac{\Gamma\left(\frac{2+k}{2}\right)}{\Gamma\left(\frac{3+k}{2}\right)}\Phi(r,k) \tag{4.14}$$

$$F_z = F_z^{(I)} = \int_0^{\rho} \sigma_{zz}^{(I)}\big|_{z=0} \cdot 2\pi r dr = \sqrt{\pi}\frac{E}{1-\nu^2}\sum_{k=0}^{n} a_k \cdot \frac{\Gamma\left(\frac{2+k}{2}\right)}{\Gamma\left(\frac{3+k}{2}\right)}a^{1+k} \tag{4.15}$$

$$M_z = M_z^{(II)} = \int_0^{\rho} \tau_{z\theta}^{(II)}\big|_{z=0} \cdot 2\pi r^2 dr = -\frac{\pi^{\frac{3}{2}}}{2}\mu \cdot \frac{E}{1-\nu^2} \cdot \sum_{k=0}^{n} a_k \cdot \frac{1+k}{2+k} \cdot \frac{\Gamma\left(\frac{2+k}{2}\right)}{\Gamma\left(\frac{3+k}{2}\right)}a^{2+k} \tag{4.16}$$

b. Model verification

(a) Verification against FEM simulations

The analytical model is first verified against FEM simulations. The ABAQUS software (version 5.8) is used for this purpose. In ABAQUS, it is easy to define rigid smooth surfaces of revolution consisting of straight lines, circular arcs and parabolic arcs. Accordingly, although the analytical solution can handle any polynomial series, only constant and quadratic terms are considered in the FEM simulation.

If we choose wafer curvature as $2a_2$, the wafer shape is defined as $f(r) = a_2r^2$ before it indents into the half space. The vertical displacement of the wafer is defined as a_0. Then, the displacement field right under the wafer can be expressed as $f(r) = a_0 + a_2r^2$. The FEM mesh consists of 135 CAX8R finite elements, and the infinite boundary (far field) is modeled via 24 CINAX5R infinite elements. The mesh is finer toward the center of the wafer so that compu-

tational results converge quickly with only a small number of elements. A contact pair is defined between the wafer and the pad. A rectangular material orientation is defined for the half space so that stress values are reported in a material coordinate frame that rotates with element deformation. This is particularly useful in investigating normal stresses in the region of the half space in contact with the wafer.

The pad material is assumed to be isotropic and linear elastic. a_0 is the vertical displacement of the wafer and $2a_2$ is the wafer curvature caused by wafer bow. The wafer is displaced downward statically by a prescribed a_0.

When $f(r) = a_0 + a_2 r^2$ and noting eqn. (3.67), we have,

$$\sigma_{zz}\big|_{z=0} = -\frac{1}{\pi} \cdot \frac{E}{1-\nu^2} \cdot \frac{4a_2 r^2 + (a_0 - 2a_2 a^2)}{\sqrt{a^2 - r^2}} \tag{4.17}$$

In the FEM simulation, we assume $a = 50mm$ and $a_2 = 0.002/mm$. Two cases are considered: (i) $a_0 = -10mm$ for the critical position which is the limiting case for the Hertzian contact, and (ii) $a_0 = -30mm$ for the general position when full contact between the wafer and the pad is established.

Fig. 4.2(a) shows the deformation profile for the critical position ($a_0 = -10mm$). Note the deformed pad surface profile is smooth.

Fig. 4.2(b) shows the comparison between the analytical and the FEM results for the normalized pressure. It is observed that the normalized pressure is highest in the center, and drops to zero at the wafer edge. The analytical results compare very well to the FEM results.

Deformation and stresses at a general position ($a_0 > -2a^2 a_2$) are investigated next. For this purpose, $a_0 = -30mm$ is chosen and the wafer is indented beyond the critical position into

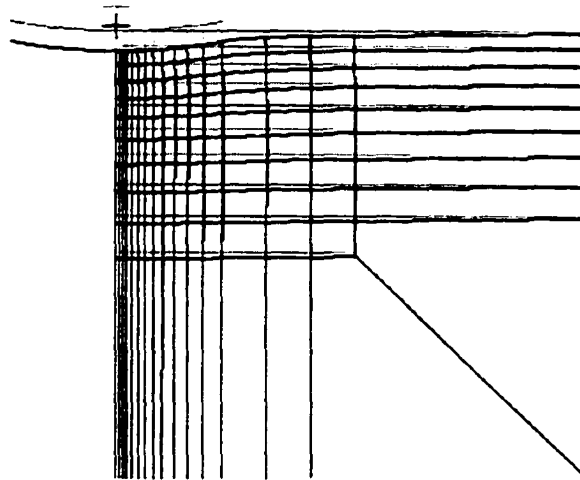

(a) Critical position: deformation profile

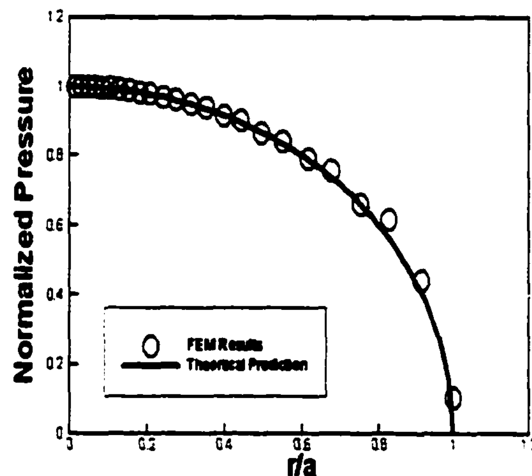

(b) Comparison of model predication with FEM result

Fig. 4.2 Comparison of normalized pressure obtained from analytical and FEM simulations for the critical position

the pad material. The deformation profile is presented in Fig. 4.3(a). Note at the wafer edge, the deformed pad surface profile is not smooth. Fig. 4.3(b) shows the comparison between the analytical and the FEM results for the normalized pressure. It is observed that the normalized pressure distribution deviates from the Hertzian profile, and shows a singularity of the order one-half at the edge of the wafer. The analytical results compare very well to the FEM results.

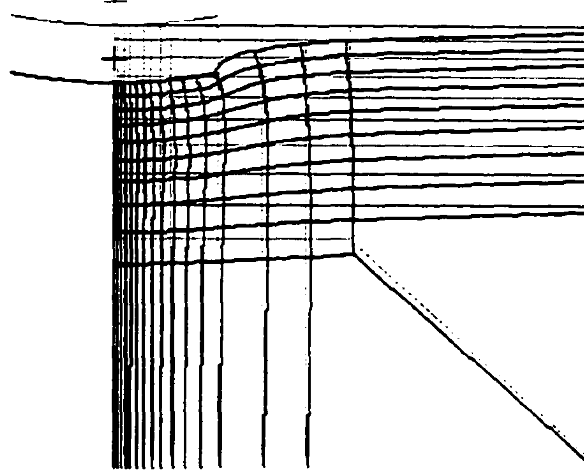

(a) General position: deformation profile

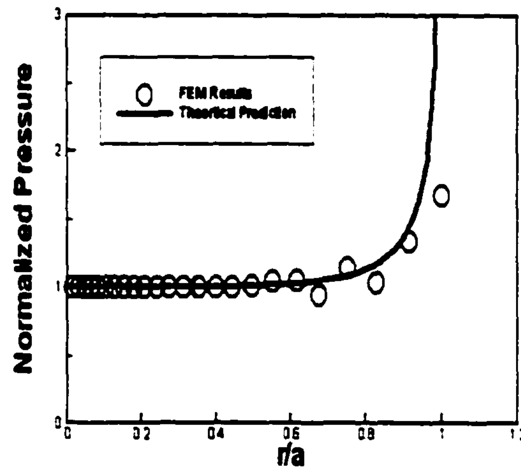

(b) Comparison of model predication with FEM result

Fig. 4.3 Comparison of normalized pressure obtained from analytical and FEM simulation for the general position

The change of normalized pressure at the pad-wafer interface for a wafer radius of 100 mm and curvature of 5×10^{-7} $1/mm$ with different depths of indentation is depicted in Fig. 4.4. It is observed that at the beginning the pressure distribution follows a Hertzian profile. As the indentation depth a_0 is increased, the pressure distribution gradually develops a singularity at the edge of the wafer, and the nature of the distribution changes drastically. It is interesting to

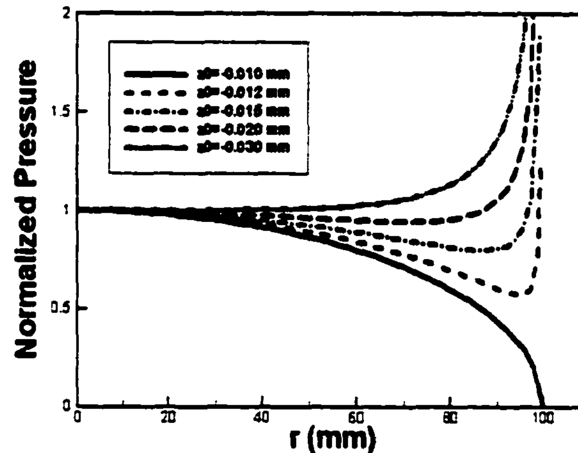

Fig. 4.4 Pressure evolution with respect to the depth of indentation. Wafer radius is 100 mm and its curvature is assumed to be 5×10^{-7} 1/mm.

observe that for a particular wafer profile, there exists a certain indentation depth for which the pressure distribution is almost uniform (for the current wafer profile, this occurs at around $a_0 = 20\mu m$). Since the indentation depth is related to the nominal pressure and the total force applied on the wafer, this implies that, for a given wafer profile and pad properties, there exists a polishing pressure for which the pressure variations may be held within a specified tolerance band. Thus, the WIWNU may also be held within a specified tolerance band. Such a capability will be very useful for designing the CMP process set up, especially the wafer carrier.

(b) Verification against experimental observations

To compare model predictions against experimental observations, it is first assumed that the material removal rate (MRR) follows Preston equation, the MRR is directly proportional to the pressure variation at the wafer-pad interface (The MRR caused by relatively velocity variation under typical CMP conditions is assumed to be small). In reality, high contact pressure at the edge will also cause large deflection, thus partially relieving the pressure.

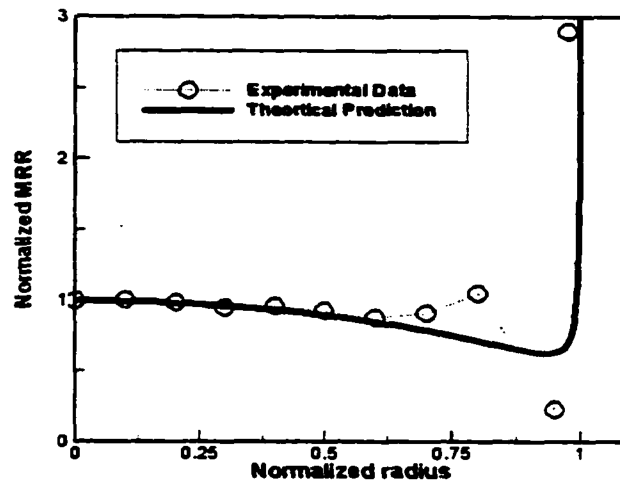

Fig. 4.5 Comparison of model predicted MRR against experimental of observations Srinivasa-Murthy et al (1997)

As a first attempt, however, a rigid wafer is assumed in the present work.

Model predictions for a wafer profile described as a parabola ($a_2 = 1.97\times10^{-4}$ m^{-1}) with indentation depth $a_0 = -5.08\times10^{-6}$ m, is compared to the experimental observations of WIWNU in MRR by Srinivasa-Murthy et al. Experiments were carried out with a R200T3 carrier film with modulus of elasticity of 6.895×10^{5} Pa. A down pressure of 4.827×10^{4} Pa, platen speed of 2.932 rad/s and carrier speed of 3.35 rad/s were used. The slurry used was SS12 and the pad was IC1000/SUBA IV (both from Rodel). The wafer was 203 mm in diameter. Fig. 4.5 shows a comparison of the model prediction with the experimental MRR distribution. The model predicts an almost constant MRR in the center region and a very high MRR at the wafer edge, which match very well with the experimental observations.

c. Discussion and conclusion

Within wafer non-uniformity (WIWNU) in material removal rate (MRR) is a critical parameter in determining the quality of a wafer planarized by a CMP process. This chapter presents an analytical model for predicting the WIWNU in MRR.

Based on the observations, it may be assumed that solid-liquid-solid interactions (hydrodynamic lubrication) is responsible for distributing the slurry, while solid-solid contact is primarily responsible for the majority of the material removal. Accordingly, we pursue a solid-solid contact model. The pad is modeled as an elastic half space, indented by a rigid wafer. An analytical solution is obtained for any wafer profile described by a polynomial. The analytical solution is verified against FEM simulations and experimental observations.

It is noted that very small wafer curvature will significantly influence the interface pressure distribution.

If only wafer curvature effect is considered, it has been observed that for a specific wafer profile, there exists an indentation depth (depending on down pressure) for which the pressure distribution transitions from an elliptic hertzian distribution to one showing a singularity at the edge of the wafer. This implies that for a given wafer profile, there exists a polishing condition for which an almost uniform pressure distribution (within a tolerance band) may be obtained at the pad-wafer interface. Alternatively, for a given polishing condition, there also exists a wafer profile (curvature) that will yield the most uniform pressure. Our analytical solution facilitates the search for this optimal solution.

To model the pressure more accurately, more terms need to be used because higher order terms may have a greater influence on the pressure profile at the wafer edge.

4.3 Rigid Wafer - Viscoelastic Pad

This section focuses on the spatial and temporal pressure variations across the entire wafer during a CMP process. Viscoelastic pad properties are incorporated. It gives the spatial pressure distribution at any given time during the polishing process. Model predictions are verified against existing experimental observations. Based on correlations between model predictions and experimental results, viscoelastic behavior of the pad may be hypothesized to be a significant contributor to the decreasing MRR phenomenon for unconditioned pads. The proposed viscoelastic model can also be utilized to help predict the thickness removal process during polishing, and process parameters may be adjusted, to optimize the performance of a CMP process.

a. Model Development

The pad is assumed to deform like a viscoelastic half-space. From the investigation, modeling the pad as a foundation cannot explain the edge effect since the influence of pad bending cannot be neglected for this purpose. In the present model, wafer shape can change and its deformation depends on the wafer carrier, slurry and pad configuration and process parameters. In the model development, we neglect friction for simplicity. However, it is not difficult to extend the solution and to include the influence of friction.

As shown in Fig. 4.6, the whole problem setup is the following:

Assuming small strains and displacements, the time variations of strains and stresses in a viscoelastic material may be expressed as (e.g., Christenson 1982),

$$2\varepsilon_{ij}(t) = u_{i,j}(t) + u_{j,i}(t) \tag{4.18}$$

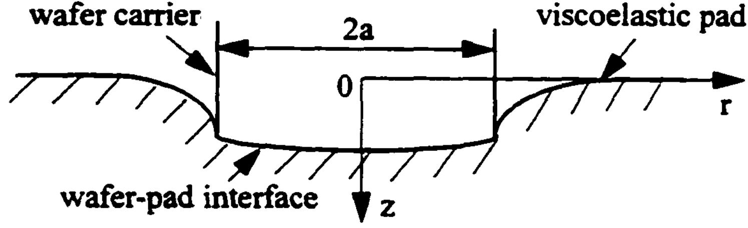

Fig. 4.6 Schematic of the contact problem

$$\sigma_{ij}(t) = \int_{-\infty}^{t}\left[2G(t-\tau)\frac{\partial}{\partial\tau}\varepsilon_{ij}(\tau) + \delta_{ij}\lambda(t-\tau)\frac{\partial}{\partial\tau}\varepsilon_{kk}(\tau)\right]d\tau \tag{4.19}$$

The eqn. (4.18) and eqn. (4.19) represent the kinematic and constitutive relations, where $\lambda(t)$ and $G(t)$ are bulk and shear relaxation moduli of the pad material, respectively.

In the absence of any body forces, the equilibrium equation is: $\sigma_{ij,j} = 0$ (4.20)

The boundary conditions at $z = 0$ are:

$$\sigma_{zr}(r,0,t) = \sigma_{z\theta}(r,0,t) = 0\,,\ r \ge 0 \tag{4.21}$$

$$\sigma_{zz}(r,0,t) = 0\,,\ r \ge a \tag{4.22}$$

and $$u_z(r,0,t) = a_0(t) + \sum_{k=1}^{n} a_k(t)r^k\,,\ 0 \le r \le a \tag{4.23}$$

where $a_0(t)$ is the depth of indentation and $\sum_{k=1}^{n} a_k(t)r^k$ describes the shape of the wafer. If a_k ($k = 1, 2, \ldots, n$) is time independent, wafer shape is fixed; if a_k ($k = 1, 2, \ldots, n$) changes with respect to time during polishing, wafer shape will be a function of time.

Initially, no interaction happens between the wafer and the pad and we have the following:

$$u_i(t) = \varepsilon_{ij}(t) = \sigma_{ij}(t) = 0\,,\ -\infty \le t \le 0 \tag{4.24}$$

$$a_0(t) = 0, -\infty \le t \le 0 \tag{4.25}$$

$$\bar{u}_z(r, 0, s) = \sum_{k=0}^{n} \bar{a}_k(s) r^k, \ 0 \le r \le a \tag{4.26}$$

From inverse Laplace transform, we have for interface pressure (eqn. (3.54)):

$$\sigma_{zz}|_{z=0} = \frac{1}{2\sqrt{\pi}} \cdot \sum_{k=0}^{n} L^{-1}\left[\frac{s\bar{E}\bar{a}_k}{1-(s\bar{\nu})^2}\right] \cdot (1+k) \cdot \frac{\Gamma\left(\frac{2+k}{2}\right)}{\Gamma\left(\frac{3+k}{2}\right)} \cdot \Phi(r,k) \tag{4.27}$$

where $E(t)$ and $\nu(t)$ are Young's modulus (stress relaxation function for a viscoelastic solid) and Poisson's ratio of the pad.

Similarly, we have the total load (eqn. (3.55))

$$F_z = -\int_0^a \sigma_{zz}|_{z=0} \cdot 2\pi r dr = \sqrt{\pi} \sum_{k=0}^{n} L^{-1}\left[\frac{s\bar{E}\bar{a}_k}{1-(s\bar{\nu})^2}\right]\left[\frac{\Gamma\left(\frac{2+k}{2}\right)}{\Gamma\left(\frac{3+k}{2}\right)} a^{1+k}\right] \tag{4.28}$$

b. Material model

To make the inverse Laplace transform simple, we assume the Poisson's ratio to be time-independent and has the value 0.1 for commonly used porous polymeric pad.

As shown in Fig. 4.7, we choose the same material model as Kim et al (2000). This Maxwell component and Kelvin component in series model is simple; but it can represent almost all the viscoelastic characteristics of the pad described by Steigerwald et al (1996). The

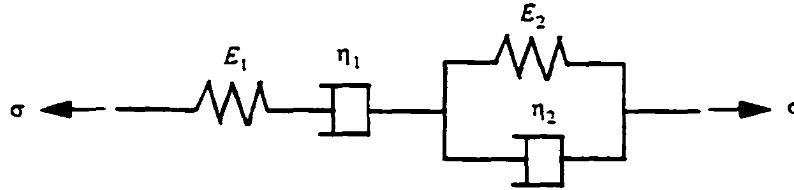

Fig. 4.7 Viscoelastic pad model

corresponding stress relaxation function $E(t)$ is derived. It decreases exponentially with respect to time and has the following format:

$$E(t) = \frac{1}{A_1}(A_2 e^{\rho_1 t} + A_3 e^{\rho_2 t}) \tag{4.29}$$

where,

$A_1 = \sqrt{\left(\frac{E_2}{E_1} - \frac{\eta_2}{\eta_1}\right)^2 + 2\left(\frac{E_2}{E_1} + \frac{\eta_2}{\eta_1}\right) + 1}$, $\rho_1 = \dfrac{-\left(\frac{E_2}{E_1} + \frac{\eta_2}{\eta_1} + 1\right) + A_1}{2\frac{\eta_2}{E_1}}$, $\rho_2 = \dfrac{-\left(\frac{E_2}{E_1} - \frac{\eta_2}{\eta_1} + 1\right) - A_1}{2\frac{\eta_2}{E_1}}$, $A_2 = E_2 + \eta_2\rho_1$ and

$A_3 = -(E_2 + \eta_2\rho_2)$

E_1, E_2, η_1 and η_2 can be measured through experiments. In the test, the specimen should be in the same working environment as in real-life CMP, e.g., wet environment with the same solution, the same soaking time and the same temperature, etc.

c. Model verification

First, we assume a viscoelastic material model and obtain its stress relaxation function; then, we give the analytical solutions for pressure distribution function $\sigma_{zz}(r,t)|_{z=0}$ for two cases: (a) constant load which is typical in CMP, and (b) constant displacement. Finally, we show the model prediction compared with experimental data in CMP.

(a) Constant load

This case is typical during the main polishing in CMP. We assume a parabolic wafer shape with fixed curvature (e.g., $f(r) = a_0 + a_2 r^2$ where $a_2 = constant$). We further assume the time interval from unloading a polished wafer to loading a new wafer is negligible compared to the time period for polishing each wafer. Under this assumption, the polishing process is

carried out under constant load and we can express it as $F_z(t) = F_0 h(t)$, where F_0 is the amplitude of the load and $h(t)$ is the step function.

From eqn. (4.27), the pressure distribution is

$$\sigma_{zz}|_{z=0} = \left[-\frac{F_0 h(t)}{2\pi a} + \frac{2a_2 a^2}{3\pi(1-\nu^2)}E(t)\right]\frac{1}{\sqrt{a^2-r^2}} + \frac{2}{\pi}\cdot\frac{E(t)}{1-\nu^2}\cdot a_2\cdot\frac{a^2-2r^2}{\sqrt{a^2-r^2}} \tag{4.30}$$

In the simulation, we choose wafer radius $a = 75mm$, $a_2 = -0.15/m^2$ and average pressure on the wafer surface is $7.5psi$. Since the actual material properties for the pads used in experiments by Bajaj et al (1994) are not available, we choose a representative set, based on IC 1400 pad properties reported by Kim et al (2000), to make a qualitative comparison. The material parameters are chosen to be $E_1 = 4.3MPa$, $E_2 = 13MPa$, $\eta_1 = 220(MPa \cdot s)$ (since η_1 is not reported by Kim et al, it is assumed to be the same as η_2), $\eta_2 = 220(MPa \cdot s)$.

Fig. 4.8 (a) shows the variation in interface pressure across the entire wafer. As the wafer edge is approached, the interface pressure rises, sharply and significantly. This causes the higher MRR at the wafer edge. It should be noted here, that depending on the combination of wafer curvature and the downpressure, the polishing may be edge-fast or edge-slow. We find even under constant load, the pressure distribution will change continuously due to the creep of the pad.

It may also be observed that the pressure over the central region (most part of the wafer excluding the edge area) of the wafer gradually drops as the polishing continues. This provides an explanation for the decreasing MRR typically observed in CMP experiments (which are usually measured based on a certain number of mapping points excluding the wafer edge region). Model predictions are compared with the experimental observations of

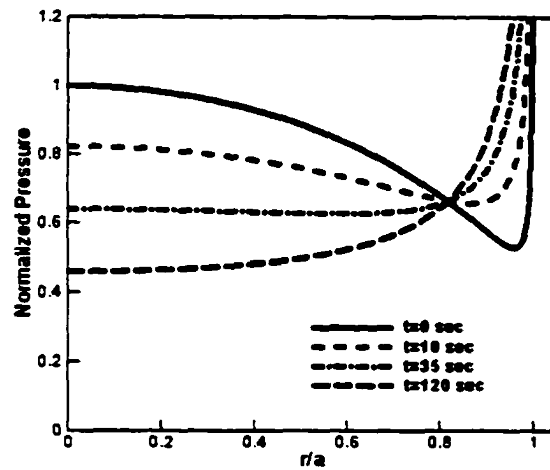

(a) Pressure evolution process

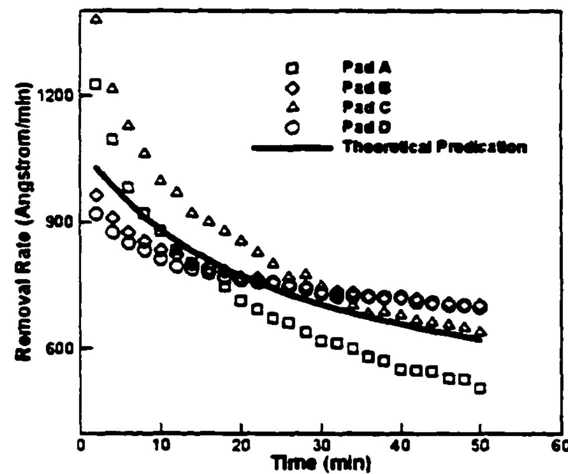

(b) MRR variation

Fig. 4.8 Comparison of model prediction against experimental observations of Bajaj et al (1994)

MRR by Bajaj et al (1994) in Figure 4.8 (b). The experiments were carried out by using Westech model 372 polishing tool. Commercially available silica slurry and commercially available polyurethane pads (Pad A, Pad B, Pad C and Pad D) were used.

To compare model predictions against experimental observations, it is assumed that the material removal rate (MRR) follows Preston equation and it is directly proportional to the pressure variation. Except the edge area which are generally not measured in the experiments, we choose the pressure at the wafer center as the reference pressure in the comparison, i.e., the MRR for the ith wafer is $\dot{H}_i(t) \sim \frac{\int_{t_i}^{t_i+\Delta t} \sigma_{zz}|_{z=0} ds}{\Delta t}$, and the wafer is polished from time t_i to time $t_i + \Delta t$. The coefficient is obtained by fitting a single experimental data point to this equation. It may be observed that the viscoelastic model predictions of the WTWNU due to MRR decay is qualitatively similar to the experimental observations. It should be noted that direct quantitative comparisons could not be made in this case, because the details of experimental conditions and pads used by Bajaj et al (1994) are not reported in their paper.

Model predictions are also compared to the experimental observations of thickness removal by Stein et al (1996) in Fig. 4.9. In the simulation, we choose $a_2 = -0.187/m^2$. The material parameters are chosen to be $E_1 = 4.3MPa$, $E_2 = 13MPa$, $\eta_1 = 220(MPa \cdot s)$, $\eta_2 = 220(MPa \cdot s)$. Because we do not have viscoelastic properties of IC1000 / Suba IV pad, we use the data for IC 1400 pad as these two pads are quite similar (Ouma 1998).

Fig. 4.9 (a) shows the variation in interface pressure across the entire wafer. Similar trend is observed. In the simulation, it is assumed that the material removal rate (MRR) follows Preston equation and the thickness removal is directly proportional to the definite integral of pressure variation with respect to time, i.e., $\Delta H(t) \sim \int_{t_i}^{t_i+\Delta t} \sigma_{zz}|_{z=0} ds$ and the ith wafer is polished from time t_i to time $t_i + \Delta t$. The experiments by Stein et al (1996) were carried out using a Cybeq 3900 polisher with carrier head pressure 7.5 psi, and the speeds for platen, car-

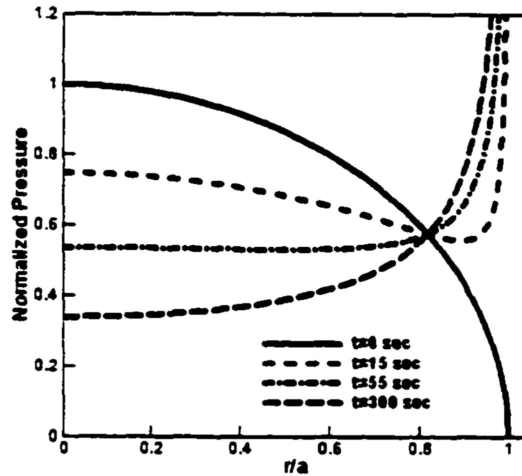

(a) pressure evolution process

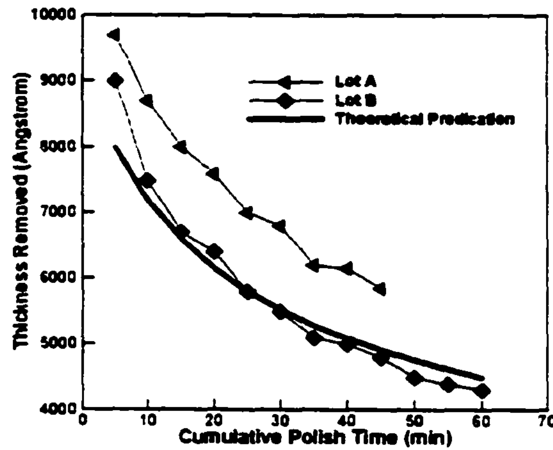

(b) Thickness removal variation

Fig. 4.9 Comparison of model prediction against experimental observations of Stein et al (1996)

ousel and carrier head are 20, 15 and 5 rpm. Polishing pads were Rodel IC1000/Suba IV stacked pads with DF200 carrier inserts. Cabot SS12 slurry was used with dispense rate of 600 ml/min. Unpatterned 150mm diameter wafer was used and film thickness was measured by a Prometrix FT-530 optical probe with 10mm edge exclusion utilizing a 17 point site map for measurement points.

In Fig. 4.9 (a), it is observed that the magnitudes of interface pressure drops over the central region (domain of experimental observation with 10 mm edge exclusion). This provides an explanation for the decreasing thickness removal in Fig. 4.9 (b). As polishing continues, the pressure at most part of the wafer excluding the edge area steadily drops. Under the cumulative effect of the drop of the interface pressure, the thickness removal also decreases in Fig. 4.9 (b). Once again, the experimental trend is compared with model predictions by first fitting a single experimental data point to calibrate the model. It is observed that the trend predicted by the viscoelastic model compares very well to the experimental trend.

It has been speculated in the past that the decreasing trend of the MRR is due to changes in the porosity structure of the pad. In the investigation by Stein et al (1996), however, flat mesa-like structures formed on the pad during the first 5 minutes of polishing, and the pad structure was observed to remain unaltered thereafter. The consistent pad topography after the first 5 minutes of polish (as indicated by the interferometer data and SEM images) does not correlate with the trend in the removal rate. The decay in the MRR occurred gradually over a period of 60 minutes. Hence, any decay in MRR between 5 and 60 minute time window cannot be attributed to the change in the surface topography of the pad. It may be observed from the present work, that incorporation of viscoelastic pad properties effectively captures this long range decay of the MRR over the appropriate time scale. Hence, it may be conjectured that such decay in MRR is caused by viscoelastic deformation of the pad.

(b) Constant displacement

Although this case is not typical in CMP, we present the results here to further emphasize how viscoelastic characteristics of the pad can influence the polishing process. We assume a parabolic wafer shape with fixed curvature and polishing is carried out under con-

stant vertical displacement, i.e., $a_0(t) = a_0 h(t)$, where a_0 is the amplitude of the displacement and $h(t)$ is the step function.

Under those assumptions, we have the interface pressure from eqn. (4.27):

$$\sigma_{zz}|_{z=0} = \frac{1}{\pi} \cdot \frac{1}{1-v^2} \cdot \frac{1}{\sqrt{a^2 - r^2}} \cdot [-a_0 + (a_2 a^2 - 2a_2 r^2)] \cdot E(t) \tag{4.31}$$

From this equation, we find that the edge-fast or edge-slow nature of the pressure distribution will not change with time, but the spatial pressure distribution will change with the same trend as the stress relaxation function $E(t)$.

Fig. 4.10 shows the simulation results for constant wafer vertical displacement. In the simulation, we choose wafer dome height to be $10\mu m$ and its vertical displacement to be $a_0 = 25\mu m$. The material parameters are assumed to be $E_1 = 4.3MPa$, $E_2 = 13MPa$, $\eta_1 = 220(MPa \cdot s)$, $\eta_2 = 220(MPa \cdot s)$ and wafer diameter is $150mm$. Fig. 4.10 (a) shows the pressure evolution process. It is observed that the overall nature of the spatial pressure distribution, along with its edge-fast or edge-slow behavior, does not change. However, as shown in Fig. 4.10 (b), the magnitude of the interface pressure on the entire wafer surface drops considerably with polishing time. This may be explained by the stress relaxation behavior of the viscoelastic pad under constant displacement.

c. Discussions and conclusions

Within-wafer-non-uniformity (WIWNU) is a critical parameter in determining the quality of a wafer planarized by a CMP process. It significantly influences the yield of good dies. Wafer-to-wafer-non-uniformity (WTWNU) is also important for a CMP process as it indicates the pad life and tool stability. This paper presents an analytical model for predicting the spatial and temporal distribution of the wafer - pad interface pressure during a CMP pro-

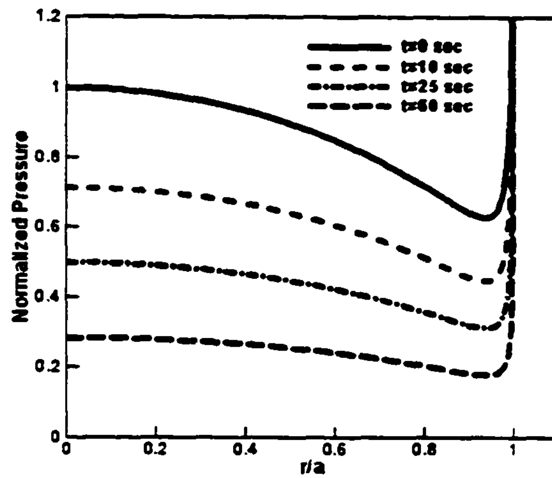

(a) Pressure evolution process

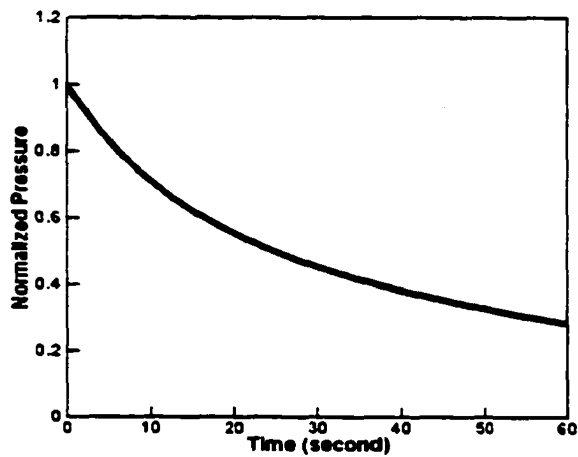

(b) Pressure vs. time

Fig. 4.10 Model simulation for constant wafer displacement

cess. The spatial distribution correlates to the WIWNU observed in a single wafer, while the long range temporal distribution correlates to the MRR decay and the resulting WTWNU over a batch of wafers. The proposed viscoelastic model shows that the MRR decay for an unconditioned pad is strongly influenced by the viscoelastic properties of the pad.

The simulations indicate that the viscoelastic properties of pad play an important role in CMP performance. Depending on how the wafer deforms, the magnitude of the load and pad properties, the pressure distribution with respect to time can have a small variation or a large variation as polishing process goes. For small variation, the pad viscoelastic properties are stable and the polishing result is almost consistent. On the other hand, for large variation, the pad properties are not stable and the polishing results will be different for different wafers even if they are polished under the same time interval and same polishing conditions. This will not end until the pad properties become stable after certain time.

In the examples, we assume polishing under constant load or constant vertical displacement conditions. We also assume fixed wafer shape. This is only for simplicity. The presented model is valid even if loading condition and wafer shape are time-dependent and are functions of time which is common for real-life CMP.

It is observed that under constant load which is typical during main polishing in CMP, the spatial distribution of the interface pressure profile may change with time from edge-slow to edge-fast, depending on the combination of wafer curvature, downpressure and pad properties. For constant displacement operations, the pressure profile retains its edge-slow or edge-fast characteristics over time. The analytical model predictions of MRR based on viscoelastic pad properties also correlate very well to existing experimental observations of MRR decay when an unconditioned pad is used to polish a number of wafers. Based on these observations, it may be conjectured that the viscoelastic material properties of the pad plays a primary role in causing the observed MRR decay. The analytical results obtained in the present work, can also provide an estimation of evolution of thickness removal distribution over the entire

wafer. This may be utilized for determining the optimum thickness of the overburden material and its polishing time, and for effective control of CMP processes.

4.4 Deformable Wafer - Elastic Pad

In this section, the relationships among wafer shape, wafer-pad interface pressure distribution and loading are investigated. When one of the three information is given, the other two are solved through contact mechanics. The purpose is to gain better understanding of carrier head design.

The assumptions are: Pad deforms like an elastic half space; Wafer is a circular plate; Wafer and pad are fully contacted. To make it simple, only axisymmetric situation is considered as shown in Fig. 4.11.

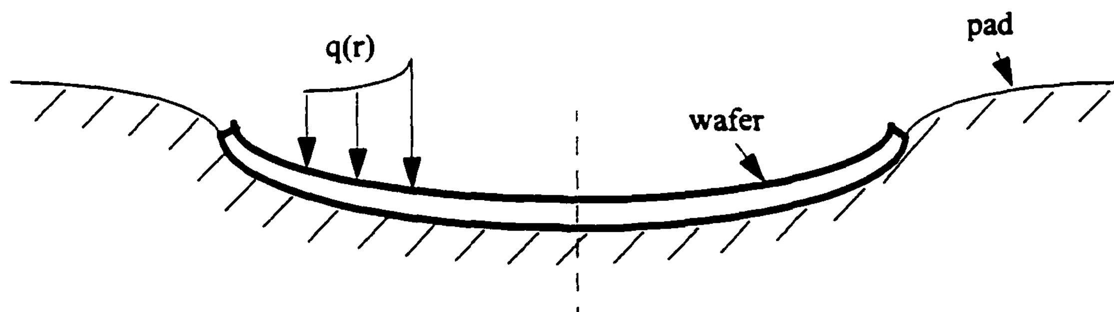

Fig. 4.11 Deformable wafer system setup

a. How to Load to Obtain the Desired Interface Pressure Distribution

(a) Theoretical Derivation

This case is common in carrier head design. As-deposited film thickness varies due to different deposition processes. A better head design will have the ability to tune the interface pressure according to the film thickness variation so that thicker portions of the film experi-

ence higher pressure or higher removal rate. In this way, global planarization ability of CMP will be improved.

If the desired interface pressure distribution is $p(r)$, the displacement of the pad under the pressure p is (Timonshenko and Goodier 1990)

$$u_z(r) = \frac{4(1-\nu_{pad}^2)}{\pi E_{pad}}\left[\int_0^r \frac{s}{r}K\left(\frac{s}{r}\right)p(s)ds + \int_r^a K\left(\frac{r}{s}\right)p(s)ds\right] \quad (0 \le r \le a) \tag{4.32}$$

Where $E(k) = \int_0^{\frac{\pi}{2}} \sqrt{1-k^2\sin^2\theta}\,d\theta$ is complete elliptic integral of the second kind.

Because wafer surface and pad surface have to conform to each other, we have $w = u_z$; then, from plate theory, the loading condition is

$$q(r) = p(r) + \frac{D_{wafer}}{r}\frac{d}{dr}\left\{r\frac{d}{dr}\left[\frac{1}{r}\frac{d}{dr}\left(r\frac{dw}{dr}\right)\right]\right\} \tag{4.33}$$

Where $D_{wafer} = \frac{E_{wafer}t_{wafer}^3}{12(1-\nu_{wafer}^2)}$;
t_{wafer} is thickness of the wafer;
E_{wafer} is Young's modulus of the wafer;
ν_{wafer} is Poisson's ratio of the wafer.

(b) Example - Uniform Interface Pressure

In this case, $p = constant$ and we have

$$u_z(r) = \frac{4(1-\nu_{pad}^2)}{\pi E_{pad}}\left[\int_0^r \frac{s}{r}K\left(\frac{s}{r}\right)p(s)ds + \int_r^a K\left(\frac{r}{s}\right)p(s)ds\right] \tag{4.34}$$

Noting $\frac{s}{r}\sin\theta = \sin t$ and Fig. 4.12, we have

$$\int_0^r \frac{s}{r}K\left(\frac{s}{r}\right)p(s)ds = \int_0^{\frac{\pi}{2}}\int_0^{\theta} \frac{\frac{\sin t}{\sin\theta}\cdot\frac{r}{\sin\theta}\cdot\cos t}{\cos t}\,dt\,d\theta = r\tan\frac{\theta}{2}\Big|_0^{\frac{\pi}{2}} = r \tag{4.35}$$

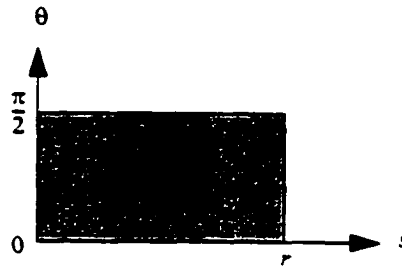

Fig. 4.12 Integration sequence change

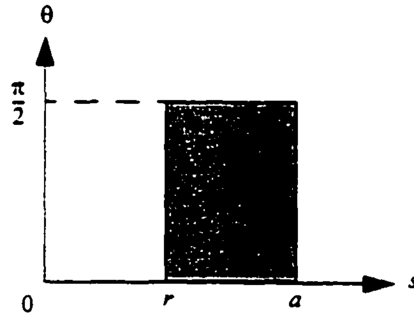

Fig. 4.13 Integration sequence change

Noting Fig. 4.13, we have

$$\int_r^a K\left(\frac{r}{s}\right)p(s)ds = \int_0^{\frac{\pi}{2}}\left(\sqrt{a^2-r^2\sin^2\theta}-r\cos\theta\right)d\theta = aE\left(\frac{r}{a}\right)-r \tag{4.36}$$

From eqn. (4.25) and eqn. (4.36), we have

$$u_z(r) = \frac{4(1-\nu_{pad}^2)pa}{\pi E_{pad}}E\left(\frac{r}{a}\right),\ (0 \le r \le a) \tag{4.37}$$

Putting eqn. (4.37) into eqn. (4.33), we have

$$q\left(\frac{r}{a}\right) = p+\frac{1}{3\pi}\cdot\frac{1-\nu_{pad}^2}{1-\nu_{wafer}^2}\cdot\frac{E_{wafer}}{E_{pad}}\cdot\left(\frac{t_{wafer}}{a}\right)^3\cdot p\cdot\left[-\frac{\left(7+\frac{r^2}{a^2}\right)}{\left(1-\frac{r^2}{a^2}\right)^3}E\left(\frac{r}{a}\right)+\frac{4}{\left(1-\frac{r^2}{a^2}\right)^2}K\left(\frac{r}{a}\right)\right] \tag{4.38}$$

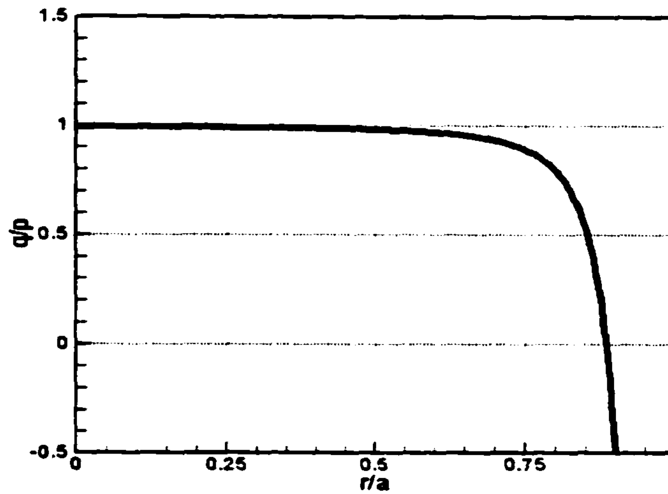

Fig. 4.14 Normalized interface pressure distribution

From the above equation, to obtain uniform interface pressure, the center part of the wafer should be loaded in compression and the edge of the wafer should be loaded in tension as shown in Fig. 4.14.

The solution may be utilized in carrier head design. After the test wafer is polished, the removal rate profile on the entire wafer surface, which is proportional to the interface pressure distribution, can be measured. From the interface pressure and referring to the given equation, one can figure out how the carrier head actually loads the wafer.

b. How to Load to Obtain the Desired Wafer Shape

(a) Theoretical Derivation

Because in the interval $0 \le r \le a$ wafer shape is smooth, its deformation can be expressed as an even polynomial series (Odd polynomial series will lead to infinite pressure at the center of the wafer, which is not observed in reality and not likely to happen) and it can be written as $w(r) = u_z(r) = \sum_{m=0}^{\infty} a_{2m} r^{2m}$. (4.39)

For this displacement, the interface pressure (eqn. (3.22)) is

$$p(r) = -\frac{1}{2\sqrt{\pi}} \cdot \frac{E}{1-\nu^2} \cdot \sum_{0}^{\infty} a_{2m} \cdot (1+2m) \cdot \frac{\Gamma(1+m)}{\Gamma\left(\frac{3}{2}+m\right)} \cdot \Phi(r, 2m) \tag{4.40}$$

The loading condition for this kind of displacement is:

$$q(r) = p(r) + D_{wafer} \sum_{m=2}^{\infty} (2m-2)^2 (2m)^2 a_{2m} r^{2m-4} \tag{4.41}$$

From the above equation, $q(r) = p(r)$ if the power of the even polynomial is less than four.

(b) Example - Second Order Even Polynomial

In this case, $u_z(r) = a_0 + a_2 r^2$. Interface pressure and the loading condition are the same and they are:

$$q(r) = p(r) = \frac{1}{2\sqrt{\pi}} \cdot \frac{E_{pad}^2}{1-\nu_{pad}^2} \cdot \left[\frac{\Gamma(1)}{\Gamma\left(\frac{3}{2}\right)} a_0 \frac{1}{\sqrt{a^2-r^2}} + 3 \frac{\Gamma(2)}{\Gamma\left(\frac{5}{2}\right)} a_2 \frac{2r^2-a^2}{\sqrt{a^2-r^2}} \right] \tag{4.42}$$

c. How to Obtain the Interface Pressure from the Loading

People generally think loading on the back of the wafer will be the same as the front of the wafer. From the following investigation, it is not true. It still has the edge effect even when the wafer is under uniform loading.

(a) Theoretical Derivation

In this case, the loading is given and expressed as

$$q(r) = \sum_{m=0}^{\infty} c_{2m} r^{2m} \tag{4.43}$$

where c_{2m} is known.

We assume $u_z(r) = \sum_{m=0}^{\infty} a_{2m} r^{2m}$, where a_{2m} is unknown. The corresponding interface pressure for $u_z(r)$ is

$$p(r) = \frac{\sum_{m=0}^{\infty} b_{2m} r^{2m}}{\sqrt{1-\left(\frac{r}{a}\right)^2}} \tag{4.44}$$

where $b_{2m} = b_{2m}(a_{2m})$ and is dependent on a_{2m}.

From eqn. (4.33) and eqn. (4.44), we have

$$\left(\sum_{m=0}^{\infty} c_{2m} r^{2m} - D_{wafer} \sum_{m=2}^{\infty} (2m-2)^2 (2m)^2 a2m r^{2m-4}\right)\sqrt{1-\left(\frac{r}{a}\right)^2} = \sum_{m=0}^{\infty} b_{2m} r^{2m} \tag{4.45}$$

If $0 \le r < a$, we have binomial expansion for $\sqrt{1-\left(\frac{r}{a}\right)^2}$:

$$\sqrt{1-\left(\frac{r}{a}\right)^2} = \left\{1+\left[-\left(\frac{r}{a}\right)^2\right]\right\}^{\frac{1}{2}} = \sum_{m=0}^{\infty} d_{2m} r^{2m} \tag{4.46}$$

where d_{2m} is known.

To make it simple, we also can write $\sum_{m=0}^{\infty} c_{2m} r^{2m} - D_{wafer} \sum_{m=2}^{\infty} (2m-2)^2 (2m)^2 a2m r^{2m-4}$ as $\sum_{m=0}^{\infty} e_{2m} r^{2m}$; then, we have

$$\left(\sum_{m=0}^{\infty} e_{2m} r^{2m}\right)\left(\sum_{m=0}^{\infty} d_{2m} r^{2m}\right) = \sum_{m=0}^{\infty} b_{2m} r^{2m} \tag{4.47}$$

where $e_{2m} = e_{2m}(a_{2m})$ and $b_{2m} = b_{2m}(a_{2m})$. This equation will give a recurrence relationship for a_{2m}, ($m = 0, 1, 2, \ldots$). After all the a_{2m} are solved, the corresponding interface pressure can be obtained.

This method is valid for infinite series; for using finite series to obtain approximative solution, the following method may be used:

$$U(a_0, a_2, \ldots, a_{2m}) = \int_0^a [err(r)]^2 w(r) dr \tag{4.48}$$

Where

$$err(r) = \sum_{i=0}^{m} c_{2i} r^{2i} - D_{wafer} \sum_{i=2}^{m} (2i-2)^2 (2i)^2 a_{2i} r^{2i-4} - \frac{\sum_{i=0}^{m} b_{2i} r^{2i}}{\sqrt{1-\left(\frac{r}{a}\right)^2}} \tag{4.49}$$

$w(r) = \sqrt{1-\left(\frac{r}{a}\right)^2}$ - weight function

$$\frac{\partial U}{\partial a_i} = 0, \; (i = 0, 2, \ldots, 2m) \tag{4.49}$$

eqn. (4.49) will minimize the error caused by the approximation.

The above equations will give a matrix which can be solved for a_i, $(i = 0, 2, \ldots, 2m)$.

(b) Example I - 2nd Order Polynomial Approximation for Uniform Loading

Assume the displacement as $u_z(r) = a_0 + a_2 r^2$.

From eqn. (4.48), we have

$$U(a_0, a_2) = \int_0^a \left[q - \frac{E_{pad}}{\pi(1-\nu_{pad}^2)} \cdot \frac{\frac{a_0}{a} - 2a_2 a + 4a_2 a \frac{r^2}{a^2}}{\sqrt{1-\left(\frac{r}{a}\right)^2}} \right]^2 \sqrt{1-\left(\frac{r}{a}\right)^2} dr \tag{4.50}$$

$$\frac{\partial U}{\partial a_0} = 0 \text{ gives } a_0 = 2\frac{1-\nu_{pad}^2}{E_{pad}} qa \tag{4.51}$$

$$\frac{\partial U}{\partial a_2} = 0 \text{ gives } a_2 = -\frac{2}{3} \cdot \frac{1-\nu_{pad}^2}{E_{pad}} \cdot \frac{q}{a} \tag{4.52}$$

Thus, the shape of the deformed wafer is

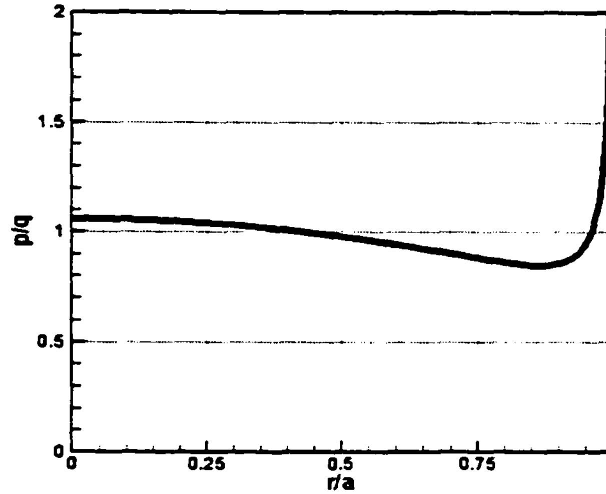

Fig. 4.15 Interface pressure distribution under uniform loading for second order polynomial approximation

$$u_z(r) = 2\frac{1-\nu_{pad}^2}{E_{pad}}qa - \frac{2}{3}\cdot\frac{1-\nu_{pad}^2}{E_{pad}}\cdot\frac{q}{a}\cdot r^2 \tag{4.53}$$

From this shape profile and eqn. (3.22), the interface pressure can be obtained and is shown in Fig. 4.15.

(c) Example II - 4th Order Polynomial Approximation for Uniform Loading

Assume the displacement as $u_z(r) = a_0 + a_2r^2 + a_4r^4$.

From eqn. (4.48), we have

$$U(a_0, a_2, a_4) =$$

$$= \int_0^a \left\{ q - 64D_{wafer}\cdot a_4 - \frac{E_{pad}}{\pi(1-\nu_{pad}^2)}\cdot\frac{1}{\sqrt{1-\left(\frac{r}{a}\right)^2}}\left[\left(\frac{a_0}{a} - 2a_2a - \frac{8}{9}a_4a^3\right) + \left(4a_2a - \frac{32}{9}a_4a^3\right)\left(\frac{r}{a}\right)^2 + \frac{64}{9}a_4a^3\left(\frac{r}{a}\right)^4\right]\right\}^2$$

$$\cdot\sqrt{1-\left(\frac{r}{a}\right)^2}\,dr \tag{4.54}$$

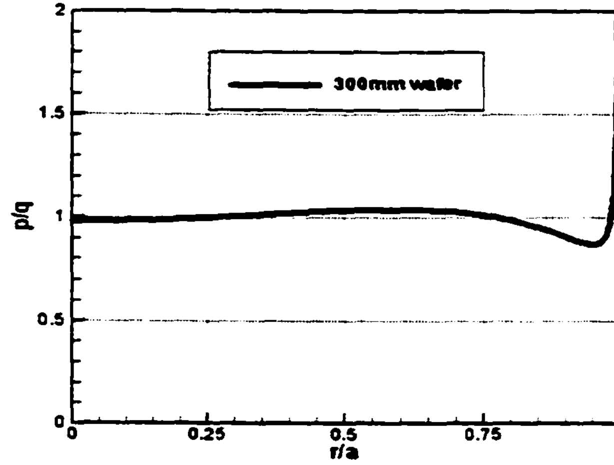

Fig. 4.16 Interface pressure distribution under uniform loading for fourth order polynomial approximation

$$\frac{\partial U}{\partial a_0} = 0 \text{ gives } \frac{\pi}{2}\left(\frac{a_0}{a}\right) + 64\pi\frac{1-\nu_{pad}^2}{E_{pad}}\cdot\frac{D_{wafer}}{a^3}\cdot(a_4a^3) = \pi q\frac{1-\nu_{pad}^2}{E_{pad}} \tag{4.55}$$

$$\frac{\partial U}{\partial a_2} = 0 \text{ gives } \frac{\pi}{2}(a_2a) + \left(\frac{4\pi}{9} - \frac{64}{3}\pi\cdot\frac{1-\nu_{pad}^2}{E_{pad}}\cdot\frac{D_{wafer}}{a^3}\right)(a_4a^3) = -\frac{\pi}{3}q\frac{1-\nu_{pad}^2}{E_{pad}} \tag{4.56}$$

$$\frac{\partial U}{\partial a_4} = 0 \text{ gives}$$

$$\left(72\pi\frac{1-\nu_{pad}^2}{E_{pad}}\cdot\frac{D_{wafer}}{a^3}\right)\left(\frac{a_0}{a}\right) + \left(\pi - 48\pi\frac{1-\nu_{pad}^2}{E_{pad}}\cdot\frac{D_{wafer}}{a^3}\right)(a_2a) +$$

$$\left[\frac{10}{9}\pi - \frac{1408}{15}\pi\left(\frac{1-\nu_{pad}^2}{E_{pad}}\cdot\frac{D_{wafer}}{a^3}\right) + 1152\pi^3\left(\frac{1-\nu_{pad}^2}{E_{pad}}\cdot\frac{D_{wafer}}{a^3}\right)^2\right](a_4a^3)$$

$$= q\left[18\pi^3\left(\frac{1-\nu_{pad}^2}{E_{pad}}\right)^2\frac{D}{a^3} - \frac{11}{15}\pi\frac{1-\nu_{pad}^2}{E_{pad}}\right] \tag{4.57}$$

Solving eqn. (4.55)~(4.57) for a_0, a_2 and a_4, we have the displacement profile $u_z(r) = a_0 + a_2r^2 + a_4r^4$ and its corresponding interface pressure distribution shown in Fig. (4.16).

One misconception in the design of carrier head is that uniform loading will lead to

uniform interface pressure. However, this is not true as shown in Fig. (4.15) and Fig. (4.16). Uniform loading will lead to nonuniform interface pressure and there will be a singularity at the wafer edge, which leads to edge effect.

d. Discussion and Conclusion

It is important to understand the relationships among wafer shape, wafer-pad interface pressure and loading for carrier design. As a preliminary study, those relationship are investigated under a simplified CMP configuration.

The model shows that under uniform pressure on backside of the wafer, there will still be edge effect due to the pressure variation at wafer-pad interface.

The model may also be used to investigate carrier head loading characteristics. From the measured removal rate on the wafer surface, the model can show the loading condition at the backside of the wafer and how the carrier head loads the wafer. A desired wafer removal rate profile can be obtained through the corresponding loading conditions on the backside of the wafer given by the model.

The model is considered in a simplified CMP system. The kinematic aspect of CMP from different polishers will influence the model prediction. Other important factors, such as retainer ring, will also influence the model result. As the understanding of those relationship is critical in carrier head design and CMP system control. It is necessary to further investigate it under more realistic CMP configurations.

4.5 Summary

Wafer scale model is based on the solution of indentation of elastic or viscoelastic half

space by a rigid frictionless polynomial punch in Chapter 3. The elastic solution is used to explain the edge effect. The elastic analytical solution is first verified against numerical results from Finite Element Method (FEM) simulation and then with experimental data. It shows wafer curvature, indentation depth and load will influence the interface pressure distribution throughout the wafer surface and it introduces parameters control as a potential avenue for completely eliminating the within wafer nonumiformity. Viscoelastic solution is used to explain within wafer nonuniformity, i.e., edge effect and wafer to wafer nonuniformity, i.e., removal rate decay for unconditioned pad. It shows the pressure distribution on the wafer surface is constantly changing due to viscoelastic deformation of the pad and the pressure on most part of the wafer except edge region drops during the polishing process. The relationships among wafer-pad interface pressure, wafer shape and wafer loading condition are also investigated. Model shows uniform loading on backside of the wafer will not give uniform pressure on front of the wafer. It is a preliminary investigation on carrier head design.

CHAPTER 5. DISHING, EROSION AND STEP HEIGHT REDUCTION

An analytical model for dishing and step height reduction is presented. The model is based on the assumption that at the feature scale, high areas experience higher pressure than low areas. The slurry is assumed to be Prestonian. The model delineates how dishing and step height reduction depend on slurry properties (selectivity and Preston's constants), pad characteristics (stiffness and bending ability), polishing conditions (pressure, relative velocity and overpolishing) and wafer surface geometry (linewidth, pitch and pattern density). Model predications are in good agreement with existing experimental observations. The present model facilitates understanding of the CMP process at the feature scale. Based on the model, design avenues for decreasing dishing and increasing the speed of step height reduction may be explored through the modification of appropriate parameters for slurry, pad and polishing conditions. It may also be used as a design tool for pattern layout to optimize the performance of the CMP process.

5.1 Literature Review

Overpolishing during metal CMP is required to remove all metallic residue on dielectric surface to guarantee the electrical isolation among circuits lines. However, during overpolishing, metal dishing and oxide erosion will occur, which instead of planarization, creates surface topography after CMP. Metal dishing will lead to line resistance deviation from its intended value and the resulting surface topography will lead to additional difficulty for the next level metal line fabrication (Pan et al 1999).

Step height reduction model is needed to accurately predict the required deposition film thickness and to reduce the cost of ownership through the reduction of film deposition, polishing time, labor and slurry usage, etc.

Based on the understanding of the CMP process, researchers have modeled the feature scale surface evolution in two different ways: one group (e.g., Runnels 1996 and Yao et al 2000) assumes there is a fluid layer between wafer and pad while the other group assumes direct wafer-pad contact. For the latter, there are also two kinds of models: one implies only high areas on the wafer feature have direct contact with pad and low areas are free of any loading and is not polished (e.g., Elbel et al 1998, Chekina 1998 and Saka et al 2001); the other assumes both high and low areas contact with pad (e.g., Gotkis et al 1998, Chen and Lee 1999, Vlassak 2001 and Saka et al 2001). The major assumptions in Chen and Lee (1999) model are: (a) the pressure difference between the high area and the low area is proportional to the step height; (b) higher area will experience higher pressure. Model shows step height is reduced exponentially with respect to time. However, the model does not show the effects of wafer feature geometry, such as linewidth, pitch and pattern density, and pad bending influence. Gotkis et al (1998) and Saka et al (2001) have the same dishing model and it only considers the case when the removal rates on metal region and on dielectric region are the same. The model cannot describe the dishing development process and cannot capture the influence of feature geometry (e.g., linewidth, pitch and pattern density) and pad properties (e.g., pad stiffness and bending ability). Vlassak (2001) models the pad as half space and the equations have to be numerically solved. Some researchers also consider pad asperities in the model (e.g., Nguyen et al 2000 and Vlassak 2001).

The physical insight for feature scale model based on direct wafer-pad contact is given

by Warnock (1991) and Gotkis et al (1998). Warnock points out that depending on the pad flexibility, polishing rate at any given point is affected by its surrounding topography, i.e., high area will experience higher removal rate because of higher pressure at that point. Gotkis et al points out the mechanism of corner rounding: protruding corners are overloaded and are convexly rounded while recessed corners are underloaded and is concavely rounded. Corner rounding is governed by pad's ability to adjust itself to the wafer surface topography and is determined by pad hardness, loading condition and the relative motion.

We classify the direct wafer-pad contact into three regions depending on pad's flexibility and wafer's surface topography:

- Pad does not touch the lower area
- pad touches lower area in some regions and does not touch in other regions
- pad touches both upper and lower areas

In the present work, we account for pad contact with both high and low areas, and attempt to develop a simply analytical model for dishing and step height reduction that is suitable for incorporation within design rules for the CMP process. We assume pad behaves like elastic foundation or linear springs with certain bending ability while influences of pad viscosity and pad asperity are ignored.

5.2 Theoretical Derivation

Major assumptions in the model are:

- Pad is assumed to deform like an elastic foundation (a set of linear elastic springs);
- Force redistribution due to pad bending is proportional to dishing height;

- The material removal rate for metal interconnect and dielectric material follows Preston's equation with different Preston's constants;
- Wafer and pad are in contact at any point of the interface;
- The same feature pattern is repeated throughout the wafer surface.

From Preston's equation ($dH/dt = K \cdot P \cdot V$), we have

$$\frac{dY_{di}}{dt} = K_{di}\{k[H-(Y-Y_{di})]\}V \tag{5.1}$$

$$\frac{dY_{met}}{dt} = K_{met}\{k[H-(Y-Y_{met})]\}V \tag{5.2}$$

The pad thickness in the dielectric region at time t is $Y(t)-Y_{di}(t)$. At this moment, the deformation of the pad corresponding to its original undeformed thickness H is $H-(Y-Y_{di})$. To cause this much of pad deformation, the pressure should be $k[H-(Y-Y_{di})]$. The total area in the dielectric region with unit thickness is $(b-a)\cdot 1$. Because the pressure on the dielectric region is the same, the total force on this region is $\{k[H-(Y-Y_{di})]\}\cdot[(b-a)\cdot 1]$. Similarly, the total force on the metal interconnect region is $\{k[H-(Y-Y_{met})]\}\cdot(a\cdot 1)$. In CMP, constant downforce is used and we have

$$\{k[H-(Y-Y_{di})]\}\cdot[(b-a)\cdot 1]+\{k[H-(Y-Y_{met})]\}\cdot(a\cdot 1) = P\cdot(b\cdot 1) \tag{5.3}$$

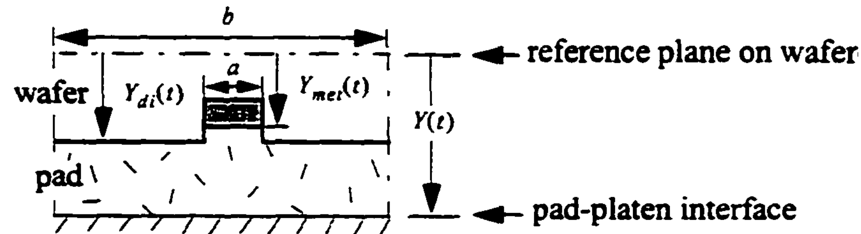

Fig. 5.1 Schematic picture of the model setup

Due to the pad bending, there is a force redistribution, i.e., the force will be higher in the dielectric region and smaller in the metal region. The three new governing equations are:

$$\frac{dY_{di}}{dt} = K_{di}\left\{k[H-(Y-Y_{di})] + \frac{\Delta F}{b-a}\right\}V \tag{5.4}$$

$$\frac{dY_{met}}{dt} = K_{met}\left\{k[H-(Y-Y_{met})] - \frac{\Delta F}{a}\right\}V \tag{5.5}$$

$$\{k[H-(Y-Y_{di})]\cdot[(b-a)\cdot 1] + \Delta F\} + \{k[H-(Y-Y_{met})]\cdot(a\cdot 1) - \Delta F\} = P\cdot(b\cdot 1) \tag{5.6}$$

Solving eqn. (5.6) for $Y(t)$, we have

$$Y = \left(1-\frac{a}{b}\right)Y_{di} + \frac{a}{b}Y_{met} + \left(H-\frac{P}{k}\right) \tag{5.7}$$

Substituting eqn. (5.7) into eqn. (5.4) and eqn. (5.5), we have

$$\frac{dY_{di}}{dt} = K_{di}Vk\left[-\frac{a}{b}Y_{di} + \frac{a}{b}Y_{met} - \frac{1}{k}\left(P + \frac{\Delta F}{b-a}\right)\right] \tag{5.8}$$

$$\frac{dY_{met}}{dt} = K_{met}Vk\left[\left(1-\frac{a}{b}\right)Y_{di} - \left(1-\frac{a}{b}\right)Y_{met} - \frac{1}{k}\left(P-\frac{\Delta F}{a}\right)\right] \tag{5.9}$$

From the second assumption, we have

$$\Delta F = \alpha(Y_{di} - Y_{met}) \tag{5.10}$$

where α is bending factor. It is zero if there is no pad bending.

Putting eqn. (5.10) into eqn. (5.8) and eqn. (5.9), we have

$$\frac{dY_{di}}{dt} = K_{di}Vk\left\{\left[-\frac{a}{b} - \frac{\alpha}{kc}\right](Y_{di} - Y_{met}) - \frac{P}{k}\right\} \tag{5.11}$$

$$\frac{dY_{met}}{dt} = K_{met}Vk\left\{\left(\frac{c}{b} + \frac{\alpha}{ka}\right)(Y_{di} - Y_{met}) - \frac{P}{k}\right\} \tag{5.12}$$

Where $c = b-a$

eqn. (5.11) and eqn. (5.12) imply that the removal rate in a region is not only governed by the topography of the considered region, but also decided by the topography of its surrounding area. It means elevated features will be under higher pressure than its surrounding area and lower areas will under lower pressure or be shadowed by the surrounding higher areas.

Rewriting eqn. (5.11) and eqn. (5.12), we have

$$\frac{dY_{di}}{dt} = C_1 Y_{di} + C_2 Y_{met} + C_3 \tag{5.13}$$

$$\frac{dY_{met}}{dt} = C_4 Y_{di} + C_5 Y_{met} + C_6 \tag{5.14}$$

Where

$C_1 = K_{di} Vk\left(-\frac{a}{b} - \frac{\alpha}{kc}\right)$, $C_2 = -C_1$, $C_3 = K_{di} Vk\left(-\frac{P}{k}\right)$, $C_4 = K_{met} Vk\left(\frac{c}{b} + \frac{\alpha}{ka}\right)$, $C_5 = -C_4$ and $C_6 = K_{met} Vk\left(-\frac{P}{k}\right)$

Using Laplace transform on eqn. (5.13) and eqn. (5.14), we have

$$s\tilde{Y}_{di} - Y_{di}(0) = C_1 \tilde{Y}_{di} + C_2 \tilde{Y}_{met} + \frac{C_3}{s} \tag{5.15}$$

$$s\tilde{Y}_{met} - Y_{met}(0) = C_4 \tilde{Y}_{di} + C_5 \tilde{Y}_{met} + \frac{C_6}{s} \tag{5.16}$$

In eqn. (5.15) and eqn. (5.16), the unknowns are $\tilde{Y}_{met}$ and $\tilde{Y}_{di}$. Those two equations can be rewritten in matrix form as

$$\begin{bmatrix} -C_2 & s - C_1 \\ s - C_5 & -C_4 \end{bmatrix} \begin{bmatrix} \tilde{Y}_{met} \\ \tilde{Y}_{di} \end{bmatrix} = \begin{bmatrix} \frac{C_3}{s} + Y_{di}(0) \\ \frac{C_6}{s} + Y_{met}(0) \end{bmatrix} \tag{5.17}$$

Solving the matrix eqn. (5.17) for $\tilde{Y}_{met}$ and $\tilde{Y}_{di}$, we have

$$\tilde{Y}_{met} = \frac{Y_{met}(0)s^2 + [C_6 + C_4 Y_{di}(0) - C_1 Y_{met}(0)]s + (C_3C_4 - C_1C_6)}{s[(s - C_1)(s - C_5) - C_2C_4]} \tag{5.18}$$

$$\tilde{Y}_{di} = \frac{Y_{di}(0)s^2 + [C_3 + C_2 Y_{met}(0) - C_5 Y_{di}(0)]s + (C_2C_6 - C_3C_5)}{s[(s - C_1)(s - C_5) - C_2C_4]} \tag{5.19}$$

From inverse Laplace transform, we have

$$Y_{met}(t) = \frac{\left\{K_{met}Vk\left(-\frac{P}{k}\right) + K_{met}Vk\left(\frac{c}{b} + \frac{\alpha}{ka}\right)Y_{di}(0) - K_{di}Vk\left(-\frac{a}{b} - \frac{\alpha}{kc}\right)Y_{met}(0) - \frac{K_{di}K_{met}(Vk)\left(-\frac{P}{k}\right)\left[1 + \frac{\alpha}{k}\left(\frac{1}{a} + \frac{1}{c}\right)\right]}{K_{di}\left(\frac{a}{b} + \frac{\alpha}{kc}\right) + K_{met}\left(\frac{c}{b} + \frac{\alpha}{ka}\right)}\right\}}{\left[K_{di}\left(\frac{a}{b} + \frac{\alpha}{kc}\right) + K_{met}\left(\frac{c}{b} + \frac{\alpha}{ka}\right)\right]Vk} +$$

$$\frac{K_{di}K_{met}(Vk)\left(-\frac{P}{k}\right)\left[1 + \frac{\alpha}{k}\left(\frac{1}{a} + \frac{1}{c}\right)\right]}{K_{di}\left(\frac{a}{b} + \frac{\alpha}{kc}\right) + K_{met}\left(\frac{c}{b} + \frac{\alpha}{ka}\right)}t +$$

$$\left(Y_{met}(0) - \frac{\left\{K_{met}Vk\left(-\frac{P}{k}\right) + K_{met}Vk\left(\frac{c}{b} + \frac{\alpha}{ka}\right)Y_{di}(0) - K_{di}Vk\left(-\frac{a}{b} - \frac{\alpha}{kc}\right)Y_{met}(0) - \frac{K_{di}K_{met}(Vk)\left(-\frac{P}{k}\right)\left[1 + \frac{\alpha}{k}\left(\frac{1}{a} + \frac{1}{c}\right)\right]}{K_{di}\left(\frac{a}{b} + \frac{\alpha}{kc}\right) + K_{met}\left(\frac{c}{b} + \frac{\alpha}{ka}\right)}\right\}}{\left[K_{di}\left(\frac{a}{b} + \frac{\alpha}{kc}\right) + K_{met}\left(\frac{c}{b} + \frac{\alpha}{ka}\right)\right]Vk}\right) \cdot$$

$$\exp\left\{-\left[K_{di}\left(\frac{a}{b} + \frac{\alpha}{kc}\right) + K_{met}\left(\frac{c}{b} + \frac{\alpha}{ka}\right)\right]Vkt\right\} \tag{5.20}$$

$$Y_{di}(t) = \frac{\left\{K_{di}Vk\left(-\frac{P}{k}\right) - K_{di}Vk\left(-\frac{a}{b} - \frac{\alpha}{kc}\right)Y_{met}(0) + K_{met}Vk\left(\frac{c}{b} + \frac{\alpha}{ka}\right)Y_{di}(0) - \frac{K_{di}K_{met}(Vk)\left(-\frac{P}{k}\right)\left[1 + \frac{\alpha}{k}\left(\frac{1}{a} + \frac{1}{c}\right)\right]}{K_{di}\left(\frac{a}{b} + \frac{\alpha}{kc}\right) + K_{met}\left(\frac{c}{b} + \frac{\alpha}{ka}\right)}\right\}}{\left[K_{di}\left(\frac{a}{b} + \frac{\alpha}{kc}\right) + K_{met}\left(\frac{c}{b} + \frac{\alpha}{ka}\right)\right]Vk} +$$

$$\frac{K_{di}K_{met}(Vk)\left(-\frac{P}{k}\right)\left[1+\frac{\alpha}{k}\left(\frac{1}{a}+\frac{1}{c}\right)\right]}{K_{di}\left(\frac{a}{b}+\frac{\alpha}{kc}\right)+K_{met}\left(\frac{c}{b}+\frac{\alpha}{ka}\right)}t+$$

$$\left(Y_{di}(0)-\frac{\left\{K_{di}Vk\left(-\frac{P}{k}\right)-K_{di}Vk\left(-\frac{a}{b}-\frac{\alpha}{kc}\right)Y_{met}(0)+K_{met}Vk\left(\frac{c}{b}+\frac{\alpha}{ka}\right)Y_{di}(0)-\frac{K_{di}K_{met}(Vk)\left(-\frac{P}{k}\right)\left[1+\frac{\alpha}{k}\left(\frac{1}{a}+\frac{1}{c}\right)\right]}{K_{di}\left(\frac{a}{b}+\frac{\alpha}{kc}\right)+K_{met}\left(\frac{c}{b}+\frac{\alpha}{ka}\right)}\right\}}{\left[K_{di}\left(\frac{a}{b}+\frac{\alpha}{kc}\right)+K_{met}\left(\frac{c}{b}+\frac{\alpha}{ka}\right)\right]Vk}\right)\cdot$$

$$\exp\left\{-\left[K_{di}\left(\frac{a}{b}+\frac{\alpha}{kc}\right)+K_{met}\left(\frac{c}{b}+\frac{\alpha}{ka}\right)\right]Vkt\right\} \tag{5.21}$$

eqn. (5.21) describes the erosion process for the dielectric region.

From eqn. (5.20) and eqn. (5.21), we can express the local dishing as

$$D(t) = Y_{di}(t)-Y_{met}(t)$$

$$= \frac{K_{met}-K_{di}}{K_{di}\left(\frac{a}{b}+\frac{\alpha}{kc}\right)+K_{met}\left(\frac{c}{b}+\frac{\alpha}{ka}\right)}\cdot\frac{P}{k}+$$

$$\left\{[Y_{di}(0)-Y_{met}(0)]-\frac{K_{met}-K_{di}}{K_{di}\left(\frac{a}{b}+\frac{\alpha}{kc}\right)+K_{met}\left(\frac{c}{b}+\frac{\alpha}{ka}\right)}\cdot\frac{P}{k}\right\}\exp\left\{-\left[K_{di}\left(\frac{a}{b}+\frac{\alpha}{kc}\right)-K_{met}\left(\frac{c}{b}+\frac{\alpha}{ka}\right)\right]Vkt\right\} \tag{5.22}$$

eqn. (5.22) shows dishing is influenced by many parameters. The following section will discuss about some special cases and how those parameters influence dishing.

5.3 Special Cases

a. $Y_{met}(0) = Y_{di}(0)$ **and** $K_{met} = K_{di} = K$

In this case, non-selectivity slurry is used and the initial step height is zero.

eqn. (5.22) becomes $D(t) = 0$, which means no dishing happens.

eqn. (5.20) becomes $Y_{met}(t) = Y_{met}(0) - KPVt$

eqn. (5.21) becomes $Y_{di}(t) = Y_{di}(0) - KPVt$

eqn. (5.20) and eqn. (5.21) shows the removal rates in metal region and in dielectric region are the same and follow the Preston's relationship.

b. $Y_{met}(0) = Y_{di}(0)$ **and** $K_{met} \neq K_{di}$

In this case, slurry has selectivity and initial step height is zero.

eqn. (5.22) becomes

$$D(t) = \frac{K_{met} - K_{di}}{K_{di}\left(\frac{a}{b} + \frac{\alpha}{kc}\right) + K_{met}\left(\frac{c}{b} + \frac{\alpha}{ka}\right)} \cdot \frac{P}{k} \cdot \left(1 - \exp\left\{-\left[K_{di}\left(\frac{a}{b} + \frac{\alpha}{kc}\right) + K_{met}\left(\frac{c}{b} + \frac{\alpha}{ka}\right)\right]Vkt\right\}\right) \tag{5.25}$$

eqn. (5.20) becomes

$$Y_{met}(t) = Y_{met}(0) - \frac{K_{met}\left(\frac{P}{k}\right)}{K_{di}\left(\frac{a}{b} + \frac{\alpha}{kc}\right) + K_{met}\left(\frac{c}{b} + \frac{\alpha}{ka}\right)} + \frac{K_{met}K_{di}\left(\frac{P}{k}\right)\left[1 + \frac{\alpha}{k}\left(\frac{1}{a} + \frac{1}{c}\right)\right]}{\left[K_{di}\left(\frac{a}{b} + \frac{\alpha}{kc}\right) + K_{met}\left(\frac{c}{b} + \frac{\alpha}{ka}\right)\right]^2} - \frac{K_{met}K_{di}Vk\left(\frac{P}{k}\right)\left[1 + \frac{\alpha}{k}\left(\frac{1}{a} + \frac{1}{c}\right)\right]}{K_{di}\left(\frac{a}{b} + \frac{\alpha}{kc}\right) + K_{met}\left(\frac{c}{b} + \frac{\alpha}{ka}\right)}t$$

$$+ \left\{\frac{K_{met}\left(\frac{P}{k}\right)}{K_{di}\left(\frac{a}{b} + \frac{\alpha}{kc}\right) + K_{met}\left(\frac{c}{b} + \frac{\alpha}{ka}\right)} - \frac{K_{met}K_{di}\left(\frac{P}{k}\right)\left[1 + \frac{\alpha}{k}\left(\frac{1}{a} + \frac{1}{c}\right)\right]}{\left[K_{di}\left(\frac{a}{b} + \frac{\alpha}{kc}\right) + K_{met}\left(\frac{c}{b} + \frac{\alpha}{ka}\right)\right]^2}\right\}\exp\left\{-\left[K_{di}\left(\frac{a}{b} + \frac{\alpha}{kc}\right) + K_{met}\left(\frac{c}{b} + \frac{\alpha}{ka}\right)\right]Vkt\right\} \tag{5.26}$$

eqn. (5.21) becomes

$$Y_{di}(t) = Y_{di}(0) - \frac{K_{di}\left(\frac{P}{k}\right)}{K_{di}\left(\frac{a}{b} + \frac{\alpha}{kc}\right) + K_{met}\left(\frac{c}{b} + \frac{\alpha}{ka}\right)} + \frac{K_{met}K_{di}\left(\frac{P}{k}\right)\left[1 + \frac{\alpha}{k}\left(\frac{1}{a} + \frac{1}{c}\right)\right]}{\left[K_{di}\left(\frac{a}{b} + \frac{\alpha}{kc}\right) + K_{met}\left(\frac{c}{b} + \frac{\alpha}{ka}\right)\right]^2} - \frac{K_{met}K_{di}Vk\left(\frac{P}{k}\right)\left[1 + \frac{\alpha}{k}\left(\frac{1}{a} + \frac{1}{c}\right)\right]}{K_{di}\left(\frac{a}{b} + \frac{\alpha}{kc}\right) + K_{met}\left(\frac{c}{b} + \frac{\alpha}{ka}\right)}t$$

$$+ \left\{\frac{K_{di}\left(\frac{P}{k}\right)}{K_{di}\left(\frac{a}{b} + \frac{\alpha}{kc}\right) + K_{met}\left(\frac{c}{b} + \frac{\alpha}{ka}\right)} - \frac{K_{met}K_{di}\left(\frac{P}{k}\right)\left[1 + \frac{\alpha}{k}\left(\frac{1}{a} + \frac{1}{c}\right)\right]}{\left[K_{di}\left(\frac{a}{b} + \frac{\alpha}{kc}\right) + K_{met}\left(\frac{c}{b} + \frac{\alpha}{ka}\right)\right]^2}\right\}\exp\left\{-\left[K_{di}\left(\frac{a}{b} + \frac{\alpha}{kc}\right) + K_{met}\left(\frac{c}{b} + \frac{\alpha}{ka}\right)\right]Vkt\right\} \tag{5.27}$$

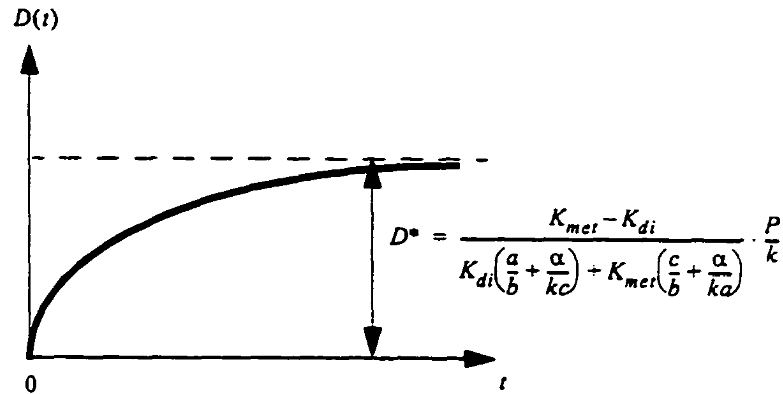

Fig. 5.2 Dishing vs. overpolishing

The following part shows how dishing in eqn. (5.25) is influenced by various factors related to CMP system and wafer surface geometry.

(a) $D = D(t)$

Model prediction trend is shown in Fig. 5.2. Two things happens: one is that even if there is an absolute flat surface at the beginning, dishing will still happen because of the selectivity; the other is that the dishing will reach a limit and cannot grow infinitely.

Fig. 5.3 explains the limit. From Preston's model, removal rate at metal region and dielectric region are almost the same at this stage and the dishing reaches the limit.

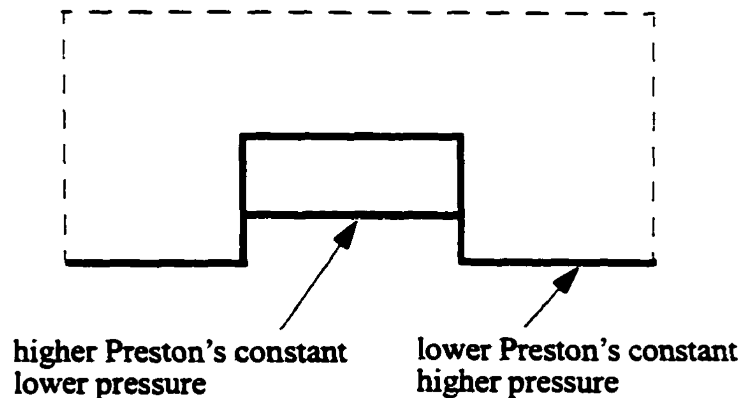

Fig. 5.3 near "steady-state" as $t \rightarrow \infty$

(b) $D = D(a)$ and $PD = const$

It is widely observed that dishing will increase with respect to linewidth. The model predicts the similar trend as shown in Fig. 5.4.

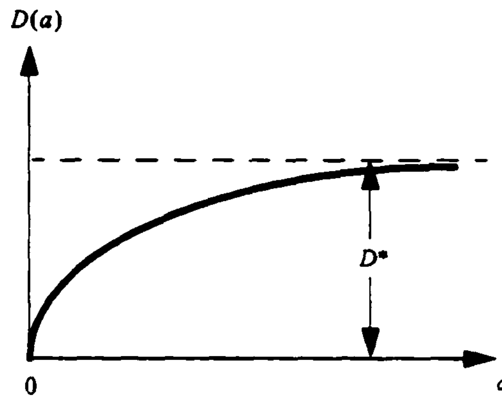

Fig. 5.4 Dishing vs. linewidth

Where $D^* = \frac{K_{met} - K_{di}}{[K_{di} \cdot PD + K_{met}(1 - PD)]} \cdot \frac{P}{k} \cdot (1 - \exp\{-[K_{di} \cdot PD + K_{met}(1 - PD)]Vkt\})$

(c) $D = D(PD)$ and $b = const$

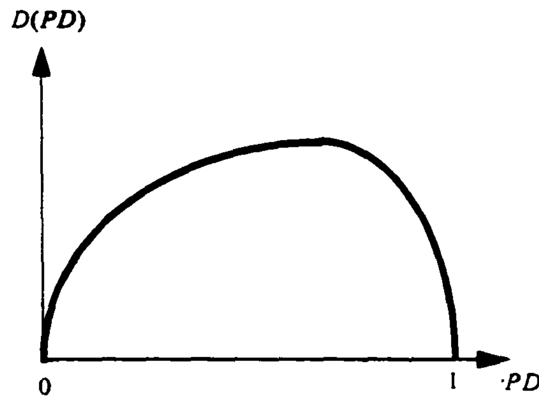

Fig. 5.5 Dishing vs. Pattern Density

Fig. 5.5 shows the model prediction. When pattern density is unity (all wafer surface is covered by metal), or zero (all wafer surface is dielectric), dishing is zero. When non-selecticity is used, dishing is also zero.

Through the changes of slurry chemistry (e.g., selectivity), processing conditions (pressure, velocity and overpolishing) and pad properties (e.g., bending ability, rigidity), dishing can be controlled at certain pattern density by the shift of the curve positions.

(d) $D = D(k)$

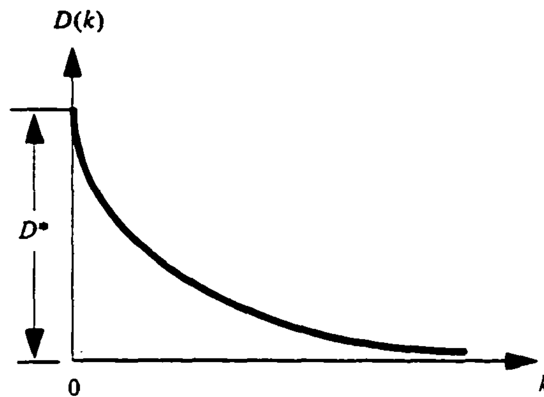

Fig. 5.6 Dishing vs. Pad Stiffness

Where $D^{*} = (K_{met} - K_{di})PVt$

Model prediction in Fig. 5.6 shows high pad stiffness will reduce dishing. Depending on its value, k can have a large influence or small influence on dishing.

(e) $D = D(P)$

Model prediction in Fig. 5.7 shows linear dependence between dishing and pressure. From the curve, lower pressure is good for lower dishing.

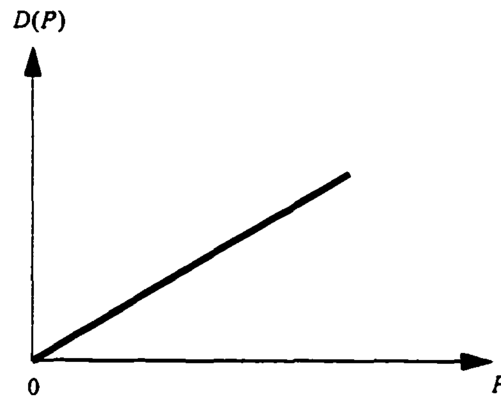

Fig. 5.7 Dishing vs. Pressure

(f) $D = D(V)$

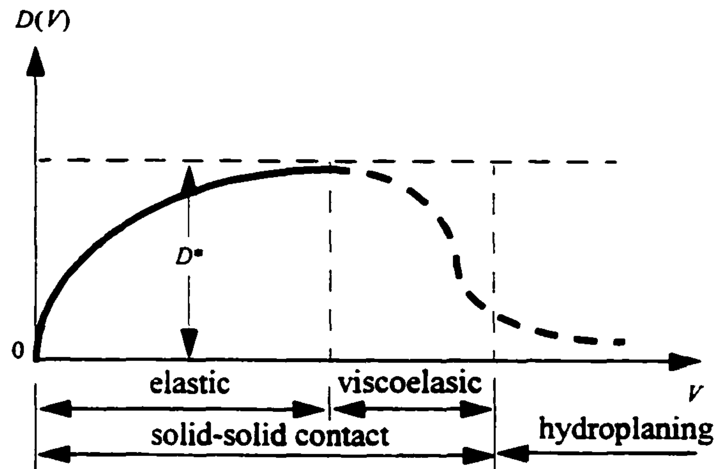

Fig. 5.8 Dishing vs. Velocity

Where $D^{*} = \dfrac{K_{met} - K_{di}}{K_{di}\left(\frac{a}{b} + \frac{\alpha}{kc}\right) + K_{met}\left(\frac{c}{b} + \frac{\alpha}{ka}\right)} \cdot \frac{P}{k}$

Model prediction is shown in Fig. 5.8 in solid line. Dashed-line is the possible trend and is not included in the model. From the model, dishing will increase with respect to line-width.

Model prediction is only valid in the elastic solid-solid contact region. Under higher velocity, viscosity of the pad will influence the dishing in the following way: As the pad passes from a high area to a low area, it cannot deform immediately due to viscosity so that less pressure is on the low area. On the other hand, as the pad passes from a low area to a high area, it cannot conform immediately the high area so that a higher pressure is on the high area. From this prospective, viscosity of pad improves the planarization efficiency and lower the dishing. Under even higher velocity (i.e., hydorplaning region), there will be a slurry layer which seperates wafer and pad.

(g) $D = D(S)$

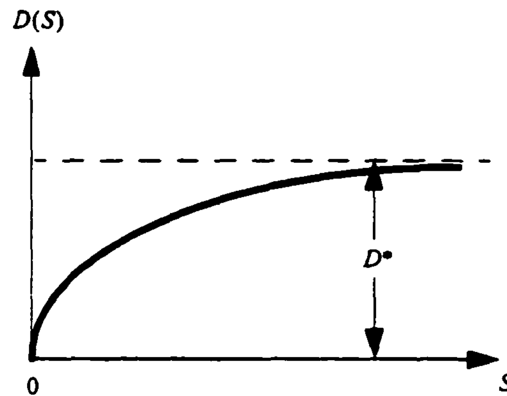

Fig. 5.9 Dishing vs. Selectivity

Where $D^* = \dfrac{1}{\dfrac{c}{b} + \dfrac{\alpha}{ka}} \cdot \dfrac{P}{k} \cdot \left(1 - \exp\left\{-\left[K_{di}\left(\dfrac{a}{b} + \dfrac{\alpha}{kc}\right) + K_{met}\left(\dfrac{c}{b} + \dfrac{\alpha}{ka}\right)\right]Vkt\right\}\right)$

Model prediction in Fig. 5.9 shows high selectivity slurry will increase dishing. At very high value, its influence will be small.

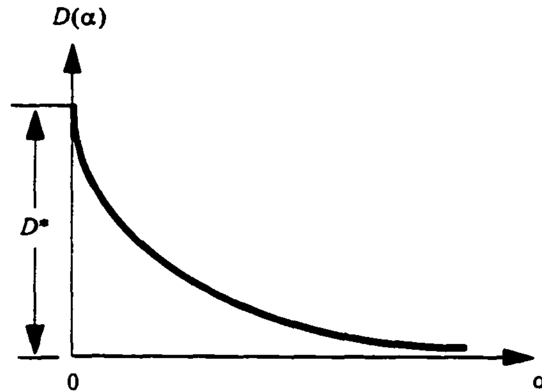

Fig. 5.10 Dishing vs. Pad Bending Ability

(h) $D = D(\alpha)$

Where $D^* = \frac{K_{met} - K_{di}}{K_{di} \cdot \frac{a}{b} + K_{met} \cdot \frac{c}{b}} \cdot \frac{P}{k} \cdot \left\{ 1 - \exp\left[-\left(K_{di} \cdot \frac{a}{b} + K_{met} \cdot \frac{c}{b} \right) Vkt \right] \right\}$

Model prediction in Fig. 5.10 shows high α value will reduce dishing.

Bending factor α describes pad bending ability. Higher α value means more difficult for pad to bend into the metal region. From the figure, higher α valure is good for lowering dishing.

Bending factor α is governed by the pad surface microstructure which is decided by the pad manufacturing processes. We can have the following conclusion about how to lower dishing:

- cross-linked fiber structure is better than free nap structure
- cellular solid structure is better than cross-linked fiber structure
- closed-cell structure is better than open-cell structure

- For closed-cell and open-cell mixture surface structure, higher percentage of closed-cell structure is better; however, if the closed-cell percentage is too high, the slurry delivery by the open-cell structure will be a problem
- solid structure without voids and naps is the best; however, it will not fulfill the other requirement of CMP (e.g., slurry delivery)

c. $Y_{met}(0) \neq Y_{di}(0)$ **and** $K_{met} = K_{di} = K$

In this case, non-selectivity slurry is used and there is an initial step height.

eqn. (5.18) becomes

$$D(t) = [Y_{di}(0) - Y_{met}(0)]\exp\left\{-K\left[1 + \frac{\alpha}{k}\left(\frac{1}{a} + \frac{1}{c}\right)\right]Vkt\right\} \quad (5.28)$$

Model prediction in Fig. (5.28) shows the planarization ability of CMP and step height is reduced exponentially with respect to time.

eqn. (5.20) becomes

$$Y_{met}(t) = \frac{\left(\frac{c}{b} + \frac{\alpha}{ka}\right)Y_{di}(0) + \left(\frac{a}{b} + \frac{\alpha}{kc}\right)Y_{met}(0)}{1 + \frac{\alpha}{k}\left(\frac{1}{a} + \frac{1}{c}\right)} - KPVt$$

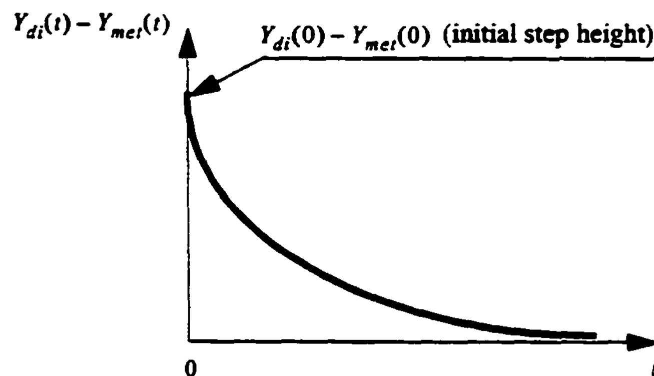

Fig. 5.8 Step height reduction in CMP

$$+\frac{\frac{c}{b}+\frac{\alpha}{ka}}{1+\frac{\alpha}{k}\left(\frac{1}{a}+\frac{1}{c}\right)}[Y_{met}(0)-Y_{di}(0)]\exp\left\{-K\left[1+\frac{\alpha}{k}\left(\frac{1}{a}+\frac{1}{c}\right)\right]Vkt\right\} \quad (5.29)$$

eqn. (5.21) becomes

$$Y_{di}(t) = \frac{\left(\frac{c}{b}+\frac{\alpha}{ka}\right)Y_{di}(0)+\left(\frac{a}{b}+\frac{\alpha}{kc}\right)Y_{met}(0)}{1+\frac{\alpha}{k}\left(\frac{1}{a}+\frac{1}{c}\right)}-KPVt$$

$$+\frac{\frac{a}{b}+\frac{\alpha}{kc}}{1+\frac{\alpha}{k}\left(\frac{1}{a}+\frac{1}{c}\right)}[Y_{di}(0)-Y_{met}(0)]\exp\left\{-K\left[1+\frac{\alpha}{k}\left(\frac{1}{a}+\frac{1}{c}\right)\right]Vkt\right\} \quad (5.30)$$

5.4 Comparison with Experimental Data

a. Dishing vs. Time

The experimental data for copper dishing (Pan et al 1999) is used in the simulation and the experiment is carried out on patterned wafers using Mirra CMP system with three polish platens and an In-Situ-Rate-MonitorTM (ISRM) on each platen. The model predictions are compared to experimental data by fitting the date point corresponding to the dishing limit to the model. Two experimental data are chosen to obtain k and α values. The comparison of model prediction with experimental data is shown in Fig. 5.12. As observed in the experiments, dishing will increase with overpolishing. In the simulation, the following parameters are specified:

- selectivity is 5
- pressure is 20 kPa
- $k = 8.027 \times 10^{10}$ N/m^3 and $\alpha = 2.16\times10^{6}$ N/m

A simple way to calculate Young's Modulus of pad is $E = k \cdot h$, where h is the thick-

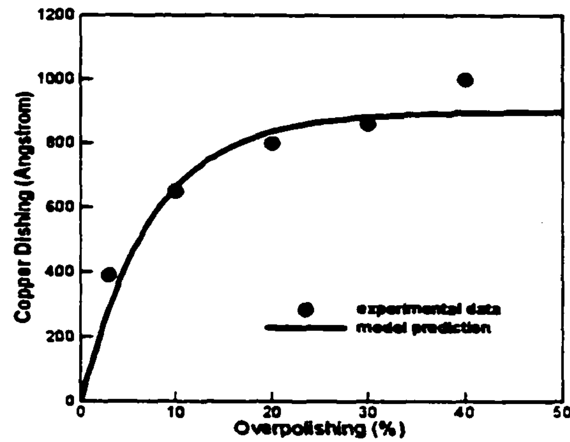

Fig. 5.12 Model prediction compared with experimental data
for dishing vs. overpolishing curve

ness of pad. If we choose $h = 1.2mm$, we have Young's Modulus of pad to be $96MPa$, which is within commonly-used pad's Young's Modulus range ($1MPa - 200MPa$).

b. Dishing vs. Line Width

The same set of experimental data (Pan et al 1999) and k, α values are used in this simulation. The comparison is shown in Fig. 5.13, which shows larger linewidth leads to larger dishing.

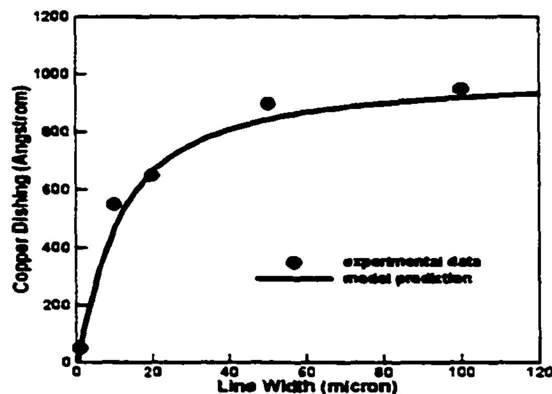

Fig. 5.13 Model prediction compared with experimental data
for dishing vs. overpolishing linewidth

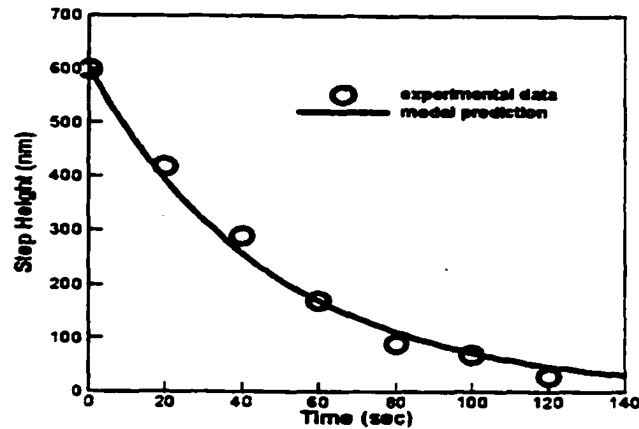

Fig. 5.14 Model prediction compared with experimental data for step height vs. time

c. Step Height vs. Time

In this simulation, we use the experimental data from Stavreva et al (1997) and in the experiments, Cu CMP is carried out by a Presi Mecapol E 460 polishing machine with a diamond conditioning tool and a perforated Rodel IC 1000 / SUBA IV stacked pad. One of the experimental data is chosen to obtain α value. Model prediction is compared with experimental data in Fig. 5.14, which shows step height is decreasing with respect to time. In the simulation, the following parameters are specified:

- removal rate is 450 nm/min
- pressure is 21.9 kPa
- pattern density is 0.5
- $k = 5.213 \times 10^{9}$
- $\alpha = 1.403 \times 10^{5}$

5.5 Summary

We find almost every part of a CMP system will influence dishing and step height reduction. The factors considered in the model are:

- slurry (selectivity and Preston's constant)
- pad (stiffness, bending ability and surface microstructure)
- polishing condition (pressure, relative velocity and overpolishing time)
- wafer surface geometry (linewidth, pitch and pattern density)

The model points out how to reduce dishing or increase the speed of step-height reduction by controlling those factors. Model may also be used in STI application.

There are many things to be done to make the model prediction more accurate, such as considering non-Prestonian slurry, viscoelastic deformation of pad and feature corner rounding, etc.

CHAPTER 6. CONCLUSIONS AND FUTURE WORK

6.1 Conclusions

Although the polishing process has existed for a long time, its mechanism is still poorly understood.

In Chemical Mechanical Polishing, there is lack of understanding about how the chemical part and the mechanical part interact together. Pure chemical part is only wet etching and pure mechanical part is only dry polishing. It is well-known that wet etching or dry polishing will not give the required surface finishing and planarity in CMP. In the mechanical part, temperature rise during polishing may be a big factor for CMP performance because pad is made of polymer, a temperature sensitive material and chemical reactions are also sensitive to temperature.

There is also lack of integration of models in different scales in CMP. For example, feature scale, die scale and wafer scale models should be related to each other; but there is not much investigation on this.

In each scale, there are lots of work to be done, e.g., when solid-solid contact is assumed in feature scale, contact mechanics has to be used. Yet, there are only limited numbers of solutions with idealized configuration available in contact mechanics. More fundamental research is needed.

For the modeling and simulation, maybe one of the most difficult things is to find experimental data to verify the model. In the experiments, not all the parameters are measured and people who carry out the experiments only measure the factors they think relevant. As the cost of experiments is high and the experiments have to be carried out by experienced techni-

cans, close cooperation between experimentalists and theorists is required. Comparing with experiments by try-and-error, modeling verification experiments is much more effective for the process improvements.

In CMP experiments, there is lack of measurement standard. For example, different mapping schemes are used in measuring WIWNU. The important information, such as where the measured points are, are often difficult to obtain.

In CMP, it is well-known that pattern density and linewidth will influence the removal rate. Test wafer made from MIT mask has different pattern density and linewidth even in the same die. To use this kind of test wafers to investigate the influence of pattern density and linewidth will give misleading results. A better mask design is needed for CMP experiments.

Not much research has been done on the model integration with other IC manufacturing processes, such as CVD and PVD. Such process models are needed to reduce cost of ownership and increase manufacturing efficiency. For example, an accurate CMP model will give the exact thickness of the overburden required and an accurate CVD model will give the conditions to carry it out. It means less material, time, labor needed to carry out deposition and less film thickness is needed to be removed in CMP with reduction of process time, labor and savings of slurry, pad, etc

Because of the complexity of CMP process, there is tremendous work to be done. Even limited results will aid the process improvement. The insight gained from the investigation will lead to better design rules that optimize CMP and the whole IC manufacturing processes.

6.1.1 Material removal mechanism

In the present model, we assume perfectly-plastic deformation of the wafer surface material happens in front of the traveling abrasives. This assumption is based on: (a) nanoindentation experimental observations; (b) softer wafer surface layer due to chemical reactions in oxide CMP. In the nano-plowing test, material cannot be removed by a single pass which leads to wear assumption built into the model.

Based on plasticity assumption, sharp particle behaves very differently compared with spherical particle, especially the load-displacement relationship.

We also find depending on pad flexibility and abrasive concentration, pad may or may not touch directly with the wafer surface. When pad does not touch wafer, all the load transfers to the wafer through the abrasives; on the other hand, only portions of the total load transfer to wafer surface when pad touches wafer. As the latter case is most likely to happen in CMP, we assume pad deforms like a beam to obtain the force partition.

We find depending on the particle size and the contact mode, i.e., whether pad touches wafer or not, material removal will have different dependencies on polishing conditions (e.g., pressure and velocity), slurry (e.g., abrasive shape, size and concentration) and pad rigidity. Model gives a reasonable good explanation about the sometimes contradictive experimental data though the model is purely based on mechanical aspect of material removal.

6.1.2 Within wafer nonuniformity

Within-wafer-non-uniformity (WIWNU) is a critical parameter in determining the quality of a wafer planarized by a CMP process. It significantly influences the yield of good dies. Wafer-to-wafer-non-uniformity (WTWNU) is also important for a CMP process as it indicates the pad life and tool stability. In the model, WIWNU and WTWNU are investigated

based on a simplified CMP setup.

From the WIWNU model, certain wafer size, shape and downforce will lead to certain wafer-pad interface pressure distribution. Through the modification of any of those factors, the pressure distribution will change. In general, there is a pressure singularity at the wafer edge which leads to extremely high material removal rate at this region. Incoming film thickness varies due to different deposition processes. In CMP, it is generally not desirable to have a uniform pressure distribution on the whole wafer. A good CMP system has the ability to tune the pressure variation according to the incoming film thickness variation. Thicker film should experience higher pressure and thinner film lower pressure. The WIWNU model will faciliate the understanding of how to obtain the desired wafer surface pressure variation though the proper control of wafer shape and loading conditions.

The WTWNU model shows the removal rate from wafer to wafer will decay due to viscoelastic deformation even if all the wafers are under the same polishing conditions. The decay is due to the pressure drop across most part of the wafer excluding the edge area. The model points out viscoelastic deformation of the pad may be one of the causes for WTWNU.

The relationships among wafer shape, loading and wafer-pad interface pressure distribution are also investigated to facilitate the carrier head design.

6.1.3 Dishing, erosion and step height reduction

The feature scale model shows almost every part of a CMP system will influence the dishing, erosion and step-height reduction. In Chemical part, slurry selectivity and Preston's constants play an important role; in mechanical part, pad stiffness and bending ability are the important part. Polishing conditions, such as pressure, velocity and overpolishing, will also

influence dishing. Wafer surface topography, such as linewidth, pattern density and pitch, is also important for understanding the feature scale surface evolution process. The influences of those parameters are generally not linear and are intertwined. To reduce dishing and increase the speed of the step height reduction may be carried out by proper control of these parameters.

6.2 Future Work

6.2.1 Particle scale model

Certainly chemical effects are very important in CMP processes. The present model attempts to account for the induced plasticity due to the chemical reaction at the wafer surface. A quantitative model for CMP will require further research and understanding of other chemical effects, e.g., redeposition, passivation, etc. How the temperature rise and material removal influence the chemical aspect of CMP needs further investigation.

The present model assumes uniform particle distribution. A model including particle size distribution and pad surface asperities needs to be considered.

A model improvement will require hydrodynamic considerations and their influence on slurry redistribution during a CMP process. A slurry distribution model is required to understand how the slurry is trapped between the wafer-pad interface and how its chemical concentration changes during the process. The insight from this model will provide the information for the improvement of slurry delivery and polisher kinematic design.

The small strain linear elastic beam bending representation of the present model is a simple approximation for the complex deformation shape of the pad. Moreover, in CMP, material is removed through simultaneous action of many such indenters (abrasive particles),

and the pad may also contact such piled-up material. Understanding of such interactions will be necessary to further develop a quantitative material removal model for a CMP process.

6.2.2 Wafer scale model

In the WIWNU model, pad is modeled as an elastic half space. A better model may consider pad as a layered half space because in reality a stacked pad is generally put on top of a rigid platen. A layered-pad model will show how the upper pad and lower pad (e.g., their thickness and Young's Modulus) influence the pressure distribution on the wafer surface. This kind of model will faciliate the stacked pad design.

In the real life CMP, a retainer ring is used. Because it will influence the deformation of the pad and wafer surface pressure distribution, a WIWNU including the information of the retainer ring should be considered.

Some researchers think slurry distribution may be one of the causes for edge effect. A slurry distribution model also needs to be investigated so that slurry distribution system could be improved.

During unloading, pad will recover some of its deformation; but there still will be a certain amount of permanent deformation which depends on the time interval of loading and unloading and the material's viscoelastic properties. Inclusion of this aspect to the model will make the WTWNU predictions more accurate. For various configurations of polishers (e.g., rotational, linear and orbital CMP polishers), the part of pad in contact with wafer is constantly changing. A model which can catch the kinematic part of CMP will be more applicable to the specific polishers. The design of the carrier head will influence how the wafer deforms during the CMP process. It is observed in our simulations that a small variation in the wafer

profile can significantly influence the pressure distribution. Accordingly, to better represent the CMP process, a time-dependent model for wafer deformation have to be considered.

It is well-known that pad conditioning and pad wear will significantly influence WTWNU. How proper pad conditioning reduce WTWNU and how pad wear causes removal rate decay needs to be incorporated into current model and to make the model prediction more accurate.

There are other factors contributing to WIWNU, such as the polisher design, wafer flats and its chamfer. There are also many other factors which lead to WTWNU and decreasing MRR, such as pad wear, glazing, pad soften by water diffusion, slurry chemistry, etc. It is essential to identify the relative importance of these factors and to combine them into a more robust model so that an appropriate control strategy can be implemented for the CMP process.

6.2.3 Die scale model

In die scale model, wafer surface topography will play a very important role. Within each die, different regions may have different linewidth, pitch and pattern density. Because all those factors influence planarity and the CMP performance, each factors has to be included in the model. Die scale model in this aspect will strongly depend on feature scale model.

On the other hand, pressure distribution in different dies will be different. The pressure distribution on each die will depend on its location and its orientation on the wafer surface. The conclusion is that die scale model also strongly depend on wafer scale model.

Die scale model may be the most important part of CMP modeling because how many good dies are produced in each wafer is the ultimate concern of chipmakers. The model will also provide the design rules for pattern layout and usage of dummy structures to optimize the

CMP performance. Not much work has been done; due to its importance, much more research efforts need to be focused on this area.

6.2.4 Feature scale model

The trend of polisher design is to use lower downforce and higher velocity. The velocity may be high enough that viscoelastic pad deformation may significantly influence the CMP planarization efficiency. The present model only considers pad elastic deformation by using a constant pad stiffness value. To capture pad viscoelastic deformation, pad stiffness has to be considered as a time-dependent function related to the viscoelastic properties of pad.

In the model, average dishing is considered. To capture the accurate dishing profile, the PDE formulation has to be considered instead of ODE formulation.

The model only consider the case when wafer surface feature and pad are fully contact with each other. It may be integrated with other models in which only upper features of wafer is in contact with pad. Those kinds of model will be able to describe the whole feature evolution process from step height reduction to dishing and erosion.

REFERENCES

Bajaj, R., Desai, M., Jairath, R., Stell, M. and Tolles, R., 1994, "Effect of Polishing Pad Material Properties on Chemical Mechanical Polishing (CMP) processes," Material Research Society Symposium proceedings, Vol. 337, pp. 637-644.

Baker, A.R., 1996, "The Origin of the Edge Effect in CMP," Proceedings of the First International Symposium on Chemical Mechanical Planarization, Vol.96, No.22, pp. 228-238.

Bibby, T. and Holland, 2000, "Equipment," Semiconductors and Semimetals, Vol. 63, pp. 5-46, Academic Press, San Diego, CA, USA.

Bielmann, M., Mahajan, U. and Singh, R.K., 1999, "Effect of Particle Size during Tungsten Chemical Mechanical Polishing," Electrochemical and Solid-State Letters, Vol.2, No.8, pp.401-403.

Borucki, L., 2001, "Mathematial Modeling of Polishing Rate Decay in Chemical-Mechanical Polishing," Journal of Engineering Mathematics (submitted).

Brown, N.J., 1987, "Some Speculations on the Mechanisms of Abrasive Grinding and Polishing," Precision Engineering, Vol.9, No.3, pp. 129-138.

Brown, N.J., Baker, P.C. and Maney, R.T., 1981, "Optical Polishing of Metals," Proc SPIE, Vol.306, pp. 42-57.

Bulsara, V. H., Ahn, Y., Chandrasekar, S. and Farris, T.N., 1997, "Mechanics of Polishing," Manufacturing Science and Technology, ASME, Vol.1, pp. 225-233.

Byrne, G., Mullany, B. and Young, P., 1999, "The Effect of Pad Wear on the Chemical Mechanical Polishing of Silicon Wafers," Annals of the CIRP, Vol. 48; No. 1, pp. 143-146.

Chekina, O.G., Meer, L.M. and Liang, H., 1998, "Wear-Contact Problems and Modeling of Chemical Mechanical Polishing," J. Electrochem. Soc., Vol.145, No.6, pp. 2100-2106.

Chen, D.-Z. and Lee, B.-S., 1999, "Pattern Planarization Model of Chemical Mechanical Polishing," Journal of the Electrochemical Society, Vol. 146, No. 2, pp. 744-748.

Christensen, R.M., 1982, Theory of Viscoelasticity, Second Edition, Academic Press, New York, USA.

Collins, W.D., 1963, "Potential Problems for a Circular Annulus," Proceedings of Edinburgh Mathematical Society, Vol. 13, Series. 2, pp. 235-246.

Cook, L.M., 1990, "Chemical Processes in Glass Polishing," Journal of Non-Crystalline Sol-

ids, Vol.120, pp. 152-171.

Cook, L.M., 2000, "CMP Consumables II: Pad," Semiconductors and Semimetals, Vol. 63, pp. 155-182, Academic Press, San Diego, CA, USA.

Elbel, N., Neueither, B., Ebersberger, B. and Lahnor, P., 1998, "Tungsten Chemical Mechanical Polishing," J. Electrochem. Soc., Vol.145, No.5, pp. 1659-1664.

Evans, C.J., Parks, R.E., Roderick, D.J. and McGlauflin, M.L., 1998, "Rapidly Renewable Lap: Theory and Practice," Annals of the CIRP, Vol. 47, pp. 239-244.

Fayolle, M. and Romagna, F., 1997, "Copper CMP Evaluation: Planarization Issues," Microelectronic Engineering, Vol. 37/38, pp. 135-141.

Gladwell, G. M. L., 1980, Contact Problems in the classical theory of elasticity, Sijthoff & Noordhoff International Publishers B. V., The Netherlands.

Gotkis, Y., Schey, D., Alamgir, S., Yang, J. and Holland, K., 1998, "Cu CMP with Orbital Technology, Summary of the Experience," 1998 IEEE/SEMI Advanced Semiconductor Manufacturing Conference, pp. 364-371.

Green, A.E. and Zema, W., 1954, Theoretical Elasticity, Oxford University Press, London, Great Britain.

Hay, J.C., Bolshakov, A. and Pharr, G.M., 1999, "Critical Examination of the fundamental relations used in the analysis of nanoindentation data," Journal of Materials Research, Vol. 14, No. 6, pp. 2296-2305.

Izumitani, T., 1979, "Polishing, Lapping, and Diamond Grinding of Optical Glasses," Treatise on Materials Science and Technology, Vol.17, Academic Press, New York, U.S., pp. 115-172.

Johnson, K.L., 1985, Contact Mechanics, Cambridge University Press, Great Britian.

Kim, H.-J., Kim, H.-Y. and Jeong, H.-D., 2000, "Viscoelastic Behavior of Polishing Pad and Its Influence on Polishing Non-uniformity," Proceedings, Fifth International Chemical-Mechanical Planarization for ULSI Multilevel Interconnection Conference (CMP-MIC), pp. 275-282.

Knapp, J.A., Follstaedt, D.M., Myers, S.M., Barbour, J.C., Friedmann, T.A., Ager III, J.W., Monteiro, O.R. and Brown, I.G., 1998, "Finite-element modeling of nanoindentation for evaluating mechanical properties of MEMS materials," Surface and Coating Technology, Vol.103-104, pp. 268-275.

Komanduri, R., Lucca, D. A. and Tani, Y., 1997, "Technological Advances in Fine Abrasive

Processes," Annal of the CIRP, Vol.46/2, pp. 545-596.

Levert, J.A., Mess, F.M., Salant, R.F. and Baker, A.R., 1998, "Mechanisms of Chemical-Mechanical Polishing of SiO2 Dielectric on Integrated Circuits," Tribology Transactions, Vol.41, No.4, pp. 593-599.

Li, S.H. and Miller, R.O., 2000, Semiconductors and Semimetals, Vol. 63, Academic Press, San Diego, CA, USA.

Liang, H., Kaufman, F., Devilla, R. and Anjur, S., 1997, "Wear Phenomena in Chemical Mechanical Polishing", Wear, Vol.211, pp. 271-279.

Lichinchi, M., Lenardi, C., Haupt, J. and Vitatli, R., 1998, "Simulation of Berkovich nanoindentation experiments on thin films using finite element method," Thin Solid Films, Vol.312, pp. 240-248.

Liu, C. W., Dai, B. T., Tseng, W. T. and Yeh, C. F., 1996, "Modeling of the Wear Mechanism during Chemical-Mechanical Polishing," J. Electrochem. Soc., vol.143, No.2, pp. 716-721.

Love, A.E.H., 1939, "Boussinesq's Problem for a Rigid Cone," Quarterly Journal of Mathematics, Vol. 10, pp. 161-175.

Luo, Q., Campbell, D.R. and Babu, S.V., 1998, "Modification of the Preston Equation for the Chemical-Mechanical Polishing of Copper," Thin Solid Films, Vol.335, pp. 160-167.

Nguyen, V.H., Velden, P.V.D., Daamen, R., Kranenburg, H.V. and Woerlee, H., 2000, "Modeling of Dishing for Metal Chemical Mechanical Polishing," IEEE International Electronic Devices Meeting, pp. 499-501.

Ouma, D. O., 1998, "Modeling of Chemical Mechanical Polishing for Dielectric Planarization", Ph.D thesis, Department of Electrical Engineering and Computer Science, MIT.

Pan, J.T., Li, P., Wijekoon, K. Tsai, S. and Redeker, F., 1999, "Copper CMP Integration and Time Dependent Pattern Effect," 1999 International Interconnect Technology Conference, San Francisco, CA, pp. 164-166.

Plummer, J.D., Deal, M.D. and Griffin, P.B., 2000, Silicon VLSI technology: fundamentals, practice and modeling, Prentice Hall, Upper Saddle River, NJ, USA.

Popov, G.Ia., 1962, "The Contact Problem of the Theory of Elasticity for the Case of a Circular Area of Contact," Journal of Applied Mathematics and Mechanics (English translation of PMM), Vol.26, No.1, pp. 207-225.

Pourbaix, M., 1966, Atlas of Electrochemical Equilibria in Aqueous Solutions, Pergamon, Oxford.

Preston, F. W., 1927, "The theory and design of plate glass polishing machine," J. Soc. Glass Tech., vol. 11, no. 44, pp. 214-256.

Runnels, S.R., 1994, "Feature-Scale Fluid-Based Erosion Modeling for Chemical-Mechanical Polishing," J. Electrochem. Soc., Vol.141, No.7, pp. 1900-1904.

Runnels, S.R., 1996, "Advances in Physically Based Erosion Simulators for CMP," Journal of Electronic Materials, Vol.25, No.10, pp.1574-1580.

Runnels, S.R. and Eyman, L.M., 1994, "Tribology Analysis of Chemical-Mechanical Polishing," J. Electrochem. Soc., Vol.141, No.6, pp.1698-1701.

Runnels, S.R. and Renteln, P., 1993, "Modeling the Effect of Polish Pad deformation on Wafer Surface Stress Distributions During Chemical-Mechanical Polishing," Dielectric Science and Technology, pp. 110-121.

Saka, N., Lai, J.-Y., Chun, J.-H., and Shu, N.P., 2001, "Mechanisms of the Chemical Mechanical Polishing (CMP) Process in Integrated Circuit Fabrication," Annals of the CIRP, Vol. 50, pp. 233-238.

Rabinowicz, E. C., 1968, "Polishing," Scientific American, vol. 218, no. 6, pp. 91-99.

Sasaki, Y., Aoyama, H., Inasaki, I., Miyairi H. and Shibaya, H., 1998, "Evaluation of Effective CMP Conditions by Estimation of Pressure Distribution on Semiconductor Wafer," Proceedings of Silicon Machining (1998 Spring Topical Meeting), Vol.17, pp. 92-95.

Shi, F.G., Zhao, B. and Wang, S.-Q., 1998, "A New Theory for CMP with Soft Pads," Proceedings of International Interconnect Technology Conference, San Francisco, CA, pp. 73-75.

Shield, T.W. and Bogy, D.B., 1989, "Some Axisymmetric Problem for Layered Elastic Media: Part I - Multiple Region Contact Solutions for Simple-Connected Indenters," Journal of Applied Mechanics, Transactions of the ASME, vol.56, pp. 798-806.

Shield, T.W. and Bogy, D.B., 1989, "Some Axisymmetric Problem for Layered Elastic Media: Part I - Solutions for Annular Indenters and Cracks," Journal of Applied Mechanics, Transactions of the ASME, vol.56, pp. 807-813.

Shield, T.W. and Bogy, D.B., 1989, "Multiple Region Contact Solutions for a Flat Indenter on a Layered Elastic half Space: Plane-Strain Case," Journal of Applied Mechanics, Transactions of the ASME, vol.56, pp. 251-262.

Sneddon, I.N., 1946, "Boussinesq's problem for a flat-ended cylinder", Proc. Cambridge Philosophical Society, Vol.42, pp. 29-39.

Sneddon, I.N., 1948, "Boussinesq's Problem for a Rigid Cone," Proceedings of Cambridge Philosophical Society, Vol. 44, pp. 492-507.

Steigerwald, J.M., Murarka, S.P. and Gutmann, R. J., 1996, Chemical Mechanical Planarization of Microelectronic Materials, Wiley-Interscience Pub. New York, USA.

Stein, D., Hetherington, D., Dugger, M. and Stout, T., 1996, "Optical Interferometry for Surface Measurements of CMP Pads," Journal of Electronic Materials, Vol. 25, No. 10, pp. 1623-1627.

Strinivasa-Murthy, C., Wang, D., Beaudoin, S.P., Bibby, T., Holland, K. and Cale, T.S., 1997, "Stress Distribution in Chemical Mechanical Polishing," Thin Solid Films, Vol.308-309, pp. 533-537.

Tichy, J., Levert, J.A., Shan, L. and Danyluck, S., 1999, "Contact Mechanics and Lubrication Hydrodynamics of Chemical Mechanical Polishing," Journal of the Electrochemical Society, Vol. 146; No. 4, pp. 1523-1528.

Timoshenko, S. P. and Goodier, J. N., 1970, Theory of elasticity, 3rd edition, McGraw-Hill, New York, USA.

Tomozawa, M., 1997, "Oxide CMP mechanisms," Solid State Technology, Vol. 40, No.7, pp 169-175.

Tseng, W.-T. and Wang, Y.-L., 1997, "Re-examination of Pressure and Speed Dependences of Removal Rate During Chemical-Mechanical Polishing Processes," J. Electrochem. Soc., Vol.144, No.2, pp. L15-L17.

Vlassak, J.J., 2001, "A Contact-Mechanics Based Model for Dishing and Erosion in Chemical-Mechanical Polishing," Mat. Res. Soc. Symp., Vol. 671, pp. M4.6.1-M4.6.6.

Wang, D., Lee, J., Holland, K., Bibby, T., Beaudoin, S. and Cale, T., 1997, "Von Mises Stress in Chemical-mechanical Polishing Processes," J. Electrochem. Soc., Vol.144, No.3, pp. 11121-1127.

Warnock, J., 1991, "A Two-Dimensional Process Model for Chemical Mechanical Polish Planarization," J. Electrochem. Soc., Vol. 138; No. 8, pp. 2398-2402.

Wolfram, S., 1991, Mathematica - A System for Doing Mathematica by Computer, second edition, Addison-Wesley, Redwood City, California, USA.

Yao, C.-H., Feke, D.L., Robinson, K.M. and Meikie, S., 2000, "Modeling of Chemical Mechanical Polishing Processes Using a Discretized Geometry Approach," Journal of the Electrochemical Society, Vol. 147; No. 4, pp. 1502-1512.

Yu, T.-K., Yu, C. C. and Orlowski, M., 1993, "A statistical polishing pad model for chemical-mechanical polishing," IEDM Tech. Dig., pp. 865-868.

Zhang, F. and Busnaina, A., 1998, "The Role of Particles Adhesion and Surface Deformation in Chemical Mechanical Polishing Processes," Electrochemical and Solid-State Letters, Vol.1, No.4, pp. 184-187.

Zhao, B. and Shi, F.G, 2000, "Chemical Mechanical Polishing in IC Processes: New Fundamental Insights," Vol. 1; No. 1, The International Journal of CMP for ULSI Multilevel Interconnection, pp. 13-25.